EFFECTS OF CHEMOTHERAPY ON MOUSE CORPUS LUTEUM AND UTERINE RECEPTIVITY

by

CHRISTIAN L. ANDERSEN

(Under the Direction of Xiaoqin Ye)

ABSTRACT

The number of childhood (from birth to adolescence) cancer survivors increases because of increased cancer incidence and a slightly more significant decrease in the mortality rate from cancer therapy. A unique side effect of concern on these cancer survivors from cancer therapy (e.g., chemotherapy and radiotherapy) is fertility impairment. Some chemotherapeutics drugs have been shown to target ovarian follicles to impair female fertility. The corpus luteum (CL) is normally developed from an ovulated follicle for producing progesterone (P4) to support early pregnancy. To fill in the knowledge gap about effects of chemotherapy on the CL, we tested the hypothesis that chemotherapy could adversely affect the CL using doxorubicin (DOX) as a representative chemotherapeutic drug in mice. We found varying effects in serum P4 levels, as well as varying effects in key aspects of CL function. CLs from DOX-treated mice with low P4 levels had less defined luteal cords, disrupted expression pattern of collagen IV (a marker of the basal lamina of endothelial cells), and reduced expression of StAR (steroidogenic acute regulatory protein) in luteal cells. A major focus in oncofertility is studying the gonadotoxic effects of chemotherapies on the ovary (sans the CL), however the uterus also plays a critical role in the future reproductive health of premenopausal patients. We showed that a single, human-relevant

dose of doxorubicin (10 mg/kg, single dose) in young adult ovariectomized CD-1 mice had a long-term effect on uterine transcriptome to E2 treatment (Andersen CL et al, 2018). Since some of the differentially expressed genes are associated with uterine receptivity, we hypothesize that chemotherapy could disrupt uterine receptivity for embryo implantation. To test this hypothesis, ovariectomized C57BL6J mice are treated with vehicle (negative control), doxorubicin (2 mg/kg, 5 daily doses), or doxorubicin (10 mg/kg, single dose, positive control) starting on PND30. Decidualization is a uterine response to an implanting embryo and an indication of uterine receptivity. We use artificial decidualization to determine uterine receptivity, visualizing the accumulation of blue-dye in the decidual sites of a receptive uterus. Preliminary data show that the above chemotherapeutic regimens have varied adverse effects on uterine receptivity.

INDEX WORDS: uterus, ovary, toxicology, reproduction, doxorubicin

EFFECTS OF CHEMOTHERAPY ON MOUSE CORPUS LUTEUM AND UTERINE RECEPTIVITY

by

CHRISTIAN L. ANDERSEN

B.S., University of Georgia, 2015

A Dissertation Submitted to the Graduate Faculty of The University of Georgia in Partial Fulfillment of the Requirements for the Degree

DOCTOR OF PHILOSOPHY

ATHENS, GEORGIA

2021

EFFECTS OF CHEMOTHERAPY ON MOUSE CORPUS LUTEUM AND UTERINE RECEPTIVITY

by

CHRISTIAN L. ANDERSEN

Major Professor:	XIAOQIN YE
Committee:	MARIA VIVEIROS
	TAI GUO

Electronic Version Approved:

Ron Walcott
Vice Provost for Graduate Education and Dean of the Graduate School
The University of Georgia
August 2021

DEDICATION

The support network I had during my collegiate education insured that I would have a strong footing to tackle a Bachelor of Science in Biochemistry and Molecular Biology, as well as a Doctor of Philosophy in Toxicology. I dedicate this dissertation to the family and friends who provided support throughout my time at the University of Georgia. My parents who encouraged me to pursue whatever I wanted and helped push me to complete my degree after some bumps in the road. My sister who always provided an ear for my troubles or included me in her own festivities. My grandparents who helped support my fraternity experience and made sure I was always taken care of during the tough financial years of graduate school. My aunt and uncle who took me into their home when I was between leases and always offered a homecooked meal if I needed it. Lastly to the many friends who also provided so much love over the years, without all the fun we had I am not sure I would have been able to handle the stress.

Researchers using *in-vivo* models to study critical aspects of the life sciences are privileged to use those organisms to gain valuable information that can relate back to our own physiology. I dedicate this dissertation to the lab animals, specifically *mus musculus*, that were used to accomplish this research in the hopes to develop better risk assessment for the future reproductive health of women. I hope with continued progress in *tissue-chip* systems we will further reduce the need for *in-vivo* systems, except where absolutely needed. This dissertation aimed to fill many critical knowledge gaps in our understanding of how chemotherapy treatment of premenopausal patients can influence their reproductive health later in life, the lab animals are owed more than we can give back to them.

ACKNOWLEDGEMENTS

I want to acknowledge my mentor, Dr. Xiaoqin Ye, without her guidance and support this dissertation would have never been completed. I was told early in my collegiate career to find mentors who want to help you succeed, not because it makes them look good, but because they enjoy helping people meet the challenges of life. I could not have asked for a better mentor than Dr. Ye. She is always willing to help, provide guidance, go on a hike and occasionally even hangout with the trainees at the conference watering hole. She made sure we always had stable sources of funding, a more difficult feat every year, and provided recommendations for grants and scholarships. She helped me pursue one of the most defining moments in my life, attending the Frontier in Reproduction training course, and without her I would not have been selected. She has spent many hours helping to refine my presentation skills, culminating in my ARCS award in 2018 and various awards for presentations later in graduate school. While she treated as her children, rather than her trainees, she also treated us as her peers and asked for my own expertise on many occasions. I am honored that Dr. Ye chose me to become one of her research children and hope that I can honor her decision through my future career as a scientist.

I also want to acknowledge all the funding support I received over the years. The UGA Interdisciplinary Toxicology Program and the department of Physiology and Pharmacology provided much of the support for my stipend, as well as funds for travel to conferences and the Frontier in Reproduction training course. The Society for the Study of Reproduction (SSR) awarded me the Anita Payne Scholarship to attend the Frontier in Reproduction training course, this award was established to support students who meet many of the ideals that the renowned

endocrinologist Anita Payne showed through her many years with SSR. I am honored to have been selected to receive such a prestigious award and will carry the weight of this award with me as I continue to investigate aspects of reproductive toxicology. The ARCS Foundation, Atlanta chapter awarded me an ARCS award in 2018, designed to provide monetary support for graduate students to use however they want. I am eternally grateful for organizations like ARCS who support graduate students with discretionary funds to provide additional monetary support.

Lastly, I would like to acknowledge the mentorship provided by my committee members, Dr. Maria Vivieros, and Tai Guo. They provided critical feedback needed to help think of the questions proposed in this dissertation, each offering valuable input into the manuscripts and research methods.

TABLE OF CONTENTS

LIST OF FIGURES

Page

Abbreviations

DPC – days post coitum

D – gestation day

LH – luteinization hormone

CL – corpus luteum

DOX – doxorubicin

E2 – 17beta-estradiol

P4 – progesterone

Bax – bcl-2-associated-x-protein

PGC – primordial germ cells

EDC – endocrine disrupting compound

HPG – hypothalamic-pituitary-gonadal

GnRH – gonadotropin releasing hormone

FSH – follicle stimulating hormone

ER – estrogen receptor

PGR – progesterone receptor

PRL – prolactin

hCG – human chorionic gonadotropin

20alpha-HSD – 20-alpha-hydroxy steroid dehydrogenase

MMP – matrix metalloproteinases

ECM – extracellular matrix

VEGF – vascular endothelial growth factor

STAR – steroidogenic acute regulatory

COLIV – collagen type 4

LDL – low density lipoprotein

HDL – high density lipoprotein

ABCA1 – ATP binding cassette subfamily A1

APOA1 – apolipoprotein A1

HSL – hormone sensitive lipase

LD – lipid droplet

ROS – reactive oxygen species

SER – smooth endoplasmic reticulum

3beta-HSD – 3beta-hydroxy steroid dehydrogenase

WOI – window of implantation

LIF – leukemia inhibiting factor

LE – luminal epithelium

GE – glandular epithelium

PDZ – primary decidual zone

IGFBP-1 – insulin growth factor binding protein 1

AYA – children, adolescents and young adults

PI3K – phosphoinositide 3-kinase

MDR1 – multidrug resistant protein 1

IVF-ET – in-vitro fertilization and embryo transfer

I.P. – intraperitoneal

S.C. – subcutaneous

BW – body weight

CHAPTER 1

Introduction

Female reproduction follows pubertal development, which prepares the ovaries, the female reproductive track, and the mammary glands for sexual maturation and reproductive capabilities. Puberty is a multistage process with dramatic changes in physical appearance and hormonal levels to obtain sexual maturation and reproductive capabilities. Although the precise mechanisms behind pubertal initiation remain largely unknown, the hypothalamic–pituitary–gonadal (HPG)-axis and proper hormonal regulation are essential for pubertal development. Female reproduction involves multiple integral processes, including ovarian folliculogenesis, ovulation, ovarian steroidogenesis, fertilization, preimplantation embryo development and transport, embryo implantation, placentation, parturition, and lactation. Female reproduction is regulated by hormones, such as progesterone (P4) and estrogen (E2) (Figure 1.1). These hormones are produced in the ovary and impart actions throughout the body (Figure 1.3). A main target of ovarian hormones is the uterus, Fallopian tubes (oviducts in rodents), and vagina. Tight coordination of ovarian and uterine molecular events supports the fertility of women. Environmental toxins and biologics, such as mycotoxins and chemotherapies (respectively) can contribute to disruptions in fertility and female reproductive health.

Ovary, corpus luteum, and ovarian hormones

The ovary is a heterogenous organ responsible for maturation and activation of competent oocytes for fertilization, as well as hormone production to facilitate pubertal development and pregnancy. The main structures of the ovary are the ovarian follicle, corpus luteum, blood vessels,

and medullary stroma and is conserved among most mammals (Figure 1.2) (Bahr, 2018). Follicles will mature and grow in conjunction with the oocyte it harbors until it undergoes regulated apoptosis, through atresia or the oocyte ovulates from the follicle. After ovulation, the follicle undergoes rapid morphological and molecular changes to form the corpus luteum. This represents the transition from directly supporting oocyte development and maturation to support of pregnancy through interactions with the uterus. Hormones produced by the ovary through the follicles and corpus luteum also contribute to the support of follicles, pregnancy, reproductive tract function, metabolic cues, as well as secondary sexual characteristics and cyclicity in humans (Bahr, 2018). 17b-Estradiol (E2) and progesterone (P4) are the primary effector steroid hormones produced by the ovary through interactions between the various cell types that inhabit the multiple structures in the ovary. These hormones and other signaling molecules are imported and exported from the ovary through a vast network of vasculature supported by the mesovarium. The utero-ovarian artery, venous blood, and nerves enter the ovary at the hilus. From here the vasculature dramatically invades into the medullary stromal area, surrounding follicles and corpora lutea in the cortex as well, thus making the ovary one of the most vascular organs (Feng *et al.*, 2017).

Development of the follicular population that contribute to the fertility of humans and mice begin as early as D9.5 DPC. Primordial germ cells (PGCs) migrate from the allantois to genital ridge and begin to divide mitotically, generating ~25,000 PGCs by D13.5. These PGCs will cease dividing, form oogonia, multiple PGCs grouped into cysts/nests, then enter meiosis (Bertolin and Murphy, 2014). These nests are interconnected by cytoplasmic bridges which are hypothesized to help increase storage of materials that will be used later in development (Tingen, Kim and Woodruff, 2009). Near birth, the cysts/nests will undergo programmed cell death through apoptotic pathways, activating Caspase 9 and Bax, further reducing the number of oocytes that will form

primordial follicles, reviewed by Sun, YC. *et. al.*(Sun *et al.*, 2017). Recent single cell 'omics data, along with previous dogma support the long-held theory that these initial mitotic events generate all the oocytes that will be ovulated in the adult ovary (Wagner *et al.*, 2020). The early days after birth represent the most important phase of oocyte loss and is critical to establishing the pool of primordial follicles. Oocytes will become completely surrounded by granulosa cells, thus starting their journey as a primordial follicle. Previous work has shown that survival of oocytes during this time is dependent on the ability to resist activation of atresia pathways, through mechanisms involving intraovarian growth factors and the health of the granulosa cell-oocyte interconnections (Bahr, 2018). Primordial follicle formation is sensitive to endocrine disrupting compounds (EDCs), suggesting that estrogen regulation is a key part of the process as well (Gura and Freiman, 2018). The establishment of the oocyte and granulosa cells represents a key stage in the development of both. Each will provide factors and support to the other to further the development of the follicle (Da Silva-Buttkus *et al.*, 2008; Gura and Freiman, 2018). It is estimated, that only 300-500 of 1,000,000 primordial follicles will reach ovulation during the reproductive lifespan of an adult woman. Follicles are organized based on morphologic characteristics, specific gene expression, and position in the ovary (Bertolin and Murphy, 2014; Fan *et al.*, 2019). Primordial follicles represent the initial phase of the follicle as a functional unit, the primordial follicle has four potential fates, reviewed by Patrick Hannon and Thomas Curry: (1) remain quiescent and establish the ovarian reserves, (2) undergo atresia, (3) undergo initial recruitment and eventually ovulate, (4) or undergo initial recruitment and then atresia, representing the most likely scenario (Hannon and Curry, 2018). In the mouse, quiescence is maintained by repressing activation pathways, survival factors preventing atresia, and maintenance of the Balbiani body, organized Golgi complexes that stores key transcripts for follicle activation (Gura and Freiman, 2018; Lei *et*

al., 2020). Initial recruitment is the process by which primordial follicles will transition to primary follicles. During this time, the oocyte grows, granulosa cells transition from flat-squamous to cuboidal, the zona pellucida forms between the oocyte and granulosa cells, and theca cells begin to migrate from ovarian stroma to the cortex. Signaling factors related to this initial recruitment are extensively reviewed in Chen, Y. et al. 2020. (Chen *et al.*, 2020). Precursor theca cells migrate from the ovarian stroma towards primary follicles and begin surrounding the granulosa layer, which has proliferated and expanded. With the establishment of multiple granulosa cells, the preantral follicle has formed. Theca cells will proliferate to form the theca interna, the steroid hormone producing theca cells, and theca externa, site of fibroblast-like theca cells that regulate the connective tissue surrounding the follicle (Richards, 2018b). Prior to this recruitment and invasion by theca cells, follicle development is entirely gonadotropin independent. However, as granulosa cells continue to proliferate, deposits of secretory/nutrient/waste products form spaces that will coalesce to create the antrum. This antrum will define the follicle as an early antral follicle. Similarly to initial recruitment, a range of intraovarian factors support the initiation of early antral follicles, however early antral follicles appear to be gonadotropin-responsive (Hannon and Curry, 2018). These follicles have been documented as the most likely to undergo atresia, likely through autophagic pathways, while antral follicle atresia is likely through apoptotic pathways (Meng *et al.*, 2018). Follicles undergo cyclic recruitment, the process that mediates careful activation and atresia of follicles, is dependent on hypothalamic-pituitary-gonad (HPG) signaling events. Careful regulation of apoptosis during primordial follicle generation, cyclic recruitment during follicle activation, and the HPG axis maintain the pool of oocytes needed for pregnancy.

In general, menstrual/estrous cyclicity begins around reproductive maturity in mammals. Inbred mice strains typically reach puberty around 6-8 weeks, but outbred strains will reach

puberty around 4 weeks (Bell, 2018). Our understanding of the exact molecular mechanisms that initiate pubertal onset in mammals is continually evolving. The "central drive" hypothesis proposes that a network of neurons impart stimulatory and inhibitory action onto gonadotropin releasing hormone (GnRH) neurons in the hypothalamus, eventually stimulatory events will cause an increase in GnRH pulsatility leading to initiation of puberty (Figure 1.3). Slower GnRH pulsatility stimulates follicle stimulating hormone (FSH) release from the pituitary that will support the growth of follicles through granulosa cell proliferation, follicle growth, and priming of luteinizing hormone (LH) receptor (LHR), while increased pulsatility will favor the release of LH that supports androgen synthesis, dominant follicle support, and follicle ovulation. The GnRH release and further selection of different gonadotropins results in feed-forward and feedback (positive and negative) regulation on the HPG axis through the end hormonal products. This gonadotropin release will cause follicles, the primary site of E2 synthesis, to begin producing and secreting E2 into circulation (Terasawa and Fernandez, 2001; Ojeda and Skinner, 2006). A two-cell, two-gonadotropin model has been proposed as the mechanism for E2 synthesis in the follicle (Figure 1.4) (Fortune, 2018). Aromatase (*CYP19A1*), regulated by FSH in granulosa cells, is responsible for the conversion of androstenedione to estrone, as well as testosterone to E2. Estrone can be converted to E2 by 17beta-hydroxysteroid dehydrogenase (*17B-HSD*) in granulosa cells. Estrogen steroidogenesis is reviewed extensively in Figure 1.4. E2 can intern impart regulatory actions back onto the HPG axis as a form of both positive and negative feedback, dependent on actions in the hypothalamus or pituitary, respectively (Figure 1.3) (Padmanabhan, Puttabyatappa and Cardoso, 2018). The kisspeptin, neurokinin B, and dynorphin (KNDy) expressing neurons are the hypothesized site of gonadal hormone negative regulation due to the expression of the key receptors, estrogen receptors and progesterone receptor. Estradiol also has negative feedback

regulation on the FSH-beta subunit, which is responsible for effector FSH, thus limiting FSH stimulation but not preventing it. In conjunction, estradiol has positive feedback regulation on kisspeptin neurons in the anteroventral periventricular area, leading to increase GnRH release favoring LH surge. Pubertal onset and the menstrual and estrous cycles are critical for pregnancy and require the careful activation and maintenance of the HPG axis. Estrogen, an important component of the HPG axis, and its' regulation are key for follicular and corpora lutea health and function.

E2 also has local actions in the ovary, supporting granulosa cell mechanisms by enhancing FSH stimulation of aromatase expression (in turn estradiol synthesis), LH receptor (LHR) expression and LH responsiveness, antrum formation, gap-junction formation and prevention of follicular atresia (Couse *et al.*, 2005). E2's effects directly on granulosa cells through estrogen receptor action, besides previous mentioned actions through ERbeta, are minimal (Couse *et al.*, 2005). Estradiol's paracrine action on theca cells culminates in the interactions with activins, protein hormones produced by granulosa cells and the pituitary that in conjunction with inhibins regulate the stimulation and inhibiting of FSH release (respectively) (Figure 1.3). It is hypothesized that estradiol suppresses activin expression, therefore increased estradiol and inhibin production by preovulatory follicles would act to suppress activin and increase theca cell androgen production (Young and McNeilly, 2010). Estradiol has significant action in stimulating angiogenesis in the developing corpus luteum, progesterone production, and cholesterol uptake from circulation (Stocco, Telleria and Gibori, 2007). Estradiol's positive feedback regulation on the hypothalamus is key to regulating the LH surge needed for ovulation.

Ovulation is the process by which a mature follicle will be extruded from the ovary to be fertilized in the oviduct (in rodents). The preovulatory follicle is composed of multiple cell layers,

consisting of the theca externa and interna, the mural and syncytial granulosa cells, and the cumulus cells that directly surround the zona pellucida and oocyte. Intercommunication between these layers is critical for successful ovulation. This process is regulated by the relationship of LH and FSH to stimulate LHR found on the granulosa cells of antral/preovulatory follicles. Once LH binds the LHR, molecular events throughout the ovary, such as thinning of the surrounding stromal tissue will permit the release of the cumulus cell-oocyte complex (COC) to release into the bursa (exclusive to rodents) where it will eventually be transported to the oviduct for fertilization. Many of the signaling cues associated with ovulation are regulated through the LH receptor (Figure 1.5) (Richards, 2018a). Increased progesterone, as well as prostaglandin, production in the preovulatory follicle aid in the breakdown of the surrounding stromal layers to facilitate ovulation. Significant upregulation of proteases aid in dissolving the theca layer and surrounding stromal layer to allow for the COC to release from the ovulation pore. Theca progesterone production increases upon the LH surge preovulation, progesterone will bind progesterone receptor (PGR) in granulosa cells to facilitate upregulation of genes involved in follicle extrusion, protein secretion, and vascular endothelial cells. Upon extrusion of the oocyte, the follicle will undergo rapid molecular and structural changes to form the corpus luteum needed to provide further support of early pregnancy events.

The corpus luteum (CL) is a transient organ formed from the luteinization of granulosa and theca cells of the ovulated follicle to provide steroid hormone support of embryo development and embryo implantation (in rodents). Compared to humans, rodents are polyovulatory, only form a functional corpus luteum after fertilization has occurred and have a significantly shorter lifecycle of the corpus luteum. In humans the granulosa cells form large luteal cells, while theca cells form small luteal cells. This difference in size and shape is not as evident in rodents as in primates and

humans, however some molecular differences have been noted between the two subpopulations (Smith *et al.*, 1989; Nelson *et al.*, 1992). The consensus from these two groups reflects that small luteal cells have large nuclei, few lipid droplets, and a stellate shape, while large luteal cells have small, spherical nuclei and a high lipid content. This represents the culmination of analysis between subpopulation of luteal cells in the rodent, but progress is being made in our understanding in humans and other animals using more advanced techniques (Weber *et al.*, 1987; Niswender *et al.*, 2000; Wiltbank *et al.*, 2012; Romereim *et al.*, 2017a; Baddela *et al.*, 2018; Hryciuk *et al.*, 2019). The rodent and human corpus luteum can be classified into either the CL of pregnancy, the CL of the cycle, and the CL of lactation. The CL of pregnancy is the most comparable between the two species, but aspects are shared in the other two types (Stocco, Telleria and Gibori, 2007; Accialini *et al.*, 2017). The CL of the cycle in rodents is extremely short-lived and is considered nonfunctional, undergoing rapid regression without signals from a fertilized embryo. The CL of the cycle cannot synthesize enough progesterone and the little progesterone synthesized by follicular cells immediately after ovulation ensure that follicular recruitment will begin within the 4-5 day cycle timeline. CLs can be classified as distinct types during either pregnancy, the cycle, or lactation. While each type of CL is critical for overall reproductive health, the CL of pregnancy and the molecular events associated with it will be the main focus of this review.

Hours after ovulation, granulosa cells will undergo cell cycle arrest and molecular changes induced by LH will lead to alterations to hormone receptors. A drop in FSH and LH receptors, as well as a short-term increase in P4 and PGR (previously discussed), increase in prostaglandin E2 (*Pge2*), prolactin (*Prl*) receptor (*Prlr*), and shift from ERbeta to ERalpha, indicating a reliance on estrogen as a direct luteotropic factor (Stocco, Telleria and Gibori, 2007; Bachelot *et al.*, 2009; Accialini *et al.*, 2017). *Prl* secreted from the pituitary during early pregnancy and the decidua later

in pregnancy, plays an important role in conversion to the CL of pregnancy and CL maintenance (respectively) (Bachelot and Binart, 2005; Bachelot *et al.*, 2009). Human chorionic gonadotropin (hCG) and LH can rescue CL regression in *Prlr* deficient mice, but cannot prevent progesterone metabolism by 20alpha-HSD, a key function of *Prl* (Bachelot *et al.*, 2009).Other molecular changes will influence maintenance, vascularization, and steroidogenesis in the CL (Figure 1.6) (McRae *et al.*, 2005). A significant restructuring of collagens, proteoglycans, and glycoproteins will form the underlying extracellular matrix to support luteal and endothelial cell function, while matrix metalloproteinases (MMPs) will be responsible for regulated degradation of the follicular-specific extracellular matrix (ECM). In rodents, and to less extent humans, migration and intermixing of ovarian stromal cells (granulosa and theca) with immune cells, pericytes, and endothelial cells is extensive and produces a heterogenous tissue. Upon the surge of LH, the basement membrane separating the granulosa and theca cells breaks down allowing for significant invasion of endothelial cells (Hennebold, 2018). Continued proliferation of endothelial cells contribute to maintenance of CL and provide continual import of progesterone substrate, cholesterol, and progesterone export (Davis, Rueda and Spanel-Borowski, 2003; Stocco, Telleria and Gibori, 2007; Andersen, 2021 *submitted*). In rodents, by D4.5, it is estimated that the number of endothelial cells equals the luteal cell population, providing support to the hypothesis that angiogenesis in the CL rivals that of the placenta and tumors (Hennebold, 2018). Luteal cells provide additional paracrine support of endothelial cells through vascular endothelial growth factors (VEGFs) secretion, partially regulated by LH (Stocco, Telleria and Gibori, 2007; Hennebold, 2018). Collagen type IV (*ColIV*) is a critical protein responsible for proper endothelial cell basal lamina formation and secreted by granulosa cells during luteinization and luteal cells in the CL (McRae *et al.*, 2005; Accialini *et al.*, 2017). Increases in steroidogenesis transcripts during

luteinization, like low-density lipoprotein (*Ldl*) receptor (*Ldlr*), scavenger receptor class B member 1 (*Scarb1*), and steroid acute regulatory protein (*StAR*), as well as corresponding decreases in 3B-HSD and aromatase will gear the luteal cells up for progesterone production (McRae *et al.*, 2005). Molecular cues lead to initiation of morphological changes ultimately altering the functions of the follicle and creating the corpus luteum.

The primary function of the corpus luteum is to produce progesterone for early pregnancy (Jiménez *et al.*, 2010; El Zowalaty, Li, Zheng, *et al.*, 2017; Plewes *et al.*, 2018; Z. Wang *et al.*, 2019; Bildik *et al.*, 2020). Cholesterol needed for steroid hormone synthesis exceeds de-novo synthesis of cholesterol within luteal cells, meaning that cholesterol must be imported into luteal cells to produce the progesterone needed to support early pregnancy (Figure 1.4). Cholesterol import by theca, granulosa, cumulus and luteal cells is dependent on circulating lipoprotein-bound cholesterol, HDL and LDL; however different species have different dependencies on which is the primary source. In humans cholesterol import through LDL and the LDL receptor is the favored source, while in the rodent it is HDL and *Scarb1* (Jiménez *et al.*, 2010; Chang *et al.*, 2017; Talbott and Davis, 2017). Cholesterol is imported through both these pathways as cholesterol esters then can undergo bidirectional conversion to free cholesterol and used for progesterone production. ATP-binding cassette transporter A1 (*Abca1*) and apolipoprotein A1 (*ApoA1*) have been shown to contribute to HDL formation and homeostasis, with the latter being effected by progesterone potentially creating a feedback loop for cholesterol import (Kojima *et al.*, 2001). Cholesterol can be stored in the cytoplasmic lipid droplets as cholesteryl esters, which will undergo hydrolysis via the intracellular neutral hormone-sensitive lipase (*Hsl*, also named cholesteryl ester hydrolase (CEH)) and/or lysosomal acid lipase (*Lal*) to free cholesterol for P4 steroidogenesis (Singh and Cuervo, 2012; Wang, 2016; Talbott and Davis, 2017; Talbott *et al.*, 2020). Activated lipid droplet

(LD) reserves in luteal cells are primarily responsible for the homeostasis of the cholesterol needed for progesterone synthesis (Talbott *et al.*, 2020). Transport of cholesterol from the outer to the inner mitochondrial membrane for P4 steroidogenesis is the rate-limiting step carried out by steroidogenic acute regulatory protein (StAR) (Christenson and Devoto, 2003; Manna, Dyson and Stocco, 2009). P450 side chain cleavage (P450SCC/CYP11A1) converts cholesterol to pregnenolone on the inner mitochondrial membrane, and 3β-hydroxysteroid dehydrogenase (3β-HSD) then converts pregnenolone to P4 in the smooth endoplasmic reticulum (SER) (Christenson and Devoto, 2003). Serum P4 levels increase with CL development and reach a plateau by 3.5 days post coitum (D3.5, embryo implantation initiates ~D4.0 in mice) in mice to support early pregnancy events, such as preimplantation embryo transport from the oviduct to the uterus and establishment of uterine receptivity for embryo implantation (Ye, 2020). Progesterone autocrine action on luteal cells increases availability of progesterone (through downregulation of 20aHSD) and prevents luteal cell apoptosis. However, these actions are mediated through nontraditional steroid receptor actions and the exact mechanisms are still being investigated (Stocco, Telleria and Gibori, 2007; Z. Wang *et al.*, 2019). If pregnancy does not occur, such as during pseudopregnancy, the CL will undergo luteal regression, which is marked by structural and functional degradation of the CL, such as lipid droplet accumulation in luteal cells, luteal cell death, and a sharp drop in serum P4. Leutolysis is the regulated degradation of the CL following the end of gestation or absence of fertilization, and composed of the function and structural regression (Stocco, Telleria and Gibori, 2007; Hennebold, 2018; Pate, 2018). The functional regression happens earlier in luteolysis as progesterone cessation is critical for parturition. Prostaglandin F2 alpha (PGF2alpha), from the uterus and lesser extent the CL itself, is the primary effector protein needed to reduce progesterone levels and alter luteal cell signaling mechanisms (Stocco, Djiane and Gibori, 2003;

Stocco, Telleria and Gibori, 2007). PGF2alpha stimulates increased luteal 20alphaHSD production, causing the immediate metabolism of produced progesterone into its inactive form, 20alpha-dihydroprogesterone (20alphaDHP). The molecular effects of the relationship between *Prl* support of CL and PGF2alpha luteolysis are summarized in Figure 1.7 (Stocco, Telleria and Gibori, 2007). It is hypothesized that factors related to the functional luteolysis lead to stress-induced activation of apoptosis in luteal cell leading to structural luteolysis. Structural luteolysis is regulated through apoptosis of luteal and endothelial cells culminating in the corpus albicans, a scar present in the ovarian interstitium. Sustained PGF2a along with molecular cues from *Prl* activation of immune cell invasion lead to the breakdown of ECM and apoptosis of endothelial and luteal cells. Reduced availability of cholesterol substrate, through increased accumulation into lipid droplets (LDs), might reduce free cholesterols ability to sequester reactive oxygen species (ROSs) and aid in activation of apoptotic pathways (Pate, 2018). While the exact mechanism surrounding luteolysis are still unknown, the current understanding is that: PGF2a induces 20aHSD leading to a reduction in progesterone which facilitates the expression of Fas receptor (FasR), increasing immune cell invasion and activation of apoptosis.

Uterus, uterine receptivity, and decidualization

Currently, the uterus is the only site for the maturation of an embryo to term and represents the site of pregnancy. Upon ovulation of an egg, fertilization in the oviduct, and formation of the CL, a competent embryo will implant into the receptive uterus. After implantation, molecular signals from the embryo, uterus, and ovaries initiate decidualization which will eventually lead to placentation.

The mouse uterus is a bicornuate uterus, with two horns that eventually connect at the cervix, while the human uterus is a singular uterine body (comparison of Figure 1.1 and Figure

1.8). Besides the ovary, the mouse female reproductive tract forms from the Müllerian ducts early in development. The uterus is initially composed of a lumen lined with epithelial cells that surround the undifferentiated mesenchyme (Vue *et al.*, 2018). The endometrium, myometrium, and perimetrium are fully developed postnatally (in rodents) by radial patterning morphogenesis. The endometrium is composed of two different epithelial layers, the luminal and glandular epithelium (LE and GE, respectively), as well as two stratified stromal areas including a stromal zone, blood vessels, and immune cells (Figure 1.8). The GE develop in an initially ovarian steroid-independent mechanism, but can be susceptible to programming by hormones and EDCs (Kelleher, DeMayo and Spencer, 2019). The myometrium is the smooth muscle layer composed of an inner circular layer and outer longitudinal layer (Figure 1.8). Similarly, in humans the myometrium surrounds the endometrium, which contains LE and GE. The uterus is responsive to ovarian hormones E2 and P4. In humans, hormones regulate the uterine aspects of the menstrual cycle, while in mice, it regulates aspects of the 4-5 day estrous cycle (proestrus, estrus, metestrus, and diestrus) (Figure 1.8). The ratio of P4 and E2 drive specific local actions in the uterus (Figure 1.9), including specific transcription, protein synthesis and secretion, fluid accumulation, uterine elongation and thickness, and effects on the LE and GE. Ovulation (D 0.0) begins the early pregnancy timeline, with fertilization happening shortly after (D 0.5), followed by embryo development and transport (D 1.0-3.0), entrance in the uterus (D 3.5), implantation (D 4.0), and decidualization (d 4.25-9.5) (Kojima, Tam and Tam, 2014; Xiao, Li, *et al.*, 2017; Ye, 2020). Implantation occurs during the window of implantation (WOI) when a competent blastocysts initiates contact with the uterine luminal epithelium during the receptive phase, but not the pre-receptive or refractory phases (Figure 1.10). Much of our knowledge on implantation comes from mouse studies. These events are under specific control by ovarian hormones P4 and E2 and represent a sensitive window and it

is estimated that 75% of failed pregnancy could be due to implantation defects (Dey *et al.*, 2004; Cha *et al.*, 2018; Lu, Kong and Wang, 2018; W. Wang *et al.*, 2019). In mice, the preovulatory transient surge of estrogen induces LE proliferation. Around D1.5 as the CL becomes functional, P4 production increases and plateaus around D3.5 leading to stromal cell proliferation. On the morning of D3.5 there is a nidatory spike in estrogen that primes the uterus and initiates the WOI (Chen *et al.*, 2000; Dey and Lim, 2006; Ye, 2020). While uterine preparation for receptivity, through actions from P4 and E2 (PRa and ERa, respectively (Figure 1.9)), has dynamic, specific and temporal expression of genes intended to prepare the uterus for implantation and pregnancy establishment, other molecular and structural events occur as well (Figure 1.9) (Haibin Wang and Dey, 2006; Herington *et al.*, 2016; Koot *et al.*, 2016; Zhang *et al.*, 2018; W. Wang *et al.*, 2019; Ye, 2020). Mouse knockout models suggest there are a subset of genes that are absolutely critical for implantation and uterine receptivity, such as *Hoxa10/11*, *Pra*, *Lif* (Lee *et al.*, 2007). Mucin type 1 (Muc1), a mucin-type glycoprotein located on the apical membrane of the LE, is significantly downregulated (through PRalpha) at the implantation site and critical for uterine receptivity (Lu, Kong and Wang, 2018). While PRalpha has significant regulatory effect on implantation, proper implantation needs dramatic removal of PRalpha from the LE to occur (Diao *et al.*, 2011; Wetendorf *et al.*, 2017). Uterine GE will sequester at the site of implantation and are responsible for transporting Lif into the uterine lumen, a step needed for successful implantation (Goad *et al.*, 2017; Kelleher, DeMayo and Spencer, 2019). Structural changes in the uterus during the preparation for uterine receptivity are also under the control of ovarian hormones and include edema to facilitate luminal closure and changes to the LE shape and structure, including removal and reestablishment of microvilli (Lu, Kong and Wang, 2018). Sometime around 1200-2200 on D3.5 the blastocyst will initiate contact with the uterine luminal epithelium (anti-mesometrial side)

and the LE begins to evaginate the blastocyst, forming the implantation crypt (Ramathal *et al.*, 2010; Cha *et al.*, 2018). The trophectoderm of the blastocyst will begin penetrating the luminal epithelium, as the LE basal layer dissolves, and invade towards the stromal layer, depending on the species this invasion can be shallow or invasive (Figure 1.11). Between 0400-0600 on D4.5, the underlying stromal region will begin decidualization, but the full extent will not occur until the trophectoderm cells engulf the LE cells in contact with the blastocyst. Decidualization, also under strict regulation by ovarian hormones (particularly P4), is a series of changes to the underlying fibroblastic stromal cell population into decidual cells and the formation of the decidua. Decidual cells, are binucleated, large, and round cells that surround the implantation crypt and proliferate extensively (Ramathal *et al.*, 2010; Matsumoto, 2017). Decidualization in humans occurs as natural part the menstrual cycle during the secretory phase, while in mice it must be stimulated by either an embryo, oil droplet, or pinch during the WOI. However key molecular events in the LE, GE and stroma are similar between the two species (Matsumoto, 2017). Decidual cells excrete growth factors and cytokines that support implantation events, as well as support the formation of the vasculature that invades towards the implantation crypt from the mesometrial side (Figure 1.12) (Lim and Wang, 2010). As early as D4.5, vascularization of the implantation site is already visible using absorbable dyes like Evan's blue dye (Cha *et al.*, 2018). Significant upregulation PRL and insulin-like growth factor binding protein-1 (IGFBP-1) are important factors secreted by the decidual cells, however other distinct gene expression of decidual cells in the primary decidual zone (PDZ) have recently been described (Ramathal *et al.*, 2010; Zhao, Zhang and Liu, 2017). Around D7.5, placentation begins signaling an eventual end to the life cycle of the decidual cells as they undergo apoptosis to ensure placental expansion and development can occur. Generation of the placenta marks the end to the early pregnancy and entrance into later stages of pregnancy,

where events during early pregnancy can have a lasting impact (H Wang and Dey, 2006; Matsumoto, 2017; Cha *et al.*, 2018; Lu, Kong and Wang, 2018).

Doxorubicin, oncofertility, and female reproduction

Cancer incidence among adolescents and young adults (AYA) has steadily risen, with a corresponding decrease in cancer deaths of these patients (Bleyer *et al.*, 2017; Miller *et al.*, 2020). It is estimated that about 100,000 children, adolescent and young adults will be diagnosed with cancer in 2021 and the incidence rates among female patients is outpacing that of their male counterparts (Henley *et al.*, 2020). A particular concern for younger cancer patients is the prominent gonadotoxcity of cancer therapies, such as radiotherapy and chemotherapy (Levine, 2012; Massarotti *et al.*, 2019; Allen *et al.*, 2020; Szymanska, Tan and Oktay, 2020). The field of oncofertility, first coined in 2006 by Dr. T. Woodruff, has quickly aimed to fill the gap in our understanding of methods to preserve fertility in young cancer patients (Levine, 2012; Tomao *et al.*, 2016; Anazodo *et al.*, 2018; Harada and Osuga, 2018; Moravek *et al.*, 2019). The female reproductive tract relies on coordination between multiple organs to facilitate fertility, in which the ovaries, the Fallopian tubes (oviducts in mice), and the uterus are the physical sites for supporting pregnancy events. In premenopausal cancer patients, gonadotoxic trauma can lead to fertility impairment (Green, Sklar and Boice, 2009; Chow *et al.*, 2016). Specifically, special focus has been given to the mechanistic understanding of follicle loss associated with chemotherapy treatment. Phase III drug transporter, multidrug resistance protein 1 (MDR1), the DNA damage-Tap63alpha-C-CASP3 pathway and PI3K signaling all play important roles in mediating DOX effects on primordial follicles. While it has also been shown that DOX can disrupt growing follicles, disruptions to the primordial follicle reserves can lead to detrimental effects to fertility later in life (Ben-Aharon *et al.*, 2010; Xiao, Zhang, *et al.*, 2017; Wang *et al.*, 2018; Y. Wang *et al.*,

2019; Szymanska, Tan and Oktay, 2020). The significant focus on mechanisms surrounding follicular toxicity has left a gap in our understanding of the effects in the CL. Granulosa and theca cells are undergoing rapid differentiation and exposure of uncoiled DNA, like during differentiation, to DOX represent a potential sensitive timepoint for DOX. DOX has been shown to disrupt DNA transcription through interactions with DNA, topoisomerase, and RNA polymerase (Figure 1.13) (Yang *et al.*, 2014; Shrestha *et al.*, 2019). DOX has been shown to target other steroidal tissues, like the testes (Das *et al.*, 2011; Ujah *et al.*, 2021). The CL is highly vascularized with endothelial cells roughly equaling the number of luteal cells (Stocco, Telleria and Gibori, 2007). Extensive research both in-vitro and in-vivo show mechanisms associated with DOX-induced apoptosis and damage to endothelial cells (Kotamraju *et al.*, 2000a; Luu *et al.*, 2018; Clayton *et al.*, 2020; Luu *et al.*, 2021). These data suggest that the CL could be a prime target of DOX. While little research on the DOX actions against the CL exist, significant research has been highlighted on DOX effects on follicles; nevertheless, the attention has been on the ovary. Little attention has been given to assessing potential effects in disrupting uterine functions despite epidemiological data suggesting that the uterus could be a target of certain chemotherapy regiments (Griffiths, Winship and Hutt, 2020). The uterus is critical for fertility preservation methods, like *in-vitro* fertilization and embryo transfer (IVF-ET), as the embryo must be returned to the uterus for pregnancy to occur (Dekel *et al.*, 2014). This has left a significant knowledge gap in our understanding of the effect's chemotherapy can have on uterine function, like implantation and menstruation in women. Limited epidemiological data suggests that patients who were treated with chemotherapy and radiotherapy have increased incidence of preterm birth and low birth weight infants even when donor oocytes are used, suggesting that off-target effects in the uterus could alter functions related to pregnancy (Griffiths, Winship and Hutt, 2020). Little data exists

with a targeted, *in-vivo* analysis of long-term consequences from chemotherapy treatment during comparable AYA years in rodents (Griffiths, Winship and Hutt, 2020). Sensitive windows during important steps in female reproductive health, such as CL formation or the WOI, are potential targets of chemotherapy and further *in-vivo* research is needed to understand how that effects reproductive health.

Doxorubicin (DOX, Adriamycin, a cytotoxic anthracycline antibiotic) is a commonly-prescribed, broad-spectrum anthracycline chemotherapy (Krischke *et al.*, 2016; Iwamoto *et al.*, 2020). DOX is often prescribed as a part of combination therapies, like AC (Adriamycin and cyclophosphamide) in multiple treatment cycles. The label recommended dosage is a 60 mg/m2 (~20 mg/kg in mice) i.v. bolus on day 1 or each 21-day cycle, for a total of four cycles. DOX is listed as a topoisomerase inhibitor, suggesting that it prevents the availability of uncoiled DNA for replication needed in malignant cancer cells, as well as interactions with topoisomerase that lead to DNA-cleavable complexes that promote cytotoxicity. However, multiple mechanisms of action have become evident in years following initial studies. DOX has been shown to directly bind to nucleotides which prevent DNA/RNA polymerases further aiding in the primary mechanism of action. DOX can also bind to cell membrane lipids to play an important role in cell death (Thorn *et al.*, 2011; FDA, 2013; Wei *et al.*, 2015). DOX chemotherapy increases the risk for cardiovascular diseases, which could be partially contributed by oxidative stress-induced endothelial dysfunction in the conduit arteries (Clayton *et al.*, 2020). Other mechanisms include lipid peroxidation, ROS generation, mitochondrial damage, and membrane damage. Cisplatin is a platinum containing chemotherapeutic that also exhibits direct DNA intercalation as a major mechanism of action. Cyclophosphamide, an alkylating chemotherapeutic, can cause alkylation of DNA and is normally prescribed in tandem with DOX. Both Cisplatin and Cyclophosphamide

represent other commonly prescribed chemotherapeutic drugs that should be included in any risk-assessment of chemotherapeutic drug exposure. DOX is a commonly prescribed chemotherapeutic drug which has been shown to target ovarian follicles and steroidogenic cells, as well as inhibits transcriptional processes, making it a potential disruptor of CL development. Since off target effects of DOX exists, it is important to understand how those could present themselves in uterine health.

Understanding the potential for chemotherapeutic drugs to target the uterus requires careful experimental design. Uterine health and function rely on hormonal support from the ovaries. Follicles and the corpus luteum provide necessary progesterone and estradiol to support uterine gene regulation and important signaling events that aid in various uterine functions (H Wang and Dey, 2006; Diao *et al.*, 2011; S. Zhang *et al.*, 2013; Diao *et al.*, 2015; Hewitt, Winuthayanon and Korach, 2016; Soleilhavoup *et al.*, 2016). Little *in-vivo* data on the ability for chemotherapeutic drugs to alter uterine mechanisms and functions exist (Nishi *et al.*, 2018; Samare-Najaf, Zal and Safari, 2020). However, both the studies left the ovaries intact during chemotherapy treatment, creating a confounding effect between known gonadotoxcity and downstream effects seen in the uterus. Any conclusion made on changes to molecular mechanisms regulating uterine function cannot be explicitly tied to chemotherapy treatment, furthering the knowledge gap in this field. Nishi *et al.* also had extensive differences in animal weight, an important factor in understanding the individual variations involved in absorption, deposition, metabolism and excretion of chemotherapeutic drugs, specifically DOX (Rodvold, Rushing and Tewksbury, 1988; Gurney, 2002). Using ovareictomized mice to control for confounding effects, we showed that a human relevant (10 mg/kg bw I.P.) dose of DOX changed the uterine response to estrogen 1 month after treatment (Andersen *et al.*, 2019). While highlighted as the only *in-vivo* data to unequivocally

show that DOX can target the uterus and alter mechanism associated with uterine function, this preliminary research did not include the uterine response to both estrogen and progesterone, a critical omission (Griffiths, Winship and Hutt, 2020). Progesterone is needed for the full extent of estrogen action to occur in the uterus (Wetendorf and DeMayo, 2012). Proper estrogen and progesterone signaling is critical for implantation in both humans and mice, as well as key in proper regulation of the endometrium during estrous and menstrual cycles (Dey and Lim, 2006; Nowak, 2018).

Hypothesis and specific aims

Millions of prepubescent girls and reproductive aged women suffer from cancers. A unique side effect of concern from anti-cancer treatments, including chemotherapy and radiotherapy, in premenopausal cancer patients is fertility impairment. Oncofertility thus becomes an emerging discipline with the expressed goal to protect the future reproductive health of cancer patients. Female fertility depends on a functional female reproductive system, in which the ovaries, the Fallopian tubes (oviducts in mice), and the uterus are the physical sites for supporting pregnancy events, from oocyte production in the ovary, to fertilization in the Fallopian tubes as well as early embryo development and transport in both Fallopian tubes and uterus, to embryo implantation and post-implantation embryo/fetus development in the uterus. Because of the prominent gonadotoxicities of many oncologic treatments, the research in oncofertility has been mainly focused on the ovarian follicles. In addition to the follicles that produce oocytes to initiate a pregnancy, the ovary also has the CL for producing P4 to support early pregnancy events, from preimplantation embryo development and transport to embryo implantation. The CL is a temporary endocrine gland normally developed from an ovulated follicle. It has three main stages during its life span: development, maintenance, and regression. The two main cell types in the CL are luteal

cells and endothelial cells. Luteal cells differentiate from granulosa and theca cells of the follicle, undergoing massive alterations to gene expression (Romereim *et al.*, 2017b). Endothelial cells have been shown to be target by chemotherapy to undergo apoptosis. Doxorubicin is a commonly used chemotherapeutic agent in premenopausal cancer patients. DOX has previously been shown to target ovarian follicles, however no data exists on its function on the corpus luteum. Furthermore, the main focus of oncofertility have been on the gonadotoxic effects, which only represents one aspect of female reproductive health and fertility. Little information on uterine defects exist, information available left ovaries intact creating a confounding variable in the understanding of potential alterations to molecular mechanisms that drive uterine function. Recently epidemiologic data has been reviewed indicating potential disruptions to uterine health and pregnancy outcomes in patients prescribed chemotherapeutic drugs. No targeted, *in-vivo* data on direct chemotherapy actions in the uterus currently exists. Together, these knowledge gaps represent a glaring omission in the field of oncofertility and the research proposed in this dissertation aim to fill those gaps.

Our *long-term goal* is to understand mechanisms of chemotherapy action affecting female fertility. The *objective* of this dissertation research is to determine cellular and molecular effects of chemotherapy on corpus luteum and uterine functions. My *central hypothesis* is that DOX affects corpus luteum function, through aberrations of luteal and endothelial cell functions, and affects ovarian hormone signaling in the uterus, disrupting mechanisms needed for uterine receptivity.

Aim 1. Test the hypothesis that DOX affects corpus luteum function through aberrations of luteal and endothelial cell functions.

It is based on preliminary data that DOX exposure causes disruptions to ovarian size and weight, as well as directly disrupts ovarian follicle development and targets primordial follicles for apoptosis. DOX has also been shown to cause apoptosis to endothelial cells, which roughly make up 50% of the corpus luteum cell population and support functions related to corpus luteum function. Key aspects related to luteal and endothelial cell function, such as steroidogenesis and microvasculature formation (respectively) were analyzed.

Aim 2. Test the hypothesis that DOX affects ovarian steroid hormone signaling in the uterine transcriptome, resulting in functional changes to uterine receptivity.

It is based on preliminary data that patients treated with chemotherapeutic drugs had decreased uterine fluid volume and thinning uterine lining, as well as data that DOX caused long-term changes to the uterine response to E2 in mice. Artificial decidualization will be used as a marker of uterine receptivity to analyze potential disruptions to embryo implantation. Functional disruptions to uterine receptivity will be investigated by transcriptomic data from hormonally primed uteri.

Expected outcomes from this project will reveal the cellular and molecular effects of DOX (at human relevant levels) on different components of female fertility, the corpus luteum and uterine receptivity. These endeavors are important for understanding the adverse effects and molecular mechanisms of decreased fertility observed in cancer patients and aim to fill knowledge gaps in the field of oncofertility.

FIGURES

Figure 1.1

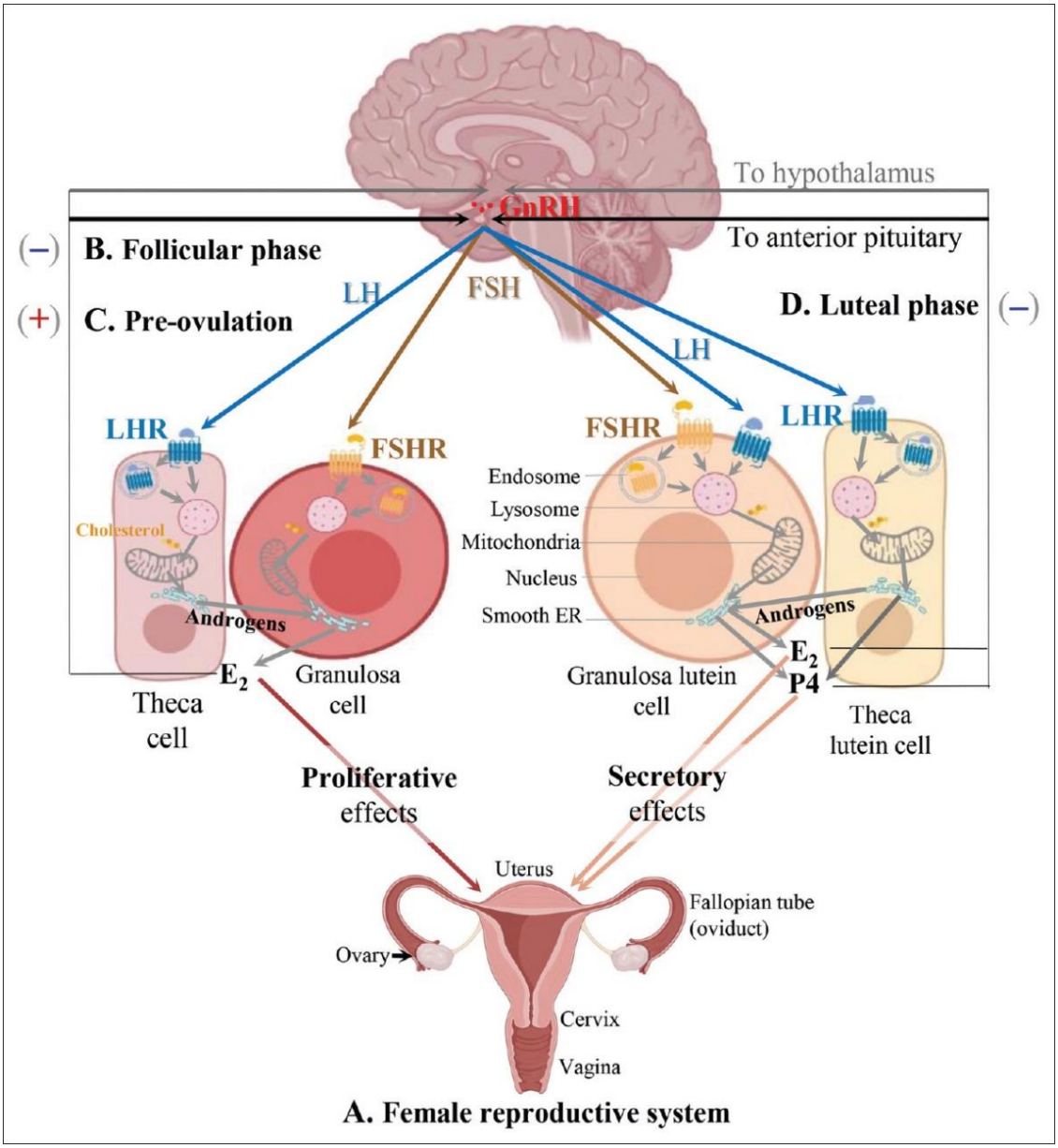

Female reproductive system. Li Yuehuan, Wang Zidao, Andersen Christian L., et al. Functions of Lysosomes in Mammalian Female Reproductive System [J] . Reprod Dev Med,2020,04 (02): 109-122. DOI: 10.4103/2096-2924.288025

Figure 1.2

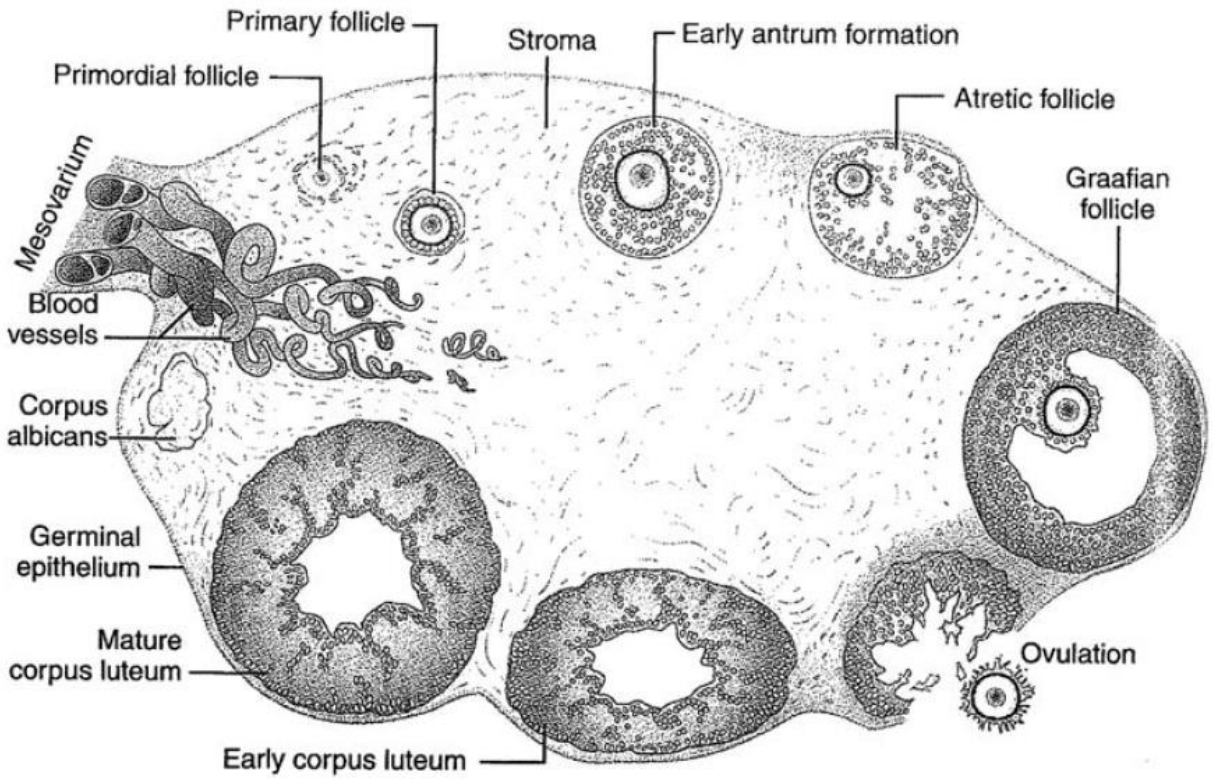

The ovary macrostructure. Bahr, J. M. (2018) 'Ovary, Overview', in Skinner, M. K. B. T.-E. of R. (Second E. (ed.). Oxford: Academic Press, pp. 3–7. doi: https://doi.org/10.1016/B978-0-12-801238-3.64389-1.

Figure 1.3

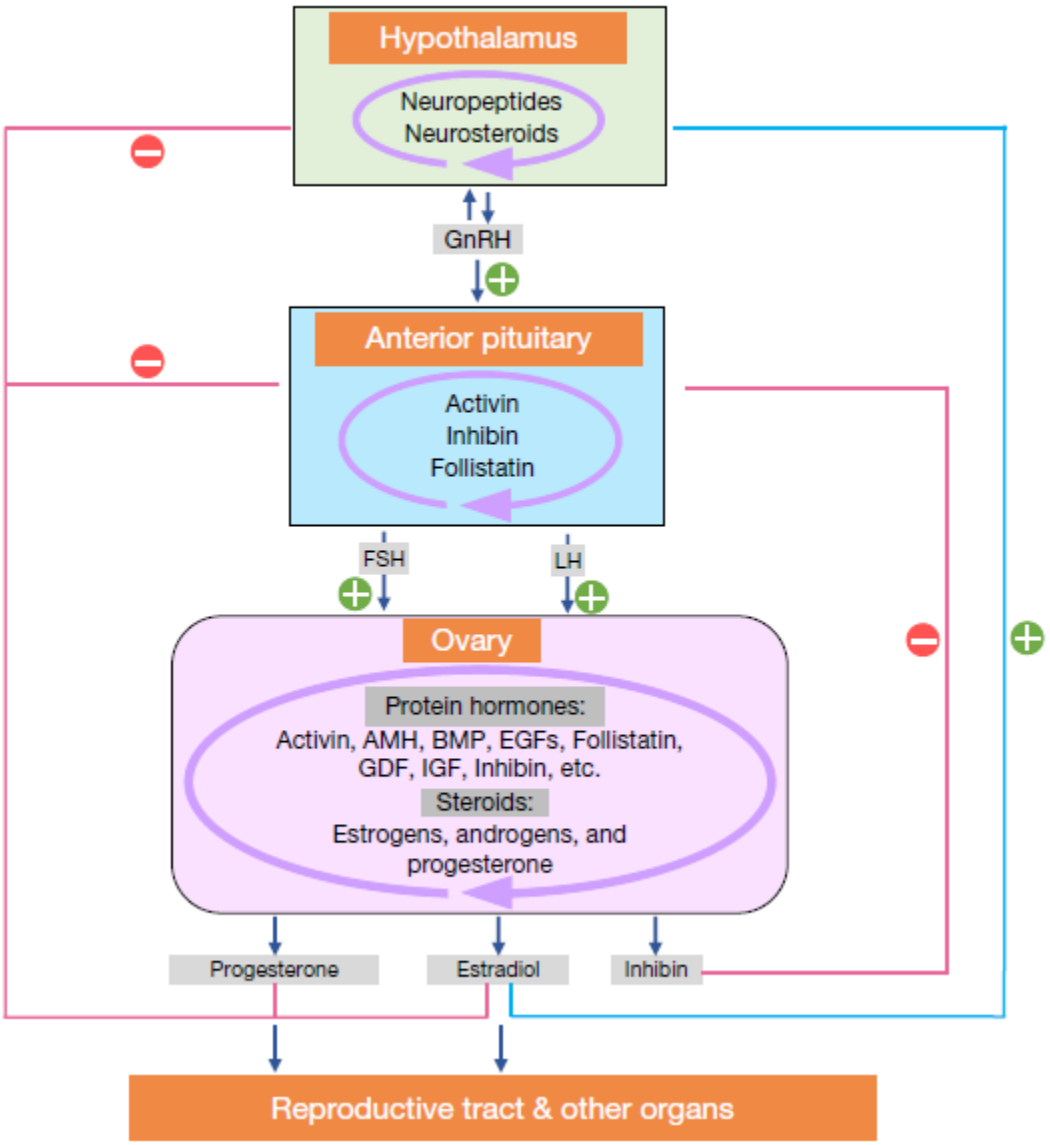

Regulation of HPG axis. Padmanabhan, V., Puttabyatappa, M. and Cardoso, R. C. (2018) 'Hypothalamus–Pituitary–Ovary Axis', in Skinner, M. K. B. T.-E. of R. (Second E. (ed.). Oxford: Academic Press, pp. 121–129. doi: https://doi.org/10.1016/B978-0-12-801238-3.64632-9.

Figure 1.4

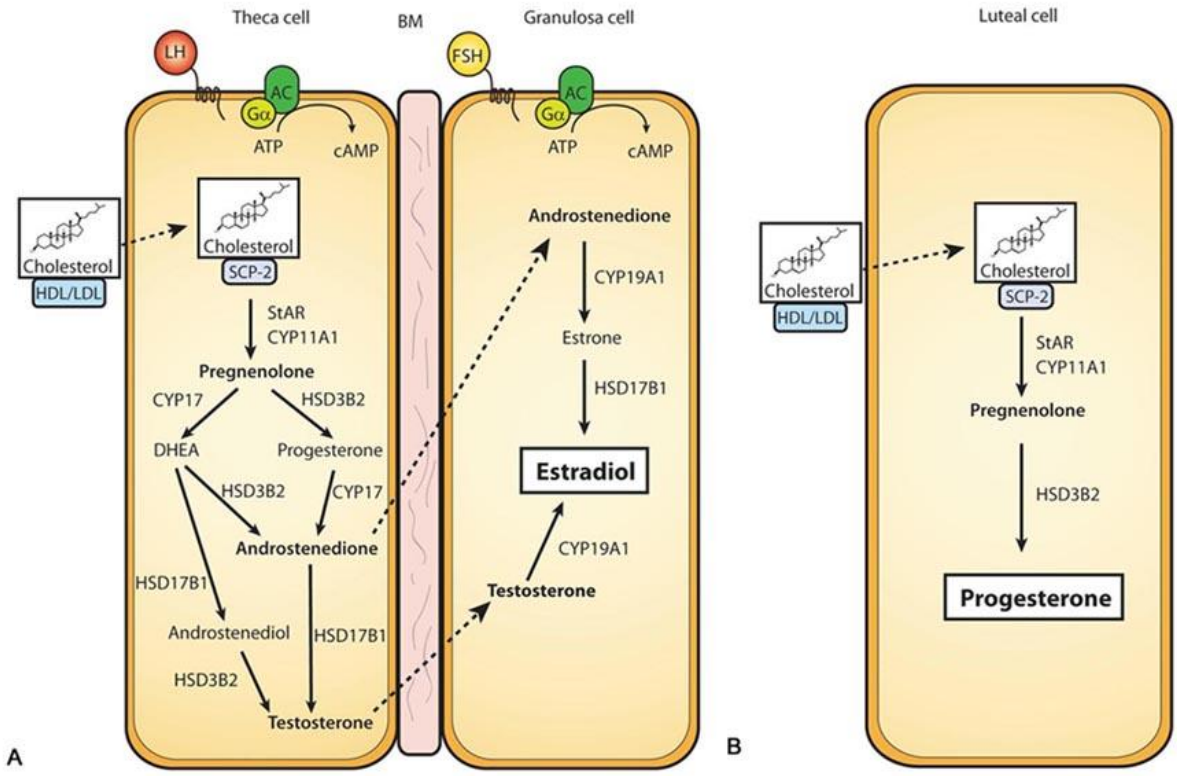

Two-cell, two-gonadotropin model of estrogen synthesis. Holesh JE, Bass AN, Lord M. Physiology, Ovulation. [Updated 2021 May 9]. In: StatPearls [Internet]. Treasure Island (FL): StatPearls Publishing; 2021 Jan-.

Figure 1.5

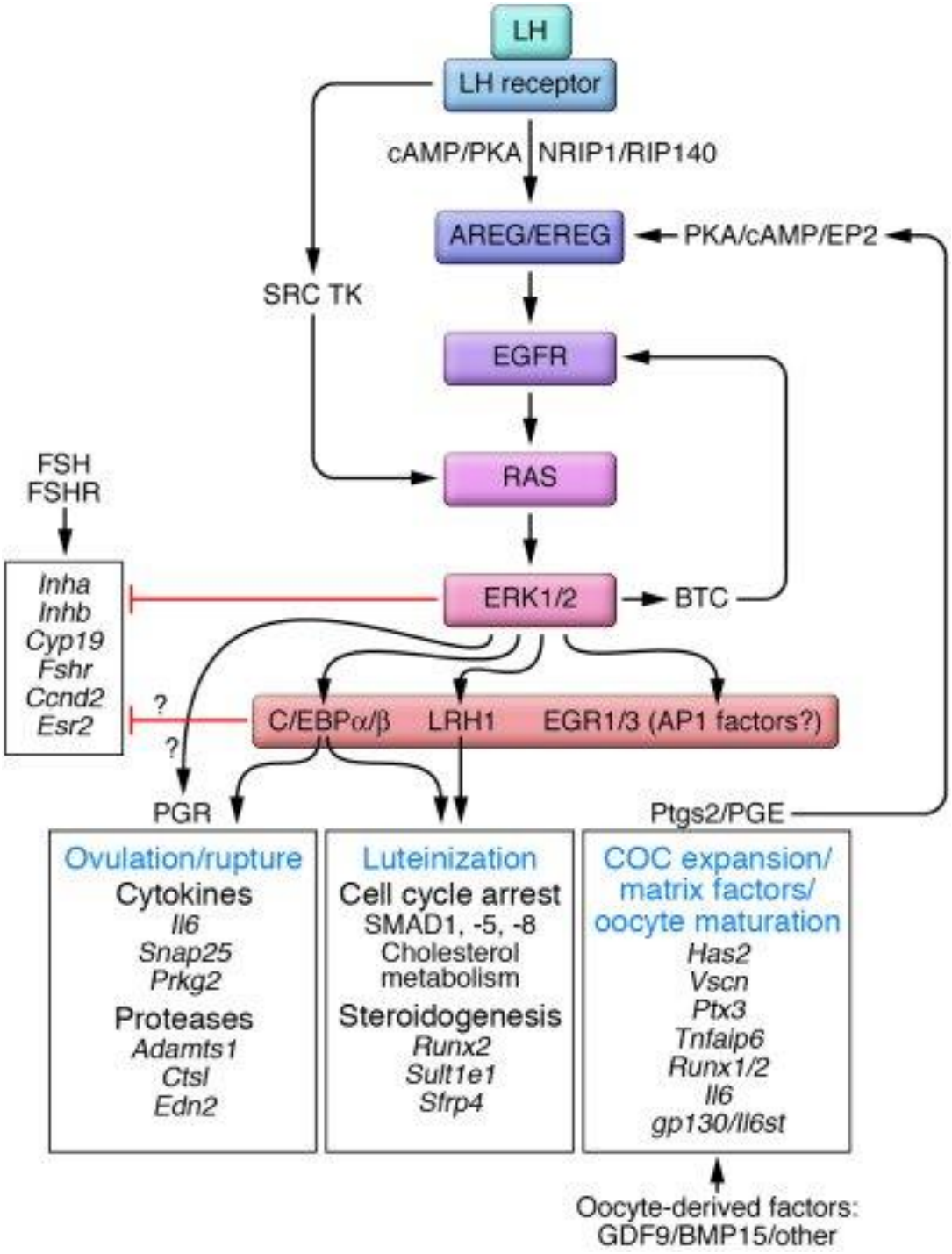

Molecular changes in the ovary during ovulation and luteinization. Richards, J. S. and Pangas, S. A. (2010) 'The ovary: basic biology and clinical implications', The Journal of Clinical Investigation, 120(4), pp. 963–972. doi: 10.1172/JCI41350.

Figure 1.6

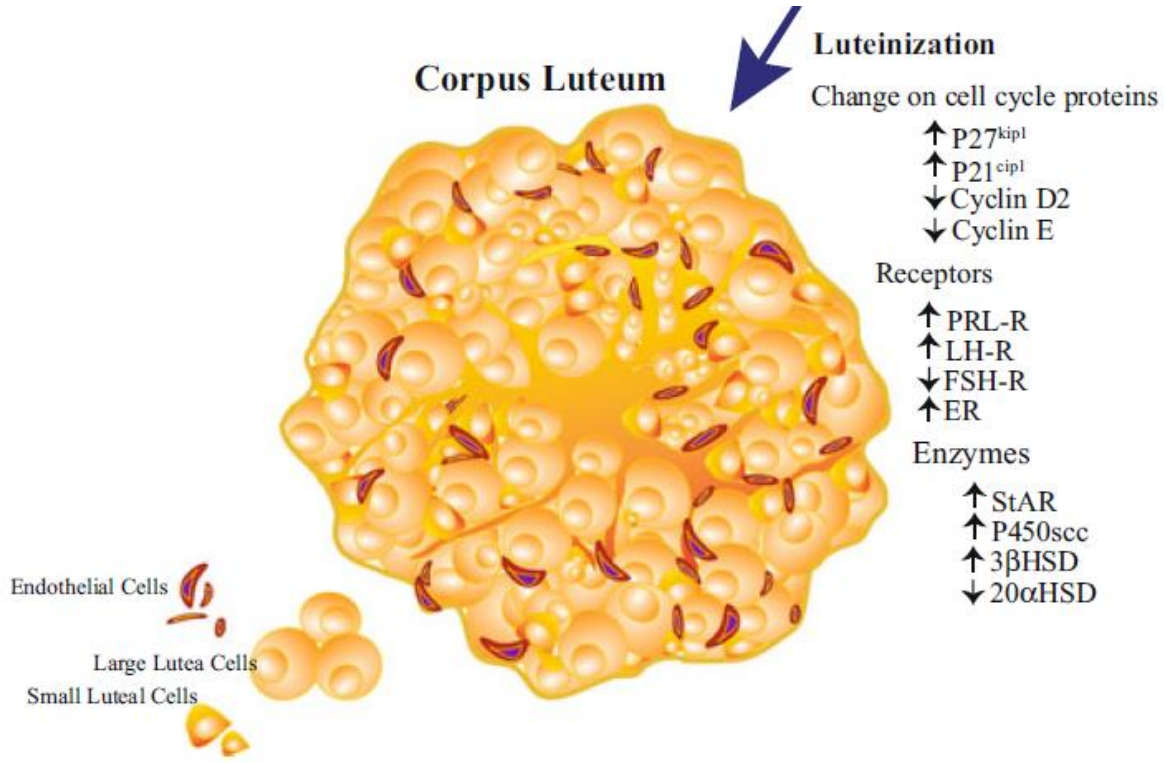

Aspects controlling luteinization, CL development, CL maintenance, CL vascularization, and CL steroidogenesis. Stocco, C., Telleria, C. and Gibori, G. (2007) 'The Molecular Control of Corpus Luteum Formation, Function, and Regression', Endocrine Reviews, 28(1), pp. 117–149. doi: 10.1210/er.2006-0022.

Figure 1.7

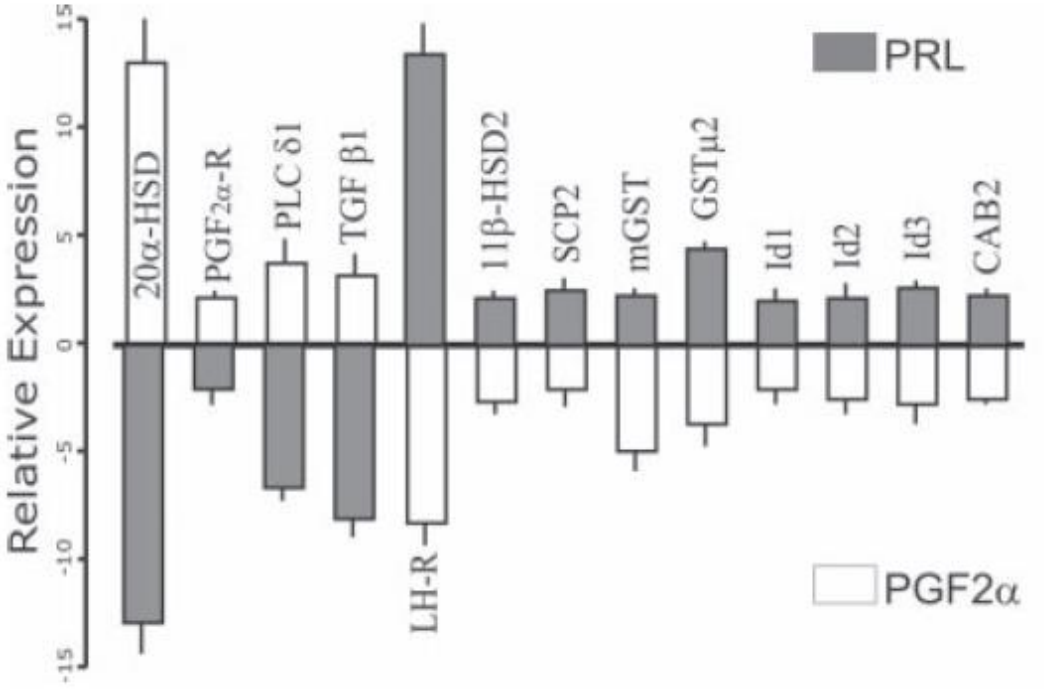

Molecular signals involved in maintenance and regression of the CL. Stocco, C., Telleria, C. and Gibori, G. (2007) 'The Molecular Control of Corpus Luteum Formation, Function, and Regression', Endocrine Reviews, 28(1), pp. 117–149. doi: 10.1210/er.2006-0022.

Figure 1.8

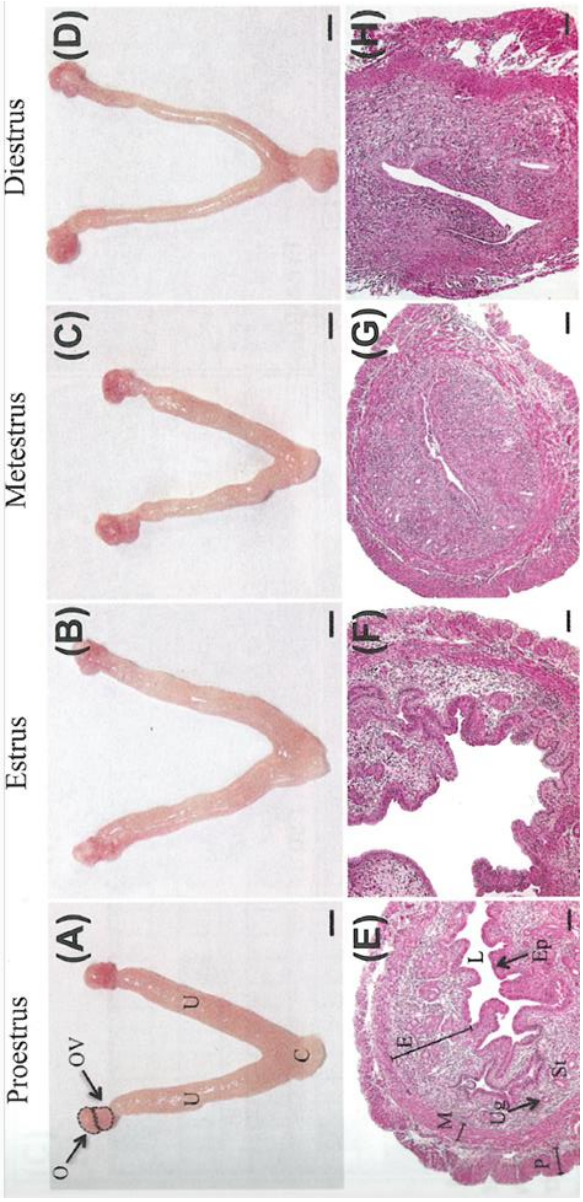

Mouse reproductive tract during different stages of estrus. O, ovary; OV, oviduct; U, uterus; C, cervix; L, lumen; E, endometrium; Ep, luminal epithelium; M, myometrium; Ug, glandular epithelium; St, stroma. Bertolin, K. & Murphy, B. D. 7 - Reproductive Tract Changes During the Mouse Estrous Cycle. in (eds. Croy, B. A., Yamada, A. T., DeMayo, F. J. & Adamson, S. L. B. T.-T. G. to I. of M. P.) 85–94 (Academic Press, 2014). doi:https://doi.org/10.1016/B978-0-12-394445-0.00007-2.

Figure 1.9

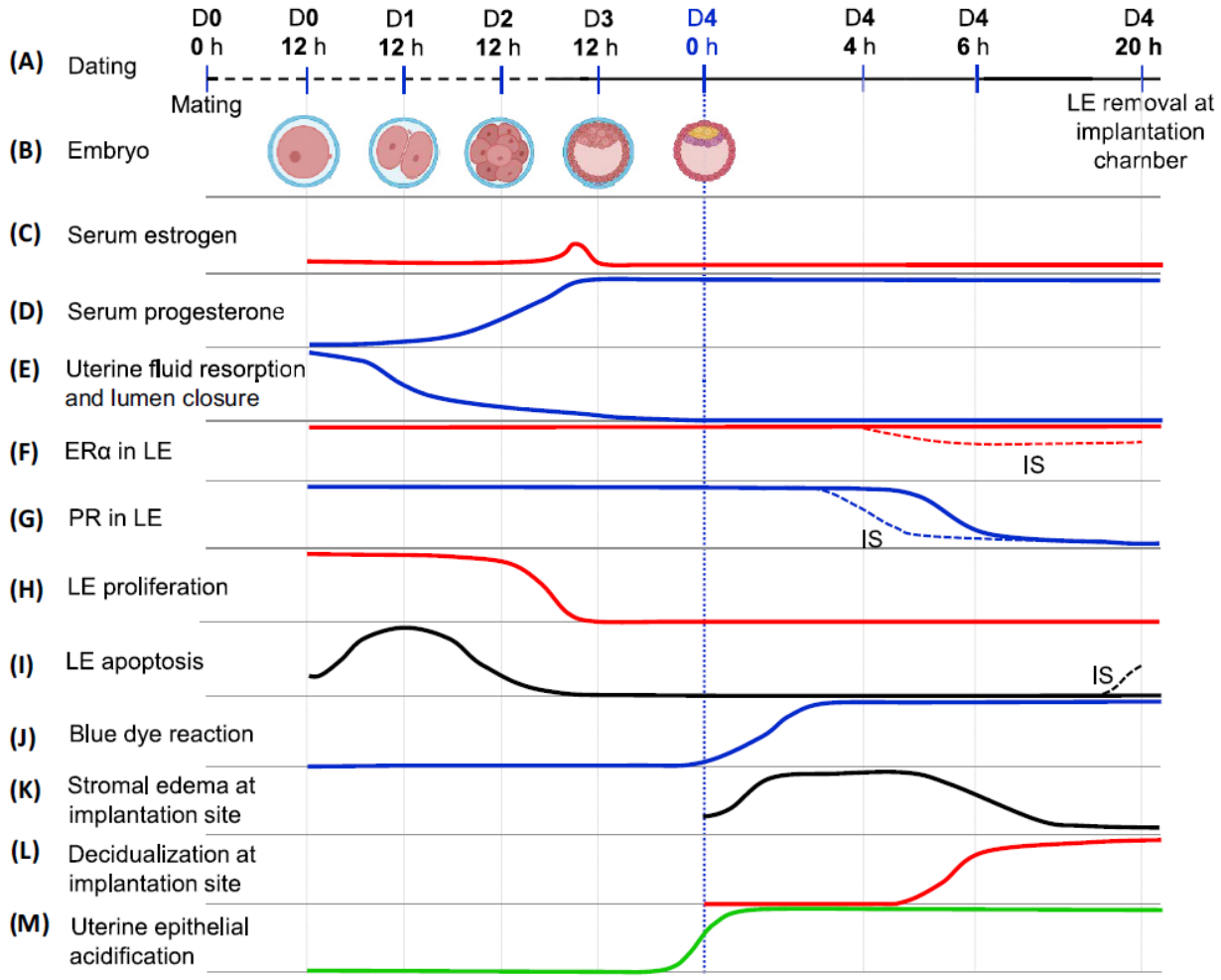

Local event in the uterus during early pregnancy. Ye, X. Uterine Luminal Epithelium as the Transient Gateway for Embryo Implantation. *Trends Endocrinol. Metab.* **31**, 165–180 (2020).

Figure 1.10

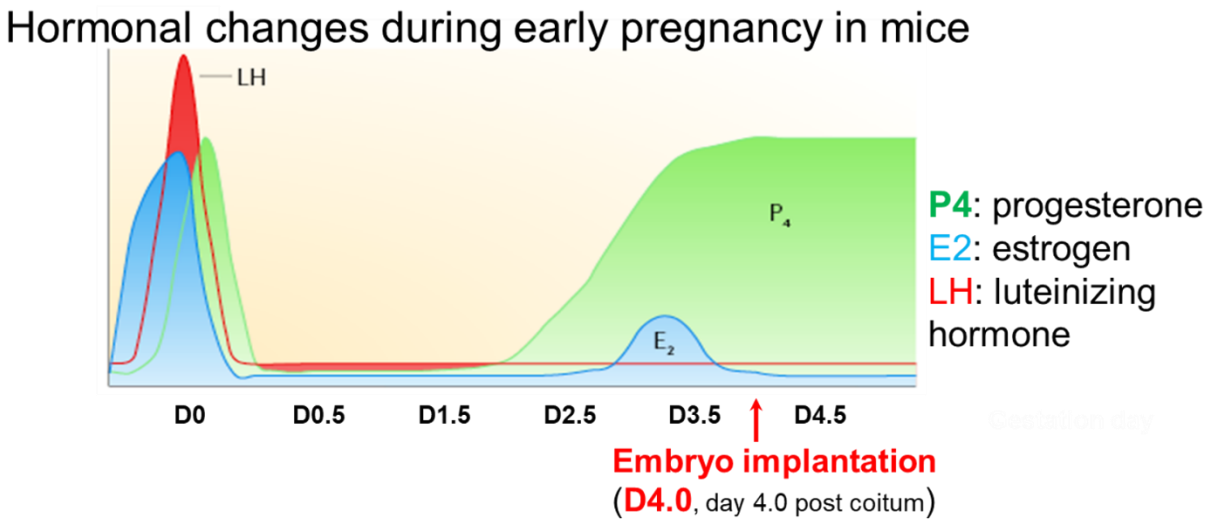

Hormonal regulation and early pregnancy. Window of implantation and receptive period of the uterus highlighted in green. Implantation occurs around D4.0. Modified from Wang, H. & Dey, S. K. Roadmap to embryo implantation: clues from mouse models. Nat. Rev. Genet. 7, 185 (2006).

Figure 1.11

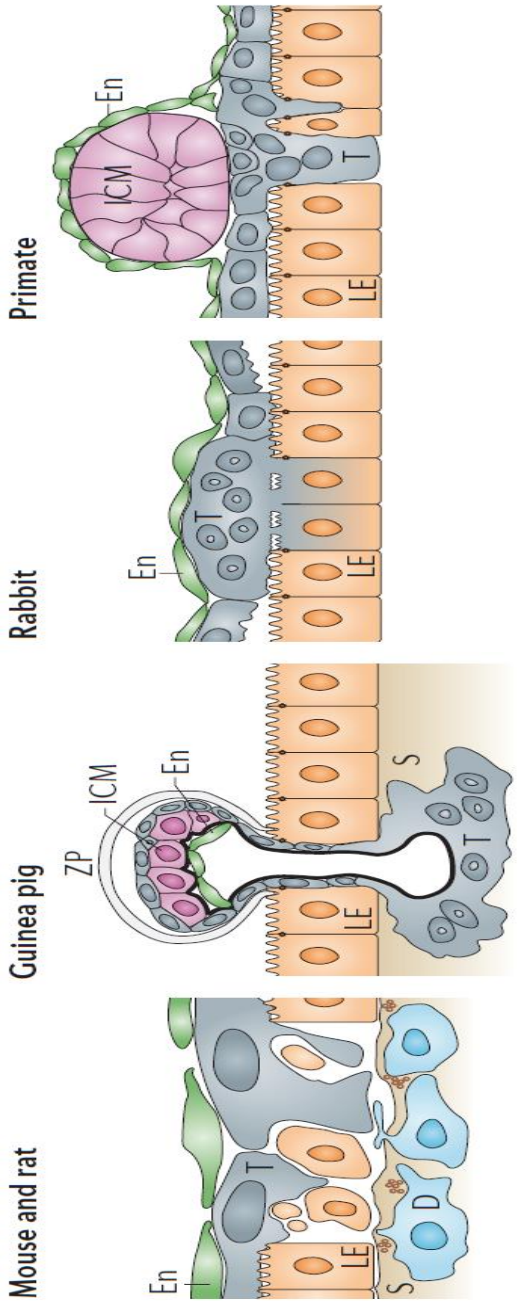

Implantation in different species. T, trophectoderm; LE, luminal epithelium; S, stromal cell; D, decidual cell. Wang, H. & Dey, S. K. Roadmap to embryo implantation: clues from mouse models. Nat. Rev. Genet. 7, 185 (2006).

Figure 1.12

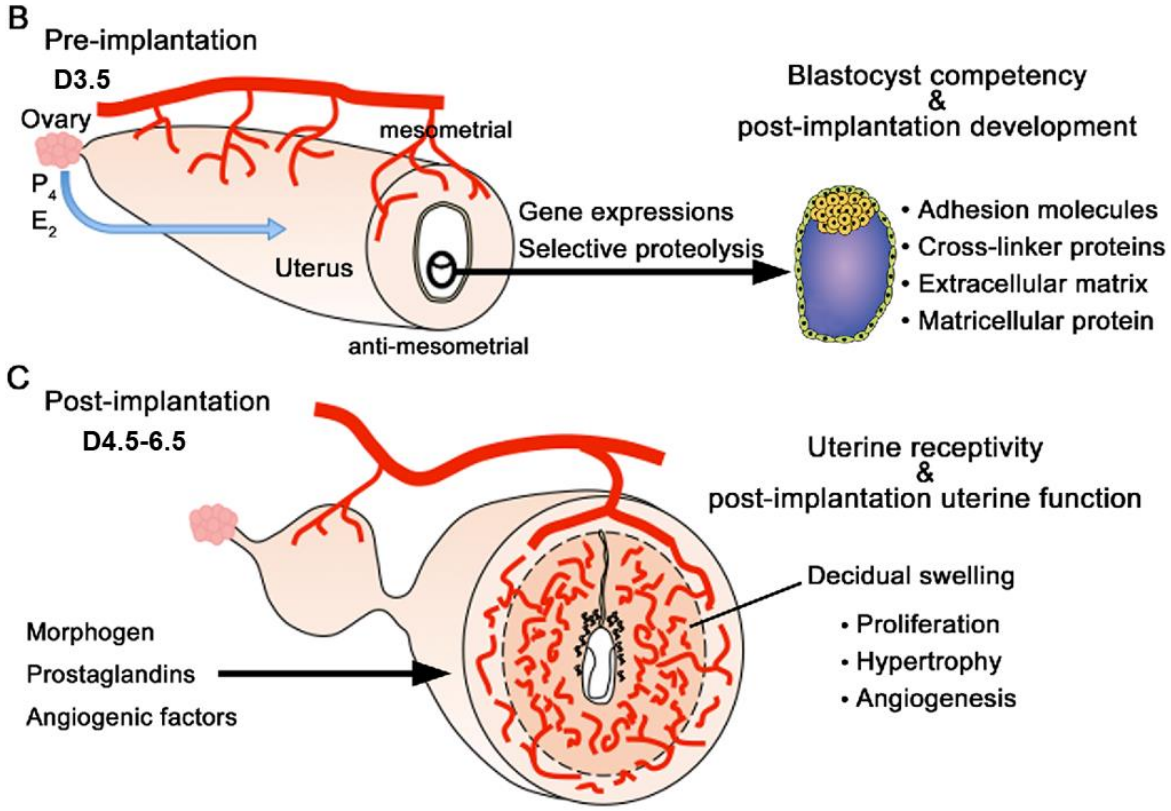

Uterine events during early pregnancy and decidualization. Modified from Matsumoto, H. Molecular and cellular events during blastocyst implantation in the receptive uterus: clues from mouse models. *J. Reprod. Dev.* **63**, 445–454 (2017).

Figure 1.13

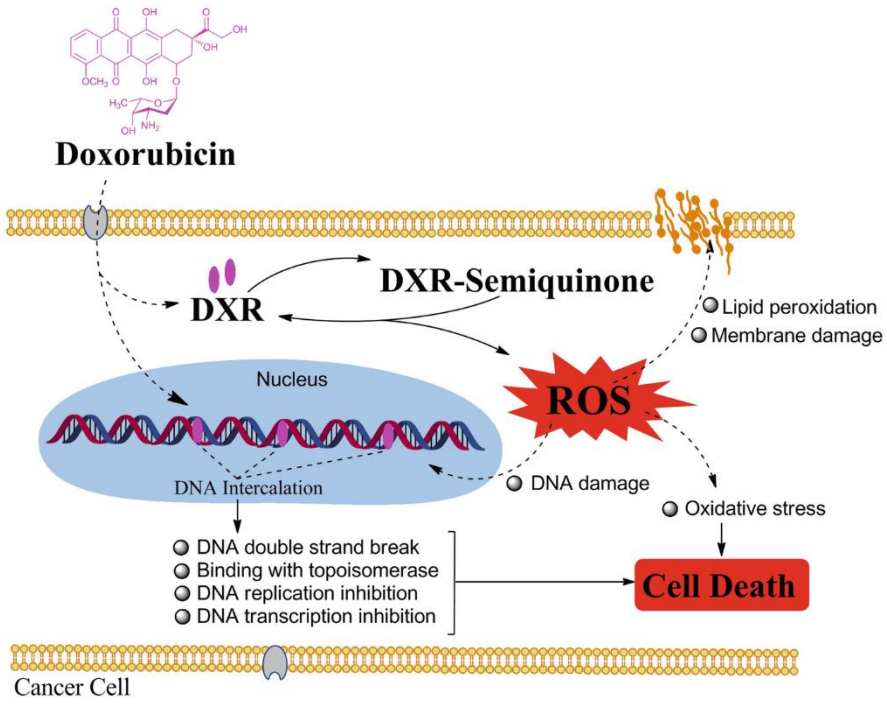

Doxorubicin common mechanisms of action in cancer cell apoptosis. Shrestha, B. *et al.* Engineering Streptomyces peucetius for Doxorubicin and Daunorubicin Biosynthesis BT - Pharmaceuticals from Microbes: The Bioengineering Perspective. in (eds. Arora, D., Sharma, C., Jaglan, S. & Lichtfouse, E.) 191–209 (Springer International Publishing, 2019). doi:10.1007/978-3-030-01881-8_7.

CHAPTER 2

VARIED EFFECTS OF DOXORUBICIN (DOX) ON THE CORPUS LUTEUM OF C57BL/6 MICE DURING EARLY PREGNANCY[1]

[1]Andersen, C.L., Byun, H., Xiao, S., Miller, D., Wang, Z., Li, Y., Viswanathan, S., Hancock, J., Bromfield, J., and Ye, X. 2021. *submitted to Biology of Reproduction*.

Title

Varied effects of doxorubicin (DOX) on the corpus luteum of C57BL/6 mice during early pregnancy

Short title

DOX and corpus luteum

Summary: Chemotherapeutic drug doxorubicin has varied toxic effects on the corpus luteum structure and function during early pregnancy.

Key words

Doxorubicin (DOX), corpus luteum, progesterone, StAR, lipid droplets, F-actin

Christian Lee Andersen[1, 2], Haeyeun Byun[1], Shuo Xiao[3], Doris M Miller[4], Zidao Wang[1,2], Yuehuan Li[1], Suvitha Viswanathan[1], Jonathan Matthew Hancock[1, 2], Jaymie Bromfield[1], and Xiaoqin Ye[1, 2, #]

[1] Department of Physiology and Pharmacology, College of Veterinary Medicine, University of Georgia, Athens, GA 30602, USA; [2] Interdisciplinary Toxicology Program, University of Georgia, Athens, GA 30602, USA; [4] Department of Pharmacology and Toxicology, Ernest Mario School of Pharmacy, Rutgers University, Piscataway, NJ 08854, USA; [4] Department of Pathology, College of Veterinary Medicine, University of Georgia, Athens, GA 30602, USA;

Grant support

R03HD097384 and R03HD100652 (XY)

[#] Corresponding author

Xiaoqin Ye, M.D., Ph.D., 501 DW Brooks Dr., Department of Physiology and Pharmacology, College of Veterinary Medicine; Interdisciplinary Toxicology Program, University of Georgia, Athens, GA 30602, USA (Tel: 1-706-542-6745; E-mail: ye@uga.edu; ORCID: 0000-0002-1037-9005)

Abstract

The corpus luteum (CL) is normally developed from an ovulated follicle to produce progesterone for supporting early pregnancy. Certain chemotherapeutic drugs are toxic to ovarian follicles but their effects in CLs remain largely unknown. We selected doxorubicin (DOX) as a representative chemotherapeutic drug and early pregnancy mice as an *in vivo* model to fill in this knowledge gap. To circumvent secondary effects on CLs from DOX-induced follicular toxicity, mice were given a single intraperitoneal injection of DOX (10 mg/kg) in days 0.5 post coitum (D0.5, post-ovulation). Varied DOX effects on D3.5 serum progesterone levels were observed in both mixed background mice and C57BL/6 mice. Further studies using D3.5 C57BL/6 ovaries revealed that all DOX-treated ovaries had increased follicular granulosa cell death, and lipid droplet accumulation and F-actin disruption in luteal cells. CLs from DOX-treated mice with progesterone deficiency also had less defined luteal cords (surrounded by endothelial cells) and disrupted expression pattern of collagen IV (a marker of basal lamina of endothelial cells), and reduced expression of steroidogenic acute regulatory protein (StAR, for the rate-limiting step of progesterone steroidogenesis in mitochondria) in luteal cells. Reduced StAR expression was not caused by lack of mitochondria but possibly by disrupted mitochondrial functions. These novel data reveal that DOX can target both endothelial cells and luteal cells, the two main cell types in the CL, and that there is varied individual sensitivity of CL to DOX toxicity during early pregnancy. This study provides important information for risk assessment of chemotherapy in female reproduction.

Introduction

Millions of prepubescent girls and reproductive aged women suffer from cancers. A unique side effect of concern from anti-cancer treatments, including chemotherapy and radiotherapy, in premenopausal cancer patients is fertility impairment (Green *et al.*, 2009; Chow *et al.*, 2016). Oncofertility thus becomes an emerging discipline with the expressed goal to protect the future reproductive health of cancer patients (Tomao *et al.*, 2016; Anazodo *et al.*, 2018; Harada and Osuga, 2018). Female fertility depends on a functional female reproductive system, in which the ovaries, the Fallopian tubes (oviducts in mice), and the uterus are the physical sites for supporting pregnancy events, from oocyte production in the ovary, to fertilization in the Fallopian tubes as well as early embryo development and transport in both Fallopian tubes and uterus, to embryo implantation and post-implantation embryo/fetus development in the uterus. Because of the prominent gonadotoxicities of many oncologic treatments, the research in oncofertility has been mainly focused on the ovarian follicles (Xiao, Zhang, *et al.*, 2017; Wang *et al.*, 2018; Winship *et al.*, 2019; Y. Wang *et al.*, 2019; Eldani *et al.*, 2020; Almeida *et al.*, 2021). In addition to the follicles that produce oocytes to initiate a pregnancy, the ovary also has the corpus luteum (CL, pl: corpora lutea) for producing progesterone (P4) to support early pregnancy events, from preimplantation embryo development and transport to embryo implantation (Bazer *et al.*, 2010; C. Zhang *et al.*, 2013; Zhang and Murphy, 2013; El Zowalaty, Li, Zheng, *et al.*, 2017; Z. Wang *et al.*, 2019; Ye, 2020). Any toxic effects of chemotherapy on the CL remain largely unknown.

The CL is a temporary endocrine gland normally developed from an ovulated follicle. It has three main stages during its life span: development, maintenance, and regression. The two main cell types in the CL are luteal cells and endothelial cells (Davis, Rueda and Spanel-Borowski, 2003b). The vasculature in the CL supports luteal cell functions, particularly P4 steroidogenesis

(Christenson and Devoto, 2003; Duffy *et al.*, 2018). The precursor cholesterol for P4 steroidogenesis in luteal cells is mainly imported from the circulation via endocytosis or selective uptake and it has a minor source via *de novo* cholesterol synthesis (Christenson and Devoto, 2003). Cholesterol can be stored in the cytoplasmic lipid droplets as cholesteryl esters, which will undergo hydrolysis via the intracellular neutral hormone-sensitive lipase (HSL, also named cholesteryl ester hydrolase (CEH)) and/or lysosomal acid lipase (LAL) to free cholesterol for P4 steroidogenesis (Singh and Cuervo, 2012; Wang, 2016; Talbott *et al.*, 2020). Transport of cholesterol from the outer to the inner mitochondrial membrane for P4 steroidogenesis is the rate-limiting step carried out by steroidogenic acute regulatory protein (StAR) (Christenson and Devoto, 2003; Manna, Dyson and Stocco, 2009). P450 side chain cleavage (P450SCC/CYP11A1) converts cholesterol to pregnenolone on the inner mitochondrial membrane, and 3β-hydroxysteroid dehydrogenase (3β-HSD) then converts pregnenolone to P4 in the smooth endoplasmic reticulum (SER) (Christenson and Devoto, 2003). P4 steroidogenesis is accompanied by dramatic changes in morphology and numbers of mitochondria and SER complexes (Christenson and Devoto, 2003). Serum P4 levels increase with CL development and reach a plateau by 3.5 days post coitum (D3.5, embryo implantation initiates ~D4.0 in mice) in mice to support early pregnancy events, such as preimplantation embryo transport from the oviduct to the uterus and establishment of uterine receptivity for embryo implantation (Ye, 2020). If pregnancy does not occur, such as during pseudopregnancy, the CL will undergo luteal regression, which is marked by structural and functional degradation of the CL, such as lipid droplet accumulation in luteal cells (Strauss *et al.*, 1977; Lee-Thacker *et al.*, 2018), luteal cell death, and a sharp drop of serum P4 level (Anupriwan *et al.*, 2008).

Doxorubicin (DOX, Adriamycin, a cytotoxic anthracycline antibiotic) is a commonly used chemotherapeutic agent in premenopausal cancer patients (Iwamoto *et al.*, 2020; Johnson-Arbor and Dubey, 2020). Its chemotherapeutic effects on cancer cells may involve different mechanisms, such as intercalation into DNA and disruption of topoisomerase-II-mediated DNA repair, as well as generation of free radicals to damage cellular membranes, DNA, and proteins (Thorn *et al.*, 2011). DOX chemotherapy increases the risk for cardiovascular diseases, which could be partially contributed by oxidative stress-induced endothelial dysfunction in the conduit arteries (Clayton *et al.*, 2020). DOX has toxicities on ovarian follicles in rodents (Xiao, Zhang, *et al.*, 2017; Nishi *et al.*, 2018; Wang *et al.*, 2018; Y. Wang *et al.*, 2019), such as follicular atresia and overactivation (Nishi *et al.*, 2018; Y. Wang *et al.*, 2019), and impaired secretion of 17beta-estradiol (E2) (Xiao, Zhang, *et al.*, 2017), and toxicities of DOX are exacerbated by deficiency of multidrug resistance protein 1 (MDR1) (Wang *et al.*, 2018). The CL is a highly vascularized transient organ in the ovary that could represent a prime target for DOX-induced toxic action. In addition, DOX can target steroidogenic tissues, such as testis (Das *et al.*, 2011; Ujah *et al.*, 2021). We hypothesized that DOX may have toxic effects on the CL. We tested this hypothesis in mice with a focus on parameters related to P4 steroidogenesis during early pregnancy.

Materials and Methods

Animals. In the initial study, mixed background (C57BL/6 and 129/SvJ (Ye *et al.*, 2005)) wild type mice (10-22 weeks old at dissection) that were available in our mouse colony were used. In the second study, C57BL/6 female mice (6 weeks old) were purchased from the Jackson Laboratory (Ellsworth, Maine). They were acclimated to the Coverdell animal facility at the University of Georgia for 2 weeks with body weight monitored twice a week to ensure well acclimation to the new environment. At 8 weeks old, the acclimated females were mated with stud

males and checked for the presence of a vaginal plug (an indication of mating) the following morning. The day of plug detection was designated as 0.5 days post coitum (D0.5). The Coverdell animal facility is on a 12-hour light/dark cycle (6:00 AM to 6:00 PM) at 23 ± 1 °C with 30–50% relative humidity. All mice had free access to regular chow 5053 (Labdiet, St. Louis, MO, USA) and water. All methods used in this study were approved by the University of Georgia IACUC Committee (Institutional Animal Care and Use Committee) and conform to National Institutes of Health guidelines and public law.

Doxorubicin (DOX) treatment and tissue collection. *Dose selection:* In humans, the recommended dosing of DOX follows a 21-28 day 40-60 mg/m^2 cycle and maximal 4 cycles based on patient information (age, body weight, disease status, etc.) and cancer type (Kabarowski, 2001). We used a single intraperitoneal (i.p.) injection of 10 mg/kg body weight of DOX in mice to determine its effects in ovarian follicles (Xiao, Zhang, *et al.*, 2017; Wang *et al.*, 2018; Y. Wang *et al.*, 2019) and the uterus (Andersen *et al.*, 2019). Based on FDA animal-human dose conversions, 10 mg/kg in adult mice is equivalent to ~30 mg/m^2 in adult humans (Nair and Jacob, 2016), which is within the clinically used chemotherapy dose range. *Treatment timing*: A CL is normally developed from an ovulated follicle and ovulation in cyclic mice occurs in the same night of mating (BINGEL and SCHWARTZ, 1969), which can be detected by the presence of a vaginal plug the next morning. Since DOX is toxic to the ovarian follicles that could affect subsequent ovulation and CL formation and development, DOX treatment was applied on post-ovulation D0.5, therefore avoiding any secondary effects on the CL from the follicular toxicity of DOX. *DOX treatment*: DOX (D-4000, LC Laboratories, Woburn, MA) was dissolved in DMSO to make a stock at 100 mg/ml, aliquoted, and kept at -20°C. A thawed aliquot was kept at 4°C and used within 3 days of thawing. Upon detection of a vaginal plug, D0.5 females were randomly assigned into two groups

to receive a single i.p. injection of vehicle control (100 μl of <2% DMSO in sterile 1x PBS, the % of DMSO was the same as that in DOX-treated group) or DOX (10 mg/kg, mouse body weight (kg) x 10 mg/kg (final dose) / 100 mg/ml (stock concentration) = ml of stock solution diluted into sterile 1x PBS in 100 ul), respectively. Although it is unclear about the half-life of DOX in the mouse ovaries via i.p. injection, studies reported a half-life of DOX ranging from 11 hours to 45 hours in different mouse tissues upon a single i.p. injection of 11-12 mg/kg (Siemann and Sutherland, 1979; Johansen, 1981). *Dissection*: On D3.5, mice were anesthetized via isoflurane inhalation. Blood was collected via the orbital sinus for serum collection as previously described (El Zowalaty, Li, Zheng, *et al.*, 2017; Z. Wang *et al.*, 2019). The left ovary was snap frozen in liquid nitrogen and kept at -80°C, while the right ovary was fixed in Bouin's solution for 24 hours, then kept in 70% ethanol at 4°C. In the D3.5 C57BL/6 mice, one side of oviduct and uterine horn was flushed to determine the effects of DOX on oocytes and embryos.

Serum progesterone (P4) and 17β-estradiol (E2) measurement. Serum was collected from the blood samples after clotting at room temperature for 45 minutes and stored at -80°C. Serum P4 and E2 were measured in the Ligand Assay and Analysis Core of the Center for Research in Reproduction at the University of Virginia (Charlottesville, Virginia).

Ovary histology and the number of corpora lutea (CLs). The fixed C57BL/6 ovaries were processed for paraffin embedding as previously described (Zhao *et al.*, 2013, 2014; El Zowalaty, Li, Zheng, *et al.*, 2017; Z. Wang *et al.*, 2019). Paraffin sections (6 μm) through the widest middle portion of the ovaries were collected, processed, and stained with hematoxylin and eosin. The numbers of CLs in ovarian sections were independently examined by four individuals who were blinded to the treatments. For the sections with inconsistent counting of CLs, they were reevaluated

by the four individuals together to agree on a final number of CLs on each section. The number of CLs from one middle section per ovary per mouse was used for statistical analysis.

Immunohistochemistry and immunofluorescence. Immunohistochemistry was employed to detect proliferating cells using anti-proliferating cell nuclear antigen (PCNA, 1:500, D3H8P, Cell Signaling Technology) in fixed C57BL/6 ovarian sections (6 μm) as previously described (El Zowalaty, Li, Chen, *et al.*, 2017). The sections were counterstained with hematoxylin. Immunofluorescence was used to detect collagen IV (Col IV), StAR, and heat shock protein 60 (HSP60). Briefly, paraffin / frozen sections were processed and subjected to antigen retrieval in 0.01 M sodium citrate (pH 6.0) at 95°C for 20 min. Sections were washed with 1xPBS followed by membrane permeabilization with 0.15% Triton X-100. The slides were then washed and blocked with 10% goat serum (16210064, ThermoFisher) with 1% BSA (B14, ThermoFisher) in 1x TBS for fixed sections or 1x PBS for frozen sections for 1 hour at room temperature; they were subsequently incubated with anti-collagen IV (1:200, Abcam, ab19808), anti StAR (1:700, Abcam, ab96637), or anti-HSP60 (1:400, Cell Signaling Technology, mAb #12165) in a humidified chamber for overnight at 4°C. The following day, the sections were washed in 1xPBS and incubated with secondary Alexa Fluor 488-conjugated goat anti-rabbit IgG antibody (1:200, Invitrogen, A11034) for 1 hour. The sections were counterstained and mounted in DAPI (4',6'-diamino-2-phenylindole)-containing Vectashield (Vector Laboratories, Burlingame, CA, USA). The negative control was processed together except without the primary antibody.

TUNEL staining. Frozen C57BL/6 ovarian sections (10 μm) were fixed in freshly-prepared 4% paraformaldehyde in 0.02 M PBS (pH 7.4) at 27°C for 10 min. Slides were washed 2x5 min in 1X PBS, and permeabilized in 1X PBS-T (0.1% Triton X-100) with 0.1% sodium citrate. TUNEL reaction mixture was made by adding 5 μL TUNEL-enzyme solution to 45 μL TUNEL-

label solution. Slides were incubated with the mixture for 1 hour at 37°C in a humidified chamber. Slides were rinsed 3 times in 1X PBS and counterstained and mounted in 4′,6′-diamino-2-phenylindole (DAPI)-containing Vectashield. The negative control was processed together except without the 5 µL TUNEL-enzyme solution.

Lipid droplet staining. Frozen C57BL/6 ovarian sections (10 µm) were fixed in 4% paraformaldehyde at room temperature for 20 minutes, washed twice in 1X PBS, then covered with 1.6 µg/ml Nile red (N3013, Sigma-Aldrich) in 1X PBS at room temperature for 15 minutes. Sections were then washed in 1X PBS and counterstained with DAPI. The numbers and sizes of lipid droplets were quantified using ImageJ (El Zowalaty, Li, Zheng, *et al.*, 2017; Z. Wang *et al.*, 2019). Briefly, original TIF images were converted to single-channel, 8-bit images. Quantile based normalization was used to standardize the image intensities. Finally, background subtraction, threshold segmentation, and quantification of lipid droplets were performed using ImageJ.

Phalloidin staining. Frozen C57BL/6 ovarian sections (10 µm) were fixed in freshly-prepared 4% paraformaldehyde in 0.02 M PBS (pH 7.4) at 23°C for 10 min. Slides were washed 2x5 min. in 1X PBS. Slides were permeabilized and blocked for non-specific staining in 1X PBS-T (0.1% Triton X-100) in 1% BSA for 30 min, washed 2x5 min in 1X PBS, and incubated with 200 µL 488-conjugated phalloidin solution (1:100 dilution) for 30 min at 23°C. The negative control received 200 µL 1X PBS. Slides were washed 2x5 min. in 1X PBS. Slides were counterstained and mounted in 4′,6′-diamino-2-phenylindole (DAPI)-containing Vectashield (H-1200-10, Vector Laboratories).

Statistical Analysis. Data are presented as dots or mean±SD where applicable. A linear mixed model fit by REML using Satterthwaite's method was used to analyze the percent weight change from D0.5 to D3.5. The percent weight change data were analyzed in R (Version 4.0.2,

package lmerTest 3.1-3). Variances between two groups were tested using the "F-test Two-Sample for Variances" in Excel. Correlation analyses between % body weight change and serum P4 levels were done using "Regression" in Excel. Two-tailed equal or unequal variance student t-test was used to compare two groups. Significance level is set at $P<0.05$.

Results

Effects of DOX treatment on body weight and serum progesterone levels

In the initial study, we used wild type mice with mixed background (C57BL/6 and 129/SvJ (Ye *et al.*, 2005)) that were available in our mouse colony. Their age range was from 10.0 to 22.1 weeks at dissection (16.2 ± 4.2 weeks in PBS group and 14.5 ± 5.4 weeks in DOX group). DOX treatment significantly reduced body weight gain on D1.5 (-3.0% ± 1.9% in PBS group and -5.1% ± 1.4% in DOX group, P=0.0262) (Fig. 2.1A). The DOX-treated mice quickly regained body weight and the body weight gains compared to D0.5 were comparable between the two groups on both D2.5 and D3.5 (Fig. 2.1A).

A main function of the CL during early pregnancy is to produce P4 for supporting early pregnancy events. The serum P4 levels reach a plateau by D3.5 in mice. Among the 13 samples in this initial experiment, four samples with the lowest P4 levels were in the DOX-treated group, which had three other samples within the full range of P4 levels in the control group (Fig. 2.1B, P=0.097). There was no significant correlation between the P4 levels and the changes of body weight on D1.5 (Fig. 2.1C, P=0.153). There was no significant difference in serum 17β-estradiol (E2) levels between the two groups (P=0.828, data not shown). Since the mice in the initial study were in mixed background and ranging from 10.0 weeks to 22.1 weeks old, the varied effects of DOX on P4 levels of individual mice promoted us to test the hypothesis in mice with C57BL/6 pure background and a narrower age range.

To control the potential variables of mouse background and age, we ordered C57BL/6 females in the 2nd set of study and only included the mice plugged within 11 days of cohabitation with stud males. They were randomly assigned into two groups on D0.5 to receive a single i.p. injection of PBS (N=6, vehicle control) and DOX (N=5), respectively. The plugging latency (duration from cohabitation to vaginal plug detection) and the body weight at the time of treatment on D0.5 were comparable between the two groups. DOX treatment also significantly reduced body weight gain on D1.5 (-0.3% ± 1.8% in PBS group and -3.9% ± 3.0% in DOX group, P=0.00774). The temporal patterns of body weight change were comparable between the two sets (Fig. 2.1A & 2.1D). In the 2nd set, the ages at dissection on D3.5 were at a narrow range of 9.9 ± 0.4 weeks in the PBS group (N=6) and 10.1 ± 0.7 weeks in the DOX group (N=5). However, even with all the potential variables controlled in the 2nd set, varied effects of DOX on P4 levels of individual mice were still present. Among the 11 samples, the three lowest ones were in the DOX-treated group, which had two other samples with comparable P4 levels as the control group (Fig. 2.1E, P=0.068). There was no significant correlation between the P4 levels and the changes of body weight on D1.5 (Fig. 2.1F, P=0.390). There was no significant difference in E2 levels between the two groups (P=0.215, data not shown). These data indicate that a single injection of DOX treatment on D0.5 can have varied effects on CL function in P4 synthesis. We focused on the 2nd set of mice for further analyses.

Preimplantation embryo development

Control mice: The timing of mouse preimplantation embryo development follows an order of zygote (D0.5/E0.5), 2-cell (D1.5/E1.5), morula (D2.5/E2.5), and blastocyst (D3.5/E3.5) stages (Zhao *et al.*, 2013; Kojima, Tam and Tam, 2014). The mouse embryos are in the oviduct by D3.0 and are in the uterus by D3.5 under the normal condition (Ye, 2020). When the C57BL/6 mice

were dissected on D3.5, one side of oviduct and uterine horn from each mouse was flushed to determine the location of oocytes and embryos as well as embryo development stages. Among the flushing from five of the six oviducts (one with nothing) in the control group, there were 4 germinal vesicle (GV) oocytes (Fig. 2.2Ai), 8 degenerated possible oocytes with low density cytoplasm (Fig. 2.2Aii), and 3 possible later stage oocytes, which had dense aggregates in the cytoplasm detached from the zona pellucida but had no identifiable nucleus or polar body (Fig. 2.2Aiii); there were 12 blastocysts (Fig. 2.2Aiv) flushed from three out of the six uterine horns but no oocytes nor earlier stage embryos flushed from any of the six uterine horns. These observations in the control group indicate that only blastocysts were present in the uterus, while unfertilized oocytes were retained in the oviduct.

DOX-treated mice: In the oviducts, among the flushing from four of the five oviducts in the DOX group (N=5 mice), there were 3 degenerated possible oocytes with low density cytoplasm (Fig. 2.2Bi), 5 possible metaphase II (MII) oocytes or zygotes with dense aggregates in the cytoplasm detached from the zona pellucida and with a polar body but without an identifiable nucleus (Fig. 2.2Bii), 1 zygote with dense aggregates in the cytoplasm and two polar bodies (one fragmented) (Fig. 2.2Biii), 1 zygote with two nuclei and one visible polar body (Fig. 2.2Biv), and 1 2-cell embryo with dense aggregates in the cytoplasm (Fig. 2.2Bv). In the uterine horns, there were 2 degenerated possible oocytes (Fig. 2.2Bvi) and 3 zygotes with dense aggregates in the cytoplasm and two polar bodies but without identifiable nuclei (Fig. 2.2Bvii) flushed from one uterine horn but no oocytes or embryos were flushed from the other four uterine horns in this group. These observations indicate that DOX treatment inhibited early embryo development *in vivo* and that DOX treatment might interfere with oocyte/embryo transport as well.

Ovary histology

The CL numbers from histology of D3.5 ovaries were comparable between the control and DOX-treated groups (Fig. 2.3A) and there was no apparent difference in the general appearance of the CLs under low magnification between the two groups (Fig. 2.3B-D). Under higher magnification, there were three obvious morphological changes in the CLs from DOX-treated mice with low P4 levels: 1) the corpus luteal cords, which were permeated by microvasculature, were less defined (Fig. 2.3C1) than that seen in the control CL (Fig. 2.3B1); 2) there was scattered cell debris that may indicate scattered luteal cell degeneration (Fig. 2.3C1); and 3) the luteal cells did not show the typical large polygonal cytoplasm and the luteal cell cytoplasm often showed small foamy areas (Fig. 2.3C1). In the ovaries from DOX-treated mice with normal P4 levels (Fig. 2.3D1), there were defined corpus luteal cords outlined by endothelial cells in the CLs; there was no obvious cell debris, but there was foamy cytoplasm and the nuclei appeared larger and less dense in the luteal cells (Fig. 2.3D1). The foamy areas in the cytoplasm were most likely occupied by lipid droplets that were dissolved during histological processing. These data indicate that DOX treatment has various effects on both endothelial cells and luteal cells in the CL, even though the effects may not be correlated with impaired P4 synthesis. Regardless of the effect of DOX treatment on the serum P4 levels, the histology also confirmed that DOX treatment increased granulosa cell death in the developing follicles (Fig. 2.3B2-2.3D2), and this observation is consistent with previous studies in non-pregnant mice (Xiao, Zhang, *et al.*, 2017; Wang *et al.*, 2018; Winship *et al.*, 2019; Y. Wang *et al.*, 2019; Eldani *et al.*, 2020; Almeida *et al.*, 2021). The increased granulosa cell death in the developing follicles was not reflected in the serum E2 levels most likely due to the normally low E2 levels during early pregnancy.

PCNA staining to detect cell proliferation in the ovary

PCNA immunostaining indicated that the overall strongest staining was in the granulosa cells of developing follicles of both control and DOX-treated ovaries (Fig. 2.4A-2.4C) despite more intense staining in the control follicles than in the DOX-treated follicles (Fig. 2.4A-2.4C), which most likely reflects reduced cell density due to the increased granulosa cell death in DOX-treated follicles as seen in the histology (Fig. 2.3B2-2.3D2). PCNA-positive cells were scattered in the CLs (Fig. 2.4A1-2.4C1). In the control CLs, most of the PCNA-positive cells were endothelial cells with an elongated nucleus surrounding the luteal cords and only occasionally the PCNA-positive cells had a round nucleus, which might be luteal cells or immune cells (Fig. 2.4A1); in the DOX-treated CLs from mice with low P4 levels, the luteal cords were not defined, and most of the scattered PCNA-positive cells do not have the typical appearances of endothelial cells (Fig. 2.4B1); in the DOX-treated CLs from the two mice with normal P4 levels (Fig. 2.1E), one had defined luteal cord but the PCNA-positive cells were reduced (Fig. 2.4C1) compared to the control (Fig. 2.4A1), the other one had comparable pattern of PCNA staining (data not shown) as the control. These data indicate that DOX treatment has varied adverse effects on the proliferation of endothelial cells in the CL.

Col IV staining to detect basal lamina of endothelial cells in the ovary

Col IV is a marker of the basal lamina of endothelial cells. Immunofluorescence of Col IV revealed that compared to the control group (Fig. 2.4D, 2.4D1), the expression level of Col IV was reduced and the expression pattern of Col IV was disorganized in the CLs from the DOX-treated mice with low P4 levels (Fig. 2.4E, 2.4E1), consistent with the lack of defined luteal cords in histology (Fig. 2.3C1) and PCNA staining (Fig. 2.4B1). The Col IV staining pattern in the CLs from DOX-treated mice with normal P4 levels was in between the above two patterns (Fig. 2.4F, 2.4F1).

TUNEL staining to detect cell death in the ovary

A distinctive pattern in the ovary sections from both groups was the intense and massive TUNEL staining in some follicles (Fig. 2.5A-2.5C) due to physiological ovarian follicle atresia in the control group and additional toxic effect of DOX in the follicles of DOX-treated group. The numbers of identifiable growing follicles in the TUNEL and DAPI double-stained sections were comparable between the control (7.5 ± 2.1) and the DOX-treated (7.2 ± 2.4, P=0.831) groups (Fig. 2.5D); however, the percentage of TUNEL positive growing follicles was significantly higher in the DOX-treated group (87.8% ± 12.6%) than that in the control group (45.9% ± 14.4%, P=0.00062) (Fig. 2.5E). It was consistent with the histology observation and served as another indication of the DOX effect on the ovarian follicles. In addition, the TUNEL-positive follicle cell density was lower in the DOX-treated group (Fig. 2.5A2-2.5C2), consistent with the histology (Fig. 2.3B2-2.3D2). This study revealed that DOX-induced cell death in the growing follicles during early pregnancy remained significant three days after treatment.

In the CLs from the control group, there was no TUNEL staining in the sections from 5 of the 6 mice in this group (Fig. 2.5A, 2.5A1). In the section from the 6^{th} mouse with the lowest P4 level (Fig. 2.1E), there were scattered TUNEL-positive cells in the CLs (data not shown). In the CLs from the DOX-treated group, the CLs from mice with low P4 levels had scattered TUNEL-positive cells (Fig. 2.5B, 2.5B1); while those from the mice with normal P4 levels had no TUNEL-positive cells (Fig. 2.5C, 2.5C1). These data indicate varied effects of DOX on cell apoptosis in the CL and increased cell apoptosis in the CL was associated with low serum P4 levels.

StAR staining to detect the enzyme for the rate-limiting step of steroidogenesis in the corpus luteum

An essential step of steroidogenesis is the conversion of the substrate cholesterol to pregnenolone in the mitochondria; while the rate-limiting step of steroidogenesis is the transport

of the substrate cholesterol from the outer to the inner mitochondrial membrane, a step carried out by the steroidogenic acute regulatory protein (StAR) (Christenson and Devoto, 2003). StAR immunofluorescence revealed that all mice except the one with the lowest P4 level (Fig. 2.1E) in the control group had strong StAR staining in the majority of luteal cells (Fig. 2.6A, 2.6A1); in the DOX-treated mice with low P4 levels, most of the luteal cells had minimal StAR staining and only a few scattered luteal cells had strong StAR staining (Fig. 2.6B, 2.6B1); and in the DOX-treated mice with normal P4 levels, the intensity of StAR staining ranged from weak to strong in the luteal cells (Fig. 2.6C, 2.6C1). These data demonstrate varied effects of DOX treatment on StAR staining in the luteal cells and a dramatic reduction of StAR expression in luteal cells was associated with low P4 levels in the DOX-treated group.

HSP60 staining to detect mitochondria in the corpus luteum

Since StAR is expressed in the mitochondria and DOX can accumulate in the mitochondria to cause oxidative stress (Sarvazyan, 1996; Yen *et al.*, 1999), to determine if DOX could affect the mitochondrial density, and thus indirectly affect the StAR expression levels in the luteal cells, we detected the expression of heatshock protein 60 (HSP60), a mitochondrial marker localized in the matrix of mitochondria (Cheng, Hartl and Norwich, 1990). HSP60 immunofluorescence indicated that all CLs in different groups had strong HSP60 staining (Fig. 2.6D-F) and the strongest HSP60 staining in the CL was in the cytoplasm of luteal cells (Fig. 2.6D1-2.6F1). Therefore, the reduction of StAR expression in the DOX-treated luteal cells (Fig. 2.6B1 & 2.6C1) was not caused by lack of mitochondria.

Nile Red staining to detect lipid droplets in the corpus luteum

The key function of StAR in steroidogenesis is to transport the substrate cholesterol and lipid droplets are a main source of cholesterol. We detected the lipid droplets in the CLs using Nile

Red staining. At low magnification, the Nile Red staining in the control CLs was relatively lighter than that in the surrounding interstitial compartment (Fig. 2.7A); while that in the DOX-treated CLs was more comparable to the surrounding interstitial compartment (Fig. 2.7B, 2.7C). At high magnification, compared to the sizes of the lipid droplets in the control luteal cells (Fig. 2.7A1), the lipid droplets in the DOX-treated luteal cells were more variable in sizes with some large ones regardless of the P4 levels (Fig. 2.7B1, 2.7C1). Quantification data revealed increased average size of lipid droplets in DOX-treated group (Fig. 2.7D). These data demonstrate lipid droplet accumulation in DOX-treated luteal cells that was not correlated with StAR expression or serum P4 levels.

Phalloidin staining to detect cytoskeleton integrity in the corpus luteum

The cytoskeleton is critical for directional lipid droplet movement in the cytoplasm. Phalloidin staining was used to detect F-actin in the CLs. In the control CLs, the individual luteal cells (w/round nuclei) were readily identifiable because the continuous sheet-like Phalloidin staining clearly outlined the positions of the nuclei (Fig. 2.7E, 2.7E1). However, in the DOX-treated CLs (Fig. 2.7F, 2.7G), the majority of luteal cells were not as readily identifiable as those in the control CLs (Fig. 7E), because the Phalloidin staining was often seen as clusters (Fig. 2.7F-2.7G1), especially in the CLs from DOX-treated mice with low P4 levels (Fig. 2.7F, 2.7F1). These data demonstrate disrupted cytoskeleton in DOX-treated luteal cells.

Discussion

Doxorubicin (DOX) is a widely used chemotherapeutic agent. A major side effect of DOX is intestinal mucositis. In our early pregnancy mouse model, the first response observed was a transient body weight loss detected 24 hours after injection, which disappeared within 48 hours of treatment. It was demonstrated in pigs and rodents that reduced food consumption and

gastrointestinal damage were contributing factors for DOX-induced weight loss (Martin *et al.*, 2014; Seiler *et al.*, 2015; Carr, King and Dekaney, 2017). We did not examine food consumption nor the intestine on D1.5 in this study when the weight loss was transiently evident. Although there was an overall reduction of body weight in the DOX-treated group on D1.5, there were different levels of reduction, indicating varied individual sensitivity. In addition, no significant correlation between body weight changes and serum P4 levels could suggest different sensitivities on different parameters within the same individual towards DOX treatment.

DOX has toxic effects on cultured embryos (WANG *et al.*, 2012; Chang *et al.*, 2014). Information about effects of DOX on early embryo development *in vivo* remains lacking. Our limited data indicated that a single therapeutical relevant dose of DOX (10 mg/kg) prevented mouse embryo development beyond 2-cell stage, mainly arrested at 1-cell zygote stage *in vivo*. Since DOX was delivered via i.p. injection shortly after fertilization when ovarian hormones P4 and E2 are at low levels (Haibin Wang and Dey, 2006; Ye, 2020), the toxic effects on the embryos were most likely caused by direct exposure to DOX in the oviduct. How does DOX reach the oocytes/embryos in oviductal lumen? DOX via i.v. or i.p. injection in mice was shown to reach the ovary and uterus within hours (Asperen *et al.*, 1998; Y. Wang *et al.*, 2019). Although there is insufficient literature on DOX pharmacokinetics in the mouse oviduct, which is localized in between the ovary and the uterus, it is reasonable to speculate that DOX could be distributed to the oviduct within hours of injection, and in our experimental setting, DOX distribution in the oviduct may peak within hours of injection before an embryo reaches the 2-cell stage on D1.5. Based on a study that i.v. injected tracers on D0.5 mice were detected in the multivesicular bodies and in numerous small vesicles in the apical portion of the preampulla oviductal epithelial cells (Parr, Tung and Parr, 1988) and another study showing the role of multidrug resistance protein 1

(MDR1) in exporting DOX from ovarian cells (Wang *et al.*, 2018), we expect that both exocytosis and ABC transporters on the oviductal epithelial cells could be involved in transporting i.p. injected DOX into the oviductal lumen to affect the zygotes on D0.5 in this study. How could DOX cause zygote arrest in the oviductal lumen? One possibility could be the adverse effect of DOX on F-actin to impair DNA damage repair (Okuno *et al.*, 2020).

Luteal cells are normally differentiated from the remaining granulosa cells and theca cells in the ovulated follicles. This study revealed that during early pregnancy, in contrast to massive apoptosis of granulosa cells in the developing follicles, the luteal cells in the CLs were rarely TUNEL positive upon DOX treatment and luteal cell apoptosis was occasionally observed in the CLs from DOX-treated mice with low P4 levels. One explanation is the expression of ATP-binding cassette family of transporters (ABC transporters), such as P-glycoprotein (also called multidrug resistance protein 1 (MDR1) / ABCB1 / CD243), that pump drugs out of the cells. DOX was accumulated in cardiac tissue of mice lacking mdr1a P-glycoprotein (Asperen *et al.*, 1998), which also had increased ovarian toxicity (Wang *et al.*, 2018) due to the expected intracellular accumulation of DOX. P-glycoprotein has a spatiotemporal expression pattern in the ovary. It was shown to be highly upregulated in the granulosa cells of rat preovulatory follicle after equine chorionic gonadotropin CG (eCG) stimulation for 42 h (pre-ovulation) and it remains highly expressed in the luteal cells post-ovulation (Lee, Croop and Anderson, 1998). The upregulation of P-glycoprotein in the CLs compared to follicles was also evident in adult mouse ovaries at estrus stage (Wang *et al.*, 2018). Since DOX treatment was administrated on D0.5 (post-ovulation), P-glycoprotein expression is expected to be already upregulated to pump out DOX from the luteal cells. Therefore, one reasonable explanation for the resistance of luteal cells in the CLs but vulnerability of granulosa cells in the follicles from DOX-induced cell death would be the

upregulation of ATP transporters, such as P-glycoprotein, in CL to reduce DOX levels in the luteal cells. Since chemotherapeutic drugs, including DOX, are preferentially targeting proliferating cells (e.g., cancer cells), and luteal cells are not typically proliferating while granulosa cells are highly proliferating, minimal cell proliferation in luteal cells can be another contributing factor for their resistance to DOX-induced apoptosis.

In addition to the luteal cells, the other main type of cells in the CL are endothelial cells (Davis, Rueda and Spanel-Borowski, 2003b). Although the area of an ovarian follicle occupied by granulosa cells lacks vasculature, the CL is highly vascularized (Duffy *et al.*, 2018). The vasculature in the CL supports CL development and luteal cell functions, including P4 steroidogenesis and transport of steroid hormones to the systemic circulation (Christenson and Devoto, 2003; Duffy *et al.*, 2018). Endothelial cells are sensitive to DOX treatment in general (Kotamraju *et al.*, 2000b; Luu *et al.*, 2021) and vascular toxicity of DOX contributes to the placental toxicity in ICR mice (Bar-Joseph *et al.*, 2020). In the CLs from DOX-treated mice with low P4 levels, the vascular toxicity of DOX could be the main contributing factor for the lack of defined luteal cord structure. However, in the CLs from DOX-treated mice with normal P4 levels, there were defined luteal cords. These observations indicate that endothelial cells in the CLs are targeted by DOX treatment and that there is individual variation in sensitivity to DOX treatment, which is different from the consistent toxic effect of DOX on the granulosa cells in the developing follicles.

The individual variation in the sensitivity to DOX treatment is also reflected in StAR expression, which was reduced in the luteal cells of mice with low P4 levels. DOX-induced suppression of *StAR* mRNA expression was observed in DOX-treated male rat testes and correlated with decreased plasma testosterone levels (Das *et al.*, 2011; Ujah *et al.*, 2021). Since StAR is the

rate-limiting enzyme for transporting the substrate cholesterol from the outer to the inner mitochondrial membrane for P4 steroidogenesis, the quantity of mitochondria in the cytoplasm could affect the overall StAR expression level in the luteal cells. DOX can accumulate in the mitochondria due to its specific binding to the abundant phospholipid cardiolipin located in the inner mitochondrial membrane. The accumulated DOX can disrupt the electron transport chain in the mitochondria to overproduce reactive oxygen species (ROS) (Davies and Doroshow, 1986; Sarvazyan, 1996; Yen *et al.*, 1999). Although the quantity of mitochondria in the luteal cells, based on HSP60 expression levels, is not significantly affected by DOX treatment, DOX-induced overproduction of ROS in mitochondria could impair mitochondrial functions and inhibit StAR expression, which will reduce the substrate cholesterol from reaching the inner mitochondrial membrane, and therefore, disrupt the mitochondrial function in supporting the enzymatical conversion of cholesterol to pregnenolone (by P450SCC/CYP11A1) on the inner mitochondrial membrane. The molecular mechanisms in DOX-induced suppression of StAR expression, which correlates with DOX-induced P4 deficiency, remain to be elucidated.

Lipid droplets store neutral lipids, including cholesteryl ester that is a main source of cholesterol for P4 steroidogenesis. They are surrounded by a phospholipid monolayer and coated with perilipins (PLIN1-5) (Singh and Cuervo, 2012). The CLs undergo development and maintenance for P4 synthesis to support early pregnancy. If pregnancy does not occur or P4 production in CL is no longer needed during pregnancy, the CL undergoes luteal regression / luteolysis, which is hallmarked by lipid droplet accumulation (Strauss *et al.*, 1977), which is also present in structurally regressing CLs from a previous cycle that coexist with current cycle CLs at maintenance stage (Lee-Thacker *et al.*, 2018). DOX treatment leads to lipid droplet accumulation in the luteal cells on D3.5 when the CLs are normally at the maintenance stage. Since DOX could

disrupt actin cytoskeleton in the luteal cells and cytoskeleton plays an important role for directional lipid movement, e.g., to the mitochondria, the disrupted cytoskeleton inevitably halted directional lipid movement leading to lipid droplet accumulation. On the other hand, there was a dramatic reduction of StAR expression in the luteal cells from DOX-treated mice with low P4 levels, therefore, the utilization of lipid droplet-derived cholesterol for P4 synthesis is diminished, which may also lead to lipid droplet accumulation. The disrupted cytoskeleton in DOX-treated CLs may be caused by DOX-induced oxidative stress (Wei *et al.*, 2015).

In summary, we identify multiple effects of DOX treatment in the preimplantation CLs. Both endothelial cells and luteal cells are targeted. There are three types of effects from DOX treatment during early pregnancy: 1) effects are present in all DOX-treated CLs but not correlated with the key function of CLs in P4 steroidogenesis, such as lipid droplet accumulation and disrupted cytoskeleton; 2) effects varied greatly and are correlated with P4 levels, such as StAR expression in the luteal cells and impaired morphology of luteal cords, which are surrounded by endothelial cells; and 3) varied effects un-correlated with P4 levels, such as body weight change on D1.5. The molecular mechanisms for DOX-induced effects, e.g., reduced StAR expression, in the CL remain to be investigated. This study fills in the knowledge gap about toxic effects of chemotherapy on the CL and provides critical information for risk assessment of chemotherapy in female reproduction.

Conflicts of Interest (COI)

The authors declare that there is no applicable COI.

Data Availability Statement

All the data are available upon request.

Acknowledgements

The authors thank the Office of the Vice President for Research, Interdisciplinary Toxicology Program, and Department of Physiology and Pharmacology at the University of Georgia, and the National Institutes of Health (NIH R03HD100652 and R03HD097384 to XY) for financial support. Serum P4 and E2 levels were determined at The University of Virginia Center for Research in Reproduction Ligand Assay and Analysis Core, which is supported by the Eunice Kennedy Shriver NICHD/NIH (NCTRI) Grant P50-HD28934.

Figure Legends

Figure 2.1. Body weigh changes and serum progesterone levels. A-C: mice in mixed background at 10.0 to 22.1 weeks old; D-F: mice in C57BL/6 pure background at 9.6 to 10.9 weeks old. Black dots, PBS-treated vehicle control group (N=6 in both sets); red triangles, DOX-treated group (N=7 in mixed background and N=5 in C57BL/6 background). A & D. Daily body weight changes of individual mice from treatment on 0.5 days post-coitum (D0.5) to dissection on D3.5. #, P=0.0262 (D1.5) in A and P=0.00774 (D1.5) in D. B & E. Serum progesterone levels of individual mice. Line, average of the group; #, P=0.097 in B and P=0.068 in E, two-tailed equal variance t-test. C & F. Lack of significant correlation between body weight changes on D1.5 and serum progesterone levels on D3.5. P=0.153 in C and P=0.390 in F.

Figure 2.2. Images of oocytes and embryos from C57BL/6 oviduct and uterine horn. The number under each image indicating the total number of oocyte/embryo with similar appearance at the same location in the same group. A. PBS control group (N=6 mice). Oviduct: Ai, germinal vesicle (GV) oocyte; Aii, degenerated possible oocyte; Aiii, possible metaphase I (MI) or metaphase II (MII) oocyte. Uterus: Aiv, blastocyst. B. DOX-treated group (N=5 mice). Oviduct: Bi, degenerated possible oocyte; Bii, possible MII oocyte or zygote; Biii, zygote with two visible polar bodies (one fragmented); Biv, zygote with one visible polar body and two nuclei; Bv, 2-cell embryo. Uterus: Bvi, degenerated possible oocyte; Bvii, zygote with two polar bodies.

Figure 2.3. Histology of D3.5 C57BL/6 ovaries. A. Numbers of corpora lutea in PBS and DOX-treated groups. N=5-6; error bar, standard deviation. B, B1, B2: PBS. C, C1, C2:

DOX-treated with low progesterone (P4) level. D, D1, D2: DOX-treated with normal P4 level. B1, C1, D1: corpus luteum enlarged from the smaller box in B, C, D, respectively; B2, C2, D2: follicles enlarged from the bigger box in B, C, D, respectively; scale bar: 200 μm (B-D), 25 μm (B1-D1), or 50 μm (B2-D2); #, corpus luteum; *, follicle; green arrow in C1 & D1, vacuolated luteal cells; black arrow in C1, C2, D2, degenerated cells. H & E staining.

Figure 2.4. PCNA immunohistochemistry and Col IV immunofluorescence in D3.5 C57BL/6 ovaries. A-C1, PCNA staining in fixed ovaries; D-F1, Col IV staining in frozen ovaries. A & D. PBS. B & E. DOX-treated with low progesterone (P4) level. C & F. DOX-treated with normal P4 level. A1-F1: enlarged from the box in A-F, respectively; scale bar: 200 μm (A-F), 25 μm (A1-F1); #, corpus luteum; *, follicle; green arrow in A1-C1, PCNA-positive endothelial cells. No specific staining in the negative control (data not shown).

Figure 2.5. TUNEL staining of D3.5 C57BL/6 ovaries. A, A1, A2: PBS. B, B1, B2: DOX-treated with low progesterone (P4) level. C, C1, C2: DOX-treated with normal P4 level. A1, B1, C1: corpus luteum enlarged from the smaller box in A, B, C, respectively; A2, B2, C2: follicles enlarged from the bigger box in A, B, C, respectively; scale bar: 400 μm (A-C), 25 μm (A1-C1), or 100 μm (A2-C2); #, corpus luteum; *, follicle. D. Numbers of identifiable growing follicles in PBS and DOX-treated groups. E. Percentage of TUNEL-positive follicles in identifiable growing follicles in PBS and DOX-treated groups. D & E: N=5-6; *, P=0.00062; error bar, standard deviation. No specific staining in the negative control (data not shown).

Figure 2.6. Immunofluorescence detection of StAR and HSP60 in D3.5 C57BL/6 ovaries. A-C1, StAR; D-F1, HSP60; A & D. PBS. B & E. DOX-treated with low progesterone (P4) level. C & F. DOX-treated with normal P4 level. A1, B1, C1: enlarged from the box in A, B, C, respectively; green: StAR staining. D1, E1, F1: enlarged from the box in D, E, F, respectively; green: HSP60 staining. #: corpus luteum; scale bar: 200 μm (A-F) or 25 μm (A1-F1). No specific staining in the negative control (data not shown).

Figure 2.7. Nile red staining of lipid droplets and Phalloidin staining of actin filaments (F-actin) in D3.5 C57BL/6 CLs. A-C1, Nile red staining; E-G1, Phalloidin staining; A & E. PBS. B & F. DOX-treated with low progesterone (P4) level. C & G. DOX-treated with normal P4 level. A1, B1, C1: enlarged from the CL marked with a red # in A, B, C, respectively; green: Nile red staining of lipid droplets; blue, DAPI staining of nuclei; #: corpus luteum; scale bar: 200 μm (A-C) or 12.5 μm (A1-C1). D. Size of lipid droplets (arbitrary units). The average size of lipid droplets in all representative areas of all CLs from the same mouse is considered as one data point. N=5-6; * P= 4.42E-05; error bar, standard deviation. E1, F1, G1: enlarged from the boxed area in E, F, G, respectively; green: Phalloidin staining of F-actin; blue, DAPI staining of nuclei; scale bar: 50 μm (E-G) or 12.5 μm (E1-G1). No specific staining in the negative control (data not shown).

FIGURES

Figure 2.1

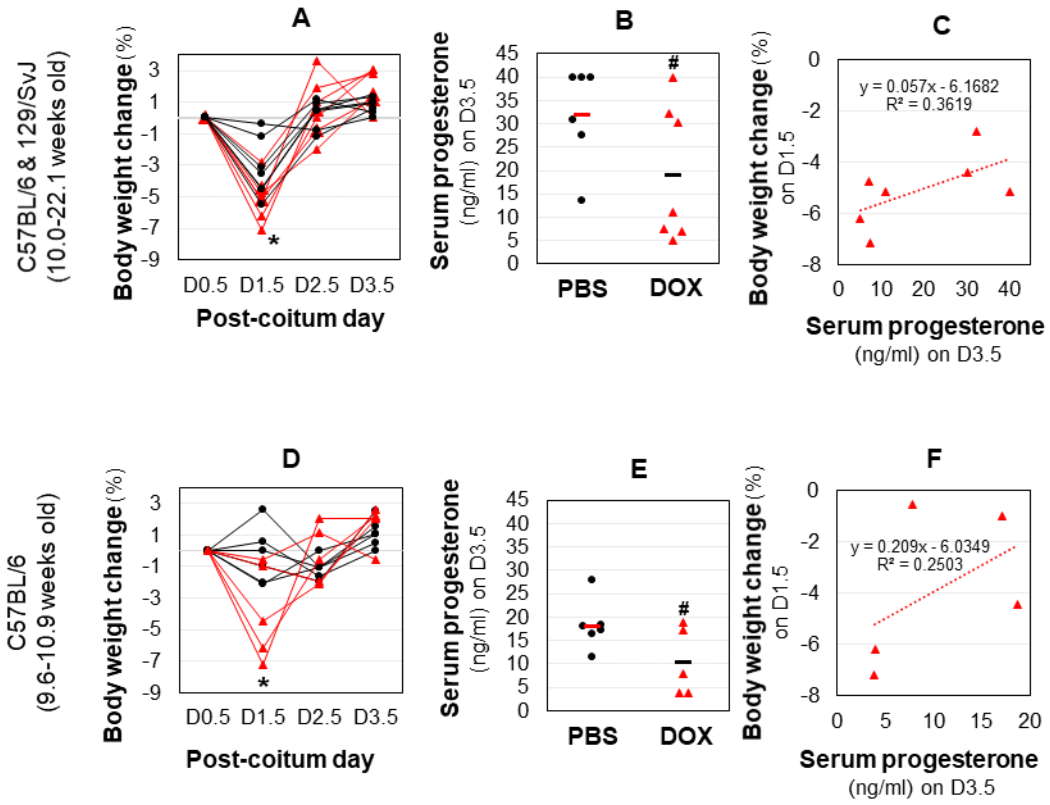

Figure 2.2

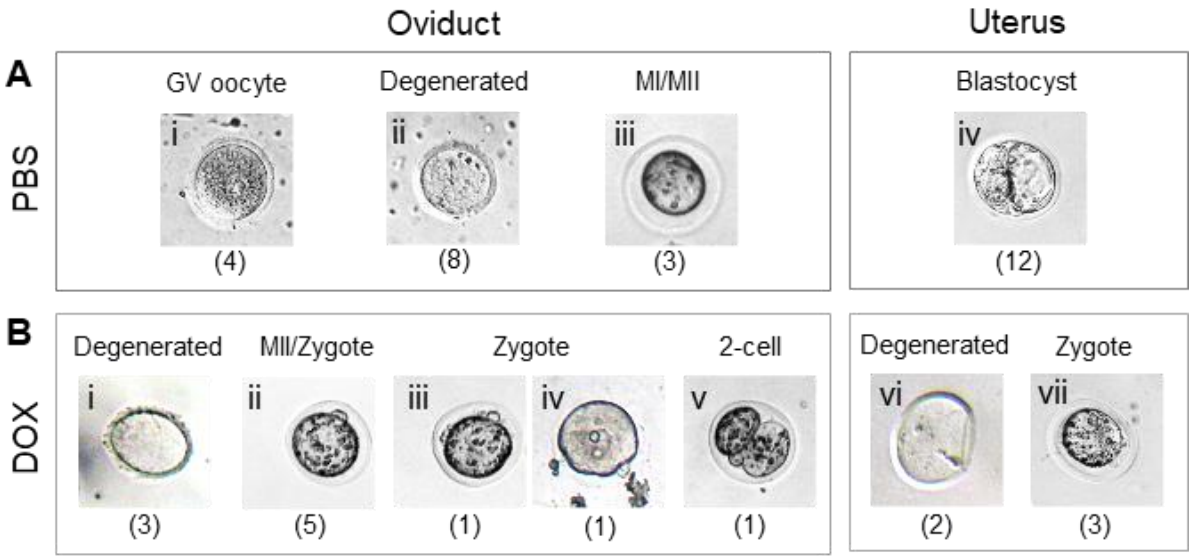
Oviduct
Uterus
A
PBS
GV oocyte
Degenerated
MI/MII
Blastocyst
i
ii
iii
iv
(4)
(8)
(3)
(12)
B
DOX
Degenerated
MII/Zygote
Zygote
2-cell
Degenerated
Zygote
i
ii
iii
iv
v
vi
vii
(3)
(5)
(1)
(1)
(1)
(2)
(3)

Figure 2.3

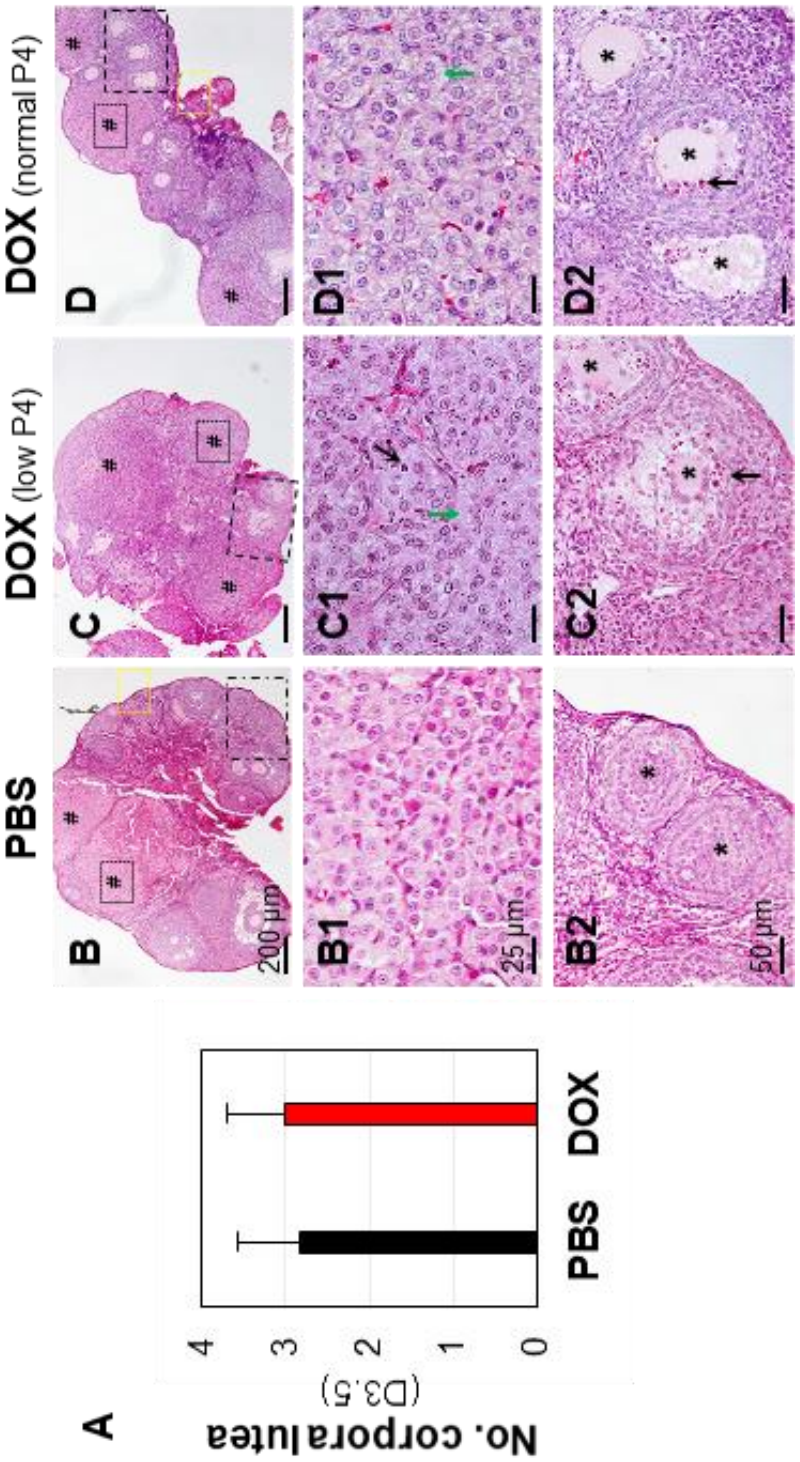
PBS
DOX (low P4)
DOX (normal P4)
B
C
D
B1
C1
D1
B2
C2
D2
200 µm
25 µm
50 µm
A
No. corpora lutea (D3.5)
0
1
2
3
4
PBS
DOX

Figure 2.4

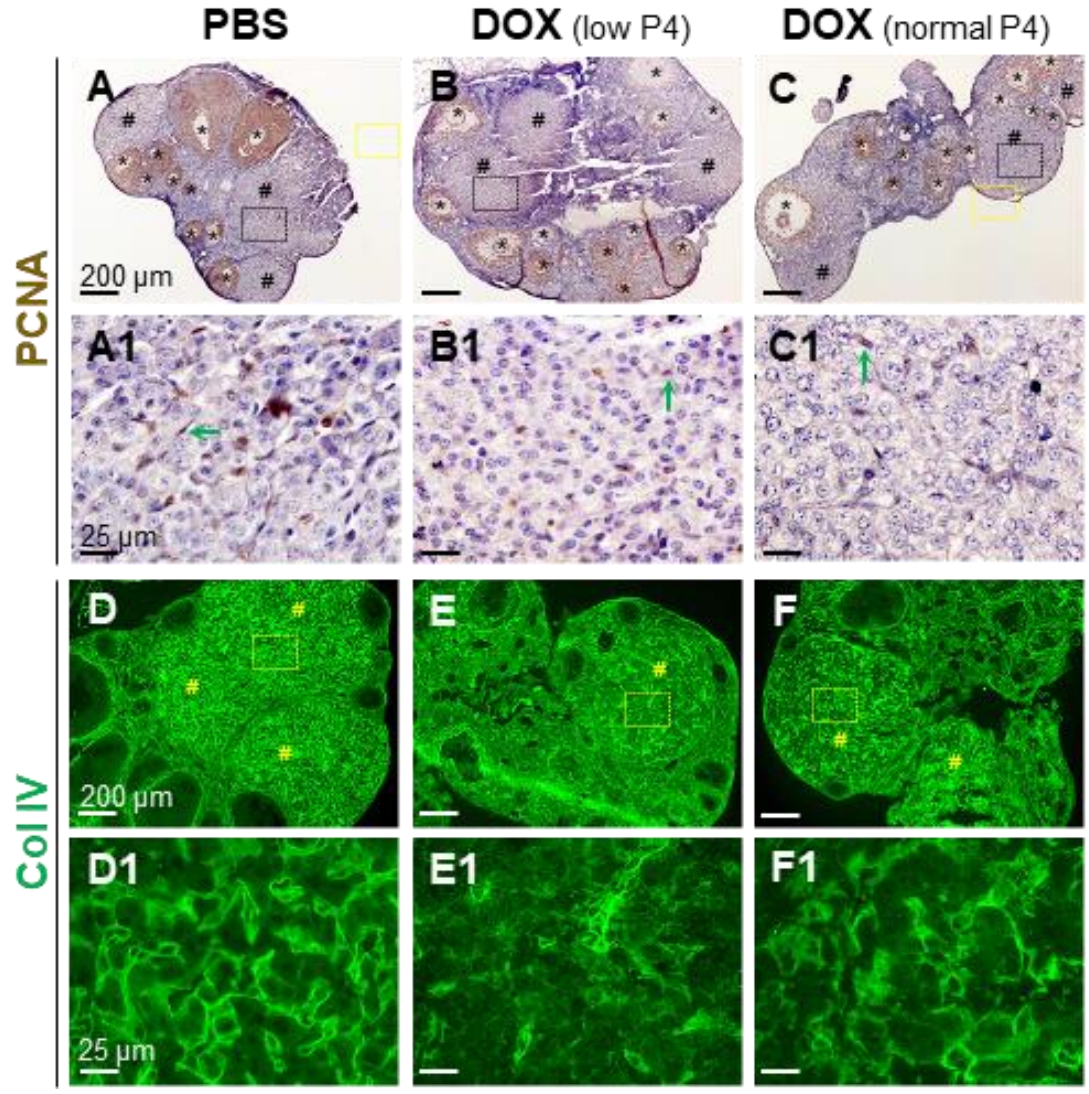
PBS
DOX (low P4)
DOX (normal P4)
PCNA
Col IV
A
B
C
A1
B1
C1
D
E
F
D1
E1
F1
200 μm
25 μm
200 μm
25 μm

Figure 2.5

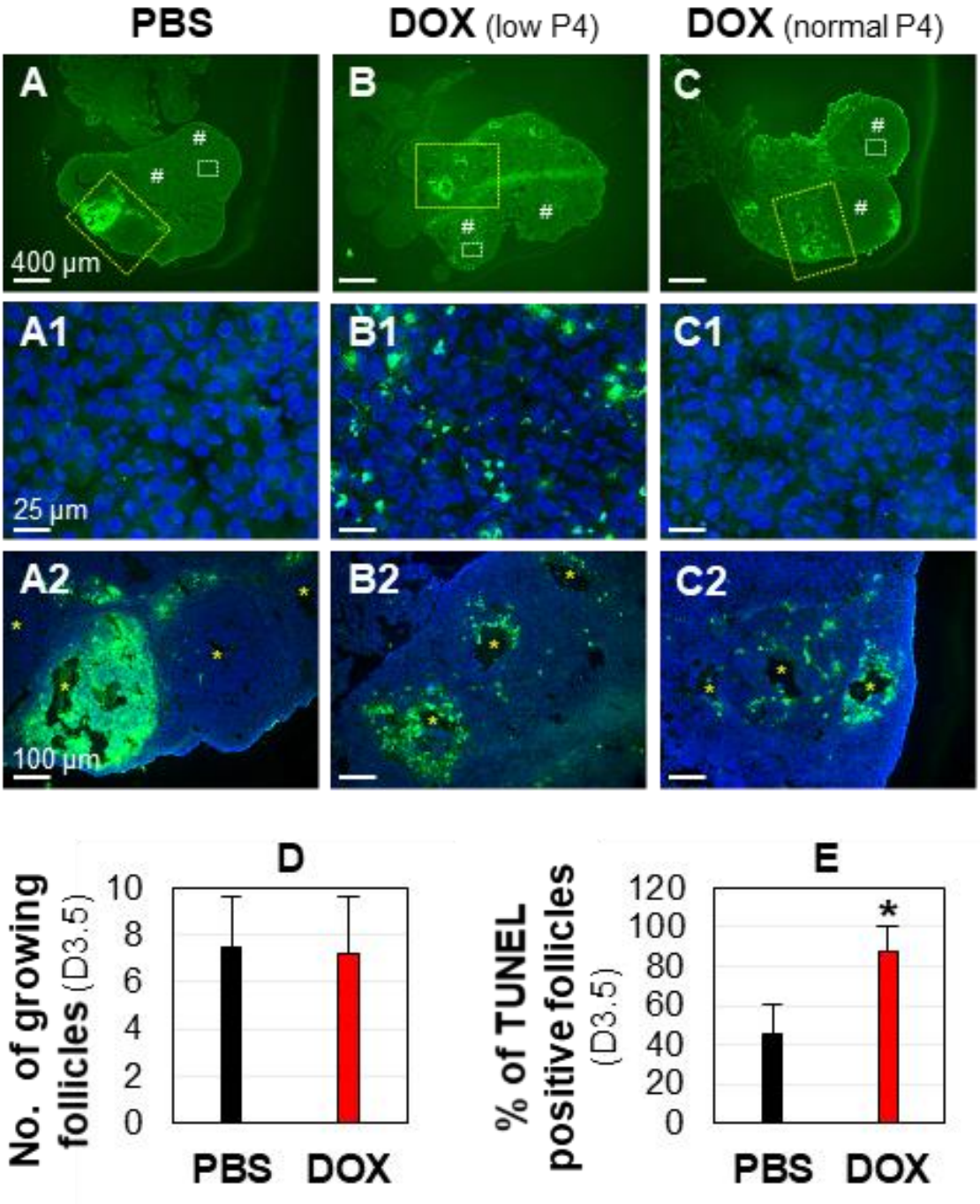
PBS
DOX (low P4)
DOX (normal P4)
A
B
C
400 μm
A1
B1
C1
25 μm
A2
B2
C2
100 μm
D
No. of growing follicles (D3.5)
10
8
6
4
2
0
PBS
DOX
E
% of TUNEL positive follicles (D3.5)
120
100
80
60
40
20
0
*
PBS
DOX

Figure 2.6

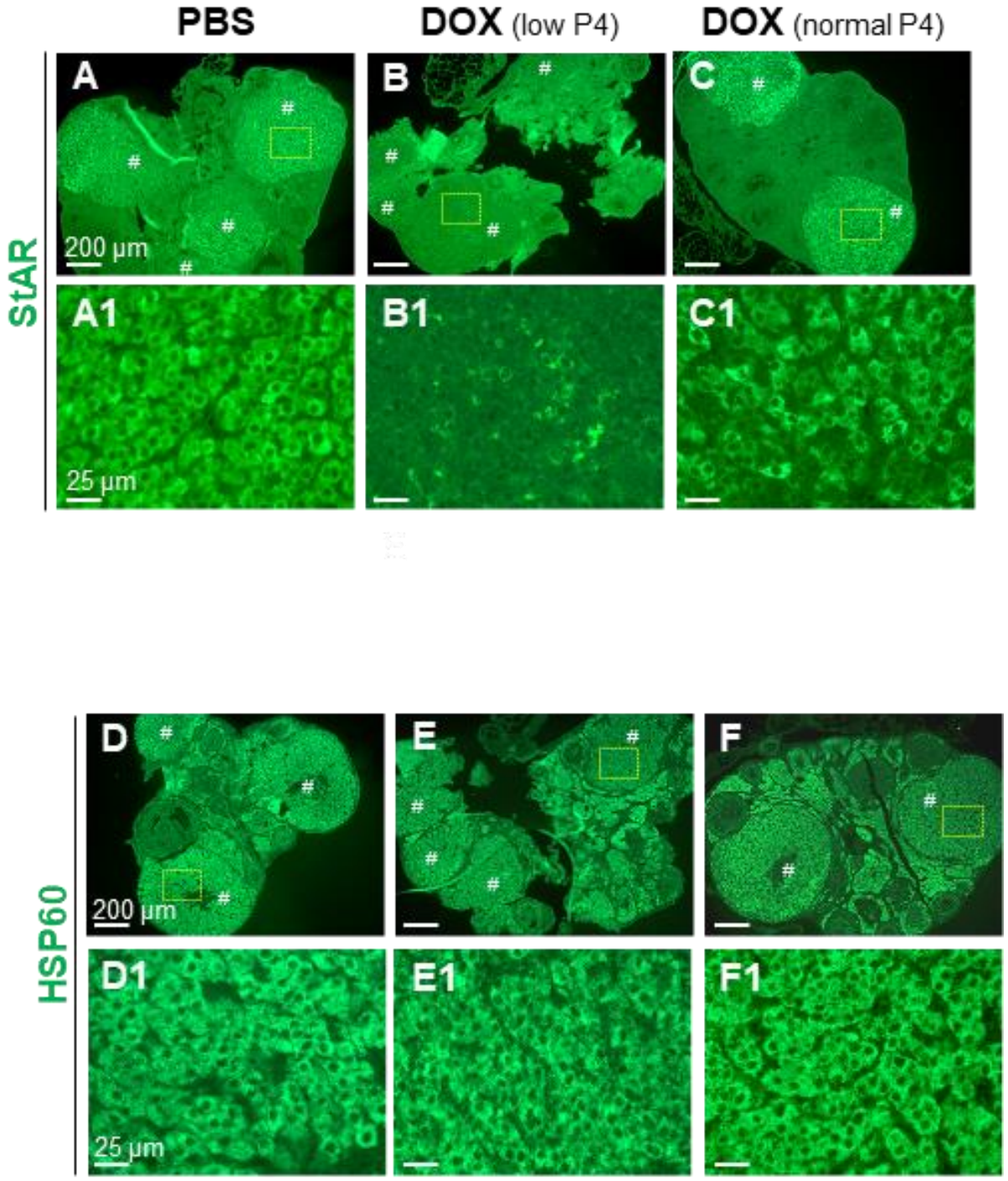
PBS
DOX (low P4)
DOX (normal P4)
StAR
A
B
C
A1
B1
C1
200 µm
25 µm
HSP60
D
E
F
D1
E1
F1
200 µm
25 µm

Figure 2.7

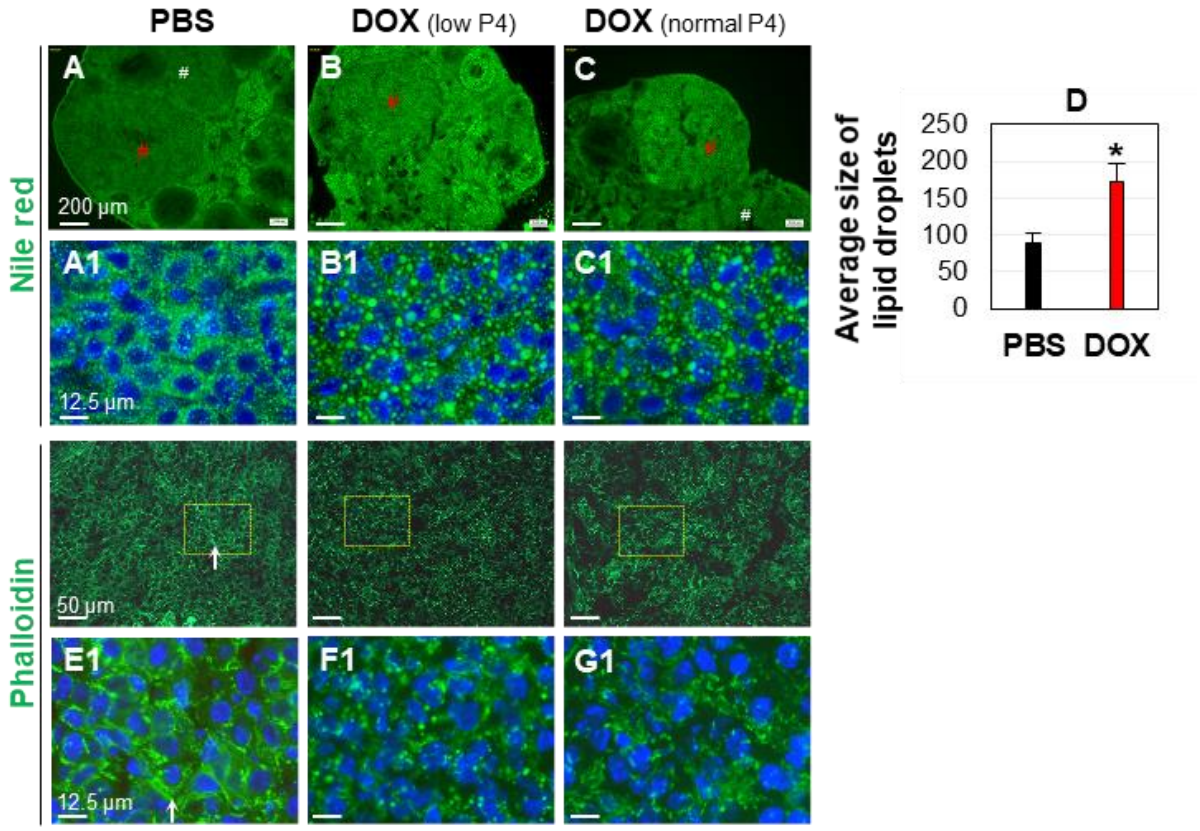
PBS
DOX (low P4)
DOX (normal P4)
A
B
C
#
200 µm
Nile red
A1
B1
C1
12.5 µm
50 µm
Phalloidin
E1
F1
G1
12.5 µm
D
Average size of lipid droplets
250
200
150
100
50
0
*
PBS
DOX

CHAPTER 3

CHEMOTHERAPEUTIC AGENT DOXORBUCIN ALTERS UTERINE GENE EXPRESSION IN RESPONSE TO ESTROGEN IN OVARIECTOMIZED CD-1 ADULT MICE[1]

[1]Andersen, C.L., M. Liu, Z. Wang, X. Ye, S. Xiao. 2019. *Biology of Reproduction*. 100:869-871.

Reprinted here with permissions of the publisher

Title

Chemotherapeutic agent doxorubicin alters uterine gene expression in response to estrogen in ovariectomized CD-1 adult mice

Short title

Doxorubicin and uterine response to estrogen

Summary sentence

Our finding that a single dose of doxorubicin relevant to human treatment level can change uterine gene expression in response to estrogen in ovariectomized mice one month later indicates that the uterus is a direct target of doxorubicin and doxorubicin has a long-term impact on the uterus.

Key words

Doxorubicin, ovariectomy, estrogen, RNA-seq, uterine gene expression

Christian Lee Andersen[1, 2], Mingjun Liu[3], Zidao Wang[1, 2], Xiaoqin Ye[1, 2, #], and Shuo Xiao[3, #]

[1] Department of Physiology and Pharmacology, College of Veterinary Medicine, University of Georgia, Athens, GA 30602, USA; [2] Interdisciplinary Toxicology Program, University of Georgia, Athens, GA 30602, USA; [3] Department of Environmental Health Sciences, Arnold School of Public Health, University of South Carolina, Columbia, SC 29208, USA.

Grant support

NIH P01ES028942 (SX)

Arnold School of Public Health Research Fund (SX)

NIH R01HD065939 (XY)

Presented in part at

- Southeastern Society of Toxicology Annual Meeting, October 25-26, 2018, Gainesville, FL.

[#] Corresponding authors

Shuo Xiao, Ph.D., 921 Assembly St., Department of Environmental Health Sciences, Arnold School of Public Health, University of South Carolina, Columbia, SC 29208, USA (Tel: 1- 803-777-6745; E-mail: sxiao@mailbox.sc.edu)

Xiaoqin Ye, M.D., Ph.D., 501 DW Brooks Dr., Department of Physiology and Pharmacology, College of Veterinary Medicine; Interdisciplinary Toxicology Program, University of Georgia, Athens, GA 30602, USA (Tel: 1-706-542-6745; E-mail: ye@uga.edu)

Abstract

Chemotherapy can potentially impair fertility in premenopausal cancer patients. Female fertility preservation has been mainly focused on the ovarian aspects and benefited greatly from assisted reproductive technologies, such as *in vitro* fertilization (IVF). The rate-limiting step for the success of IVF is embryo implantation in the uterus. Doxorubicin (DOX) is a widely used chemotherapeutic agent with ovarian toxicity. It remains unknown if the uterus is a direct target of DOX. To circumvent the indirect uterine effect from ovarian toxicity of DOX and to investigate potential long-term impact of DOX on the uterus, young adult ovariectomized CD-1 mice were given an intraperitoneal injection once with PBS or DOX (10 mg/kg, a human relevant chemotherapeutic dose), and 30 days later, each set of mice was randomly assigned into three groups and subcutaneously injected with oil, 17β-estradiol (E2, for 6 hours), and progesterone (P4, for 54 hours), respectively. Uterine transcriptomic profiles were determined using RNA-seq. Principal component analysis of the uterine transcriptomes revealed four clusters from the six treatment groups: PBS-oil & DOX-oil, PBS-P4 & DOX-P4, PBS-E2, and DOX-E2, indicating that DOX treatment did not affect the overall uterine transcriptomic profiles in the oil and P4-treated mice but altered uterine responses to E2 treatment. DAVID analysis indicated that the top affected gene cluster was “Glycoprotein”. These data demonstrate that DOX can directly target the uterus and has a long-term impact on uterine responses to E2.

Introduction

Millions of females during childhood, adolescence, and young adulthood suffer from cancers. A unique side effect of concern from cancer treatments using chemotherapy and radiotherapy in these cancer patients is fertility impairment. Oncofertility thus becomes an emerging discipline (Anazodo *et al.*, 2018). Because of the prominent gonadotoxicity of many oncologic treatments, the efforts on female fertility preservation have been mainly focused on cryopreservation of ovarian tissues, oocytes, and embryos (Harada and Osuga, 2018). Fertility preservation has benefited greatly from assisted reproductive technologies (ARTs), such as *in vitro* fertilization (IVF). The rate-limiting step for the success of IVF is embryo implantation in the uterus (Dekel *et al.*, 2014), which is under the control of ovarian hormones estrogen and progesterone (Haibin Wang and Dey, 2006).

Doxorubicin (DOX, Adriamycin) is a cytotoxic anthracycline antibiotic. It has been widely used as a chemotherapeutic agent since the 1960s to treat a variety of cancers, such as breast cancer, ovarian cancer, lymphomas, leukemia, etc. (Johnson-Arbor and Dubey, 2020). DOX can cause ovarian toxicity (Xiao, Zhang, *et al.*, 2017; Nishi *et al.*, 2018; Wang *et al.*, 2018), including impaired ovarian hormone secretion (Xiao, Zhang, *et al.*, 2017). Since uterine functions are under the control of ovarian hormones, it is expected that DOX-induced ovarian toxicity can indirectly affect uterine functions. It remains unknown if the uterus is a direct target of chemotherapeutic agents, such as DOX. Unlike the ovary/oocyte/embryo that can be removed from cancer patients for cryopreservation prior to cancer treatments, the uterus will remain with the patients (for non-uterine cancers) as they undergo cancer treatments. Any adverse effects of chemotherapy on uterine functions, such as uterine receptivity for embryo implantation, remain a significant knowledge gap.

Material and methods

To circumvent the ovarian toxicity of DOX, which will impair ovarian hormone production thus indirectly affect uterine functions, and to investigate potential long-term impact of DOX on the uterus, young adult ovariectomized CD-1 mice (8 weeks old, Envigo) were given an intraperitoneal injection once with PBS or DOX (10 mg/kg, equivalent to a human chemotherapeutic dose of ~600 mg/M^2 (Xiao, Zhang, *et al.*, 2017)). Thirty days later, each set of mice was randomly assigned into three groups and subcutaneously injected with oil, 17β-estradiol (E2, 4.5 μg/kg, one dose, dissected 6 hours later), or progesterone (P4, 60 mg/kg, three doses at 0, 24, and 48 hours, and dissected 6 hours after the last injection (Diao, Xiao, Li, *et al.*, 2013)), respectively, to mimic the changes of ovarian hormones prior to embryo implantation in mice (Haibin Wang and Dey, 2006). There were six groups of mice: PBS-oil, PBS-E2, PBS-P4, DOX-oil, DOX-E2, and DOX-P4. The uterine tissues were dissected and processed for total RNA isolation and subsequent transcriptome profiling using RNA-seq technology.

RNA-seq was performed using Illumina TruSeq (N=3/group). Each sample had over 97% alignment to the GRCm38 reference genome index using HISAT2. Transcripts were assembled and merged into a single comprehensive file using StringTie. The DESeq2 package in R was used for analysis of differential expression.

Results

Principal component analysis (PCA) indicated that 83% of the variability among the six groups were contributed by the first two principal components (PC1=66%, PC2=17%). The three groups treated with PBS (PBS-oil, PBS-E2, and PBS-P4) were well-separated, so were the three groups treated with DOX (DOX-oil, DOX-E2, and DOX-P4), indicating that E2 and P4 had distinctive effects on uterine transcriptomes (Fig. 3.1A). In addition, the six samples in both PBS-

oil and DOX-oil groups did not separate as two distinctive clusters, and neither did the six samples in both PBS-P4 and DOX-P4 groups, indicating that DOX treatment did not significantly change the overall uterine transcriptomic profiles in the oil and P4-treated mice. However, the three samples in the PBS-E2 group did separate from the three samples in the DOX-E2 group. Based on PCA analysis, the PBS-E2 group fell in between PBS-oil/DOX-oil groups and DOX-E2 group (Fig. 3.1A), suggesting that DOX treatment enhanced uterine responses to E2 treatment.

There were 292 differentially expressed transcripts out of the total 16,230 entries between PBS-E2 and DOX-E2 groups by using a criterion of log2 fold change ≥ 2 or ≤ -2 and a false discovery rate corrected P value < 0.001. The heatmap of these differentially expressed transcripts using DESeq2 is shown in Fig. 1B. By using the same criterion, there were no differentially expressed transcripts between PBS-oil and DOX-oil groups or between PBS-P4 and DOX-P4 groups.

Functional annotation tool DAVID indicated 273 DAVID IDs from the 292 differentially expressed transcripts between PBS-E2 and DOX-E2 groups. Functional annotation clustering using UP_KEYWORDS from DAVID analysis indicated that the top affected gene cluster was "Glycoprotein" (104 genes, P=2.9E-17). Other top significantly enriched clusters included "Membrane" (136 genes, P=6.8E-5) and "Extracellular matrix" (12 genes, P=1.3E-4).

Discussion

These novel data demonstrate that DOX can directly target the uterus to alter the uterine responses to estrogen. Since balanced uterine estrogen signaling is critical for embryo implantation and the most affected genes are glycoproteins, many of which play important roles in uterine preparation for embryo implantation (Haibin Wang and Dey, 2006), it is possible that DOX could potentially affect uterine receptivity for embryo implantation (Aplin and Singh, 2008), which

needs to be investigated. DOX has a half-life of elimination <48 hours. The uterine responses detected in this study were 33 days after a single injection of a clinically relevant dose of DOX, indicating that DOX at 10 mg/kg has a long-term effect on the uterus. This observation raises the concern that young female cancer patients receiving chemotherapy during childhood, adolescence, or early adulthood may have their uterine functions affected. Since the uterus is so far the only place for a mammalian embryo to survive and grow to term, it is important to include the uterus for fertility preservation of premenopausal female cancer patients.

Conflict of interest statement

The authors declare that there are no conflicts of interest.

Acknowledgments

Authors thank Dr. Teresa K. Woodruff for supporting the initiation of this project, and Arnold School of Public Health at the University of South Carolina and National Institutes of Health (NIH P01ES028942 to S.X., and NIH R01HD065939 to X.Y.) for financial support.

Figure Legends

Figure 3.1. Analysis of RNA-seq data from ovariectomized CD-1 mouse uteri. E2, 17β-estradiol, 6 hours of treatment; P4, progesterone, 54 hours of treatment; DOX, doxorubicin. A. Principal component analysis of the first two principle components. Overlapping between PBS-oil (blue dots) and DOX-oil (brown dots) groups, and between PBS-P4 (purple dots) and DOX-P4 (grey dots) groups; separation between PBS-E2 (green dots) and DOX-E2 (red dots with two overlapping) groups. B. Heatmap of top differentially expressed genes between "PBS-E2" and "DOX-E2" groups. Log2 fold change: ≥2 or ≤-2; false discovery rate corrected P value < 0.001; legend color palette: log-fold changes. Data were analyzed using DESeq2.

FIGURES

Figure 3.1

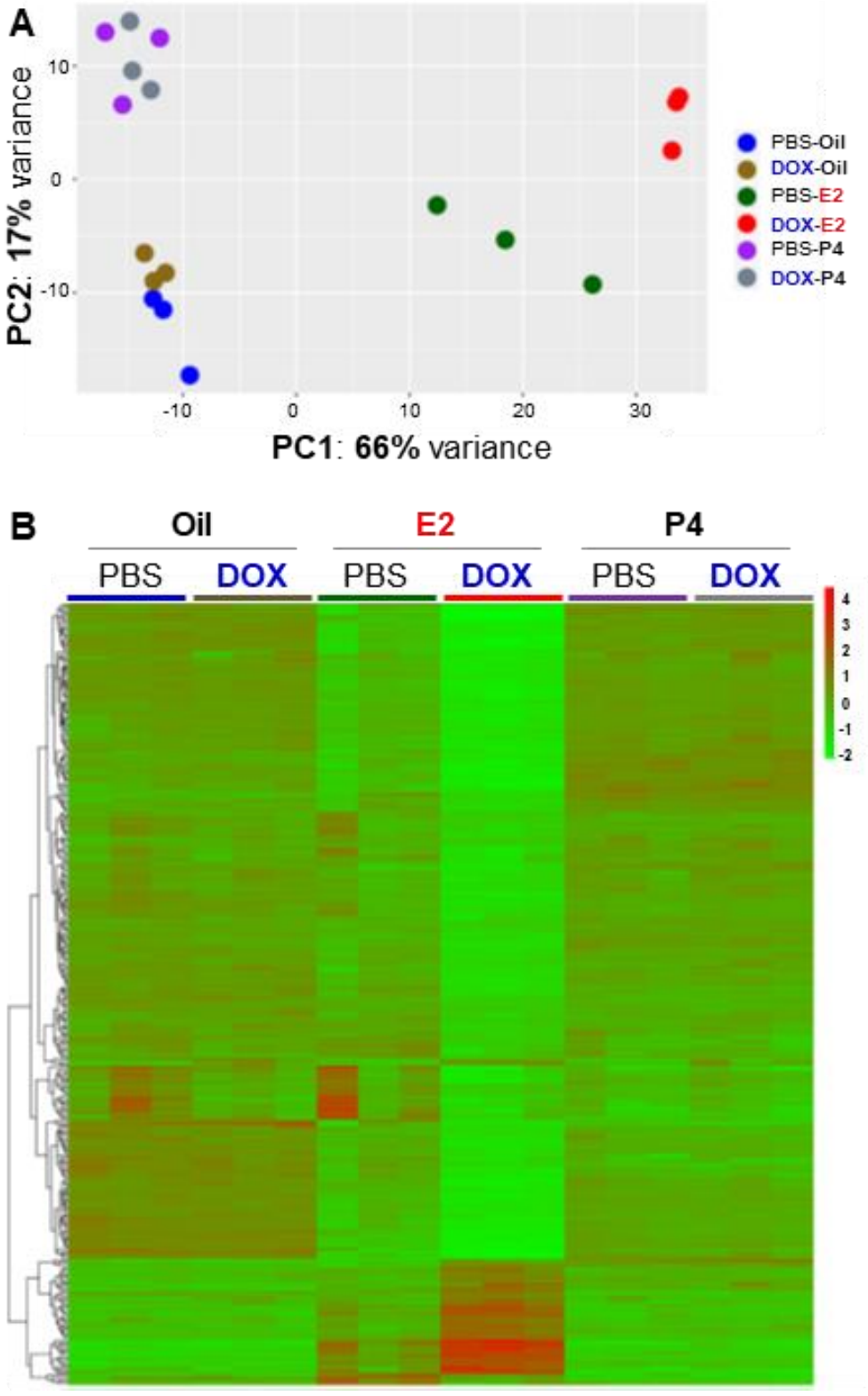

CHAPTER 4

CHANGES TO UTERINE RECEPTIVITY IN RESPONSE TO CHEMOTHERAPY TREATMENT DURING ADOLESCENCE[1]

[1]Andersen, C.L., Byun, H., Xiao, S., and Ye, X. 2021. *To be submitted to Toxicological Sciences.*

Tentative Title

Changes to uterine receptivity in response to chemotherapy treatment during adolescence

Running head

Chemotherapy and uterine receptivity

Key words

Doxorubicin (DOX), uterus, implantation, oncofertility, receptivity

Christian Lee Andersen[1, 2], Haeyeun Byun[1], Shuo Xiao[3], and Xiaoqin Ye[1, 2, #]

[1] Department of Physiology and Pharmacology, College of Veterinary Medicine, University of Georgia, Athens, GA 30602, USA; [2] Interdisciplinary Toxicology Program, University of Georgia, Athens, GA 30602, USA; [3] Department of Pharmacology and Toxicology, Ernest Mario School of Pharmacy, Rutgers University, Piscataway, NJ 08854, USA

Grant support

R03HD097384 and R03HD100652 (XY)

[#] Corresponding author

Xiaoqin Ye, M.D., Ph.D., 501 DW Brooks Dr., Department of Physiology and Pharmacology, College of Veterinary Medicine; Interdisciplinary Toxicology Program, University of Georgia, Athens, GA 30602, USA (Tel: 1-706-542-6745; E-mail: ye@uga.edu; ORCID: 0000-0002-1037-9005)

Abstract

The number of childhood (from birth to adolescence) cancer survivors increases because of increased cancer incidence and decreased mortality rate from cancer therapy. A unique side effect of concern on these cancer survivors from cancer therapy (e.g., chemotherapy and radiotherapy) is fertility impairment. Some chemotherapeutics drugs have been shown to target ovarian follicles to impair female fertility. The gonadotoxic effect on female fertility can be circumvented by cryopreservation of ovarian tissues, oocytes, and/or embryos coupled with in vitro fertilization-embryo transfer (IVF-ET). The rate-limiting step for IVF-ET success is embryo implantation, in which the uterus transiently transforms into a receptive state for an embryo to implant. Uterine receptivity is under the control of ovarian hormones estrogen (E2) and progesterone (P4). We showed that a single, human-relevant dose of doxorubicin (10 mg/kg, single dose) in young adult ovariectomized CD-1 mice had a long-term effect on uterine transcriptome to E2 treatment (Andersen CL *et al*, 2018). Since some of the differentially expressed genes are associated with uterine receptivity, we hypothesize that chemotherapy could disrupt uterine receptivity for embryo implantation. To test this hypothesis, C57BL6J mice are ovariectomized on postnatal day (PND) 23 to remove the indirect effect of ovarian toxicity on the uterus, then treated with vehicle (negative control), doxorubicin (2 mg/kg, 5 daily doses), or doxorubicin (10 mg/kg, single dose, positive control starting on PND30. Decidualization is a uterine response to an implanting embryo and an indication of uterine receptivity. We use artificial decidualization to determine uterine receptivity as following: Beginning on PND56, mice are treated with ovarian hormones E2 and P4 to establish a receptivity uterus; one PND63, mice are given an intraluminal uterine oil (mimicking embryos) injection to induce artificial decidualization, which is detected using a blue dye reaction on PND64. Preliminary data show that the above chemotherapeutic

regimens have varied adverse effects on uterine receptivity. Uterine transcriptomes will be determined to uncover molecular mechanisms of chemotherapy on uterine receptivity. We are filling in the knowledge gap about long-term effects of chemotherapy during childhood on uterine receptivity in adulthood.

Introduction

Cancer incidence among adolescents and young adults (AYA) has steadily risen, with a corresponding decrease in cancer deaths of these patients (Bleyer *et al.*, 2017; Miller *et al.*, 2020). It is estimated that about 100,000 children, adolescent and young adults will be diagnosed with cancer in 2021 and the incidence rates among female patients is outpacing that of their male counterparts (Henley *et al.*, 2020). A particular concern for younger cancer patients is the prominent gonadotoxcity of cancer therapies, such as radiotherapy and chemotherapy (Levine, 2012; Massarotti *et al.*, 2019; Allen *et al.*, 2020; Szymanska, Tan and Oktay, 2020). The field of oncofertility, first coined in 2006 by Dr. T. Woodruff, has quickly aimed to fill the gap in our understanding of methods to preserve fertility in young cancer patients (Levine, 2012; Tomao *et al.*, 2016; Anazodo *et al.*, 2018; Harada and Osuga, 2018; Moravek *et al.*, 2019). The female reproductive tract relies on coordination between multiple organs to facilitate fertility, in which the ovaries, the Fallopian tubes (oviducts in mice), and the uterus are the physical sites for supporting pregnancy events. In premenopausal cancer patients, gonadotoxic trauma can lead to fertility impairment (Green, Sklar and Boice, 2009; Chow *et al.*, 2016). Specifically, special focus has been given to the mechanistic understanding of follicle loss associated with chemotherapy treatment, through mechanisms involving follicular atresia and overactivation, primordial follicle apoptosis, and reduced secretion of 17beta-estradiol from follicular cultures (Ben-Aharon *et al.*, 2010; Xiao, Zhang, *et al.*, 2017; Wang *et al.*, 2018; Y. Wang *et al.*, 2019; Szymanska, Tan and Oktay, 2020). However, little attention has been given to assessing potential effects in disrupting uterine functions despite epidemiological data suggesting that the uterus could be a target of certain chemotherapy regiments (Griffiths, Winship and Hutt, 2020). The uterus plays a critical role in early pregnancy events, as it is the only site capable of supporting an embryo to term. After

ovulation the embryo will be fertilized and travel towards the uterus. Around D3.5, embryos enter the uterus, separate along the uterine horn, shed the zona pellucida, and during the evening will begin implanting into the uterine luminal epithelium (Yoshinaga, 2013). Events surrounding implantation are extensively reviewed by Ye, X., 2020 (Ye, 2020). Almost immediately after implantation the stromal layer begins to rapidly decidualize, as stromal cells differentiate to decidual cells and form the primary decidual zone. Increased vasculature from the mesometrial blood vessel will begin to invade towards the implantation site to support the embryo (Ramathal *et al.*, 2010). While the uterus is critical to natural pregnancy, the uterus is also critical for fertility preservation methods, like *in-vitro* fertilization and embryo transfer (IVF-ET), as the embryo must be returned to the uterus for pregnancy to occur (Dekel *et al.*, 2014). This has left a significant knowledge gap in our understanding of the effect's chemotherapy can have on uterine function, like implantation and menstruation in women. Limited epidemiological data suggests that patients who were treated with chemotherapy and radiotherapy have increased incidence of preterm birth and low birth weight infants even when donor oocytes are used, suggesting that off-target effects in the uterus could alter functions related to pregnancy. Little data exists with a targeted, in-vivo analysis of long-term consequences from chemotherapy treatment during comparable AYA years in rodents (Griffiths, Winship and Hutt, 2020).

Doxorubicin is a commonly-prescribed, broad-spectrum anthracycline chemotherapy. Doxorubicin (DOX, Adriamycin, a cytotoxic anthracycline antibiotic) is a commonly used chemotherapeutic agent in premenopausal cancer patients (Krischke *et al.*, 2016; Iwamoto *et al.*, 2020). DOX is listed as a topoisomerase inhibitor, suggesting that it prevents the availability of uncoiled DNA for replication needed in malignant cancer cells, as well as interactions with topoisomerase that lead to DNA-cleavable complexes that promote cytotoxicity. However,

multiple mechanisms of action have become evident in years following initial studies. DOX has been shown to directly bind to nucleotides which prevent DNA/RNA polymerases further aiding in the primary mechanism of action. DOX can also bind to cell membrane lipids to play an important role in cell death (Thorn *et al.*, 2011; FDA, 2013; Wei *et al.*, 2015). DOX chemotherapy increases the risk for cardiovascular diseases, which could be partially contributed by oxidative stress-induced endothelial dysfunction in the conduit arteries, suggesting that DOX could disrupt important angiogenic events during early pregnancy (Clayton *et al.*, 2020). Since off target effects of DOX exists, it is important to understand how those could present themselves in uterine health.
Uterine stem cells/uterine lining thinning

Understanding the potential for chemotherapeutic drugs to target the uterus requires careful experimental design. Uterine health and function rely on hormonal support from the ovaries. Follicles and the corpus luteum provide necessary progesterone and estradiol to support uterine gene regulation and important signaling events that aid in various uterine functions (H Wang and Dey, 2006; Diao *et al.*, 2011, 2015; S. Zhang *et al.*, 2013; Hewitt, Winuthayanon and Korach, 2016; Soleilhavoup *et al.*, 2016). Little *in-vivo* data on the ability for chemotherapeutic drugs to alter uterine mechanisms and functions exist (Nishi *et al.*, 2018; Samare-Najaf, Zal and Safari, 2020). However, both the studies left the ovaries intact during chemotherapy treatment, creating a confounding effect between known gonadotoxcity and downstream effects seen in the uterus. Any conclusion made on changes to molecular mechanisms regulating uterine function cannot be explicitly tied to chemotherapy treatment, furthering the knowledge gap in this field. Nishi et al. also had extensive differences in animal weight, an important factor in understanding the individual variations involved in absorption, deposition, metabolism and excretion of chemotherapeutic drugs, specifically DOX (Rodvold, Rushing and Tewksbury, 1988; Gurney,

2002). Using ovareictomized mice to control for confounding effects, we showed that a human relevant (10 mg/kg bw I.P.) dose of DOX changed the uterine response to estrogen 1 month after treatment (Andersen *et al.,* 2019). While highlighted as the only *in-vivo* data to unequivocally show that DOX can target the uterus and alter mechanism associated with uterine function, this preliminary research did not include the uterine response to both estrogen and progesterone, a critical omission (Griffiths, Winship and Hutt, 2020). Preliminary RNAseq data using uterine tissues during D1.5 and D3.5 provided a dataset of important genes necessary for uterine preparation for embryo implantation. Combined with data previously published by our group, we generated a list of E2-responsive genes important for uterine preparation for implantation and differentially regulated by DOX. This provided molecular mechanisms behind potential DOX disruption of uterine receptivity. To investigate the hypothesis that DOX could disrupt uterine preparation for embryo implantation, we utilized artificial decidualization as a functional measurement of uterine receptivity. Artificial decidualization (AD) mimics the normal process of decidualization but allows us to remove the ovary and follicles which have been previously shown to be negatively affected by DOX (Andersen, C.L. et al. submitted BoR 2021). Because implantation and decidualization is associated with increased vascular permeability at sites of contact with uterine luminal epithelium, AD can be visualized using an injection of absorbable dye, Evan's blue dye (Cha *et al.,* 2018). Progesterone is needed for the full extent of estrogen action to occur in the uterus (Wetendorf and DeMayo, 2012). Proper estrogen and progesterone signaling is critical for implantation in both humans and mice, as well as key in proper regulation of the endometrium during estrous and menstrual cycles (Dey and Lim, 2006; Nowak, 2018). We hypothesize that DOX can disrupt uterine mechanisms associated with the functional uterine receptivity in C57Bl6 mice. In aim 1, we investigate the effect DOX has on uterine receptivity

using an artificial decidualization model to serve as a functional endpoint of a receptive uterus. In aim 2, we evaluate the uterine response to estrogen and progesterone to determine the molecular mechanisms associated with the uterus during the window of implantation.

Materials and methods

Animals. C57BL/6 female and male mice (6 weeks old) were purchased from the Jackson Laboratory (Ellsworth, Maine). They were acclimated to the Coverdell animal facility at the University of Georgia for 2 weeks with body weight monitored twice a week to ensure well acclimation to the new environment. At 8 weeks old, the acclimated females were mated with littermate males. Subsequent litters from these initial breeding pairs were used either as breeders or as experiment mice, no runts or alphas were used based on weaning body weight. Juvenile mice were weaned at PND 21 and allowed to acclimate for 2 days. The Coverdell animal facility is on a 12-hour light/dark cycle (6:00 AM to 6:00 PM) at 23 ± 1 °C with 30–50% relative humidity. All mice had free access to regular chow 5053 (Labdiet, St. Louis, MO, USA) and water. All methods used in this study were approved by the University of Georgia IACUC Committee (Institutional Animal Care and Use Committee) and conform to National Institutes of Health guidelines and public law.

Dose selection: In humans, the recommended dosing of DOX follows a 21-28 day 40-60 mg/m^2 cycle and maximal 4 cycles based on patient information (age, body weight, disease status, etc.) and cancer type (Misset *et al.*, 1999; FDA, 2013; Völler *et al.*, 2017). In this study we used a single intraperitoneal (i.p.) injection of 10 mg/kg body weight of DOX in mice as a positive control (Xiao, Zhang, *et al.*, 2017; Wang *et al.*, 2018; Andersen *et al.*, 2019; Y. Wang *et al.*, 2019). We also used a multiple dose treatment cycle using 5 daily doses of DOX at 2 mg/kg to mimic multiple treatments seen in human dose regiments. Based on FDA animal-human dose conversions, 10

mg/kg in adult mice is equivalent to ~30 mg/m^2 in adult humans, which is within the clinically used chemotherapy dose range (Nair and Jacob, 2016).

Treatment timing: Increased detection of malignant cancers and greater access to chemotherapy has reduced the age which patients first undergo treatment. Our current goal was to examine chemotherapy exposure during pre-pubertal years and how those effects translate to the future reproductive health of patients during AYA and reproductive years (Figure 4.1).

Ovariectomy: On assigned OVX timepoint, virgin mice are weighed and given 100 uL injection of 2 mg/kg Meloxicam (Covetrus, 6451602845) 15 min. prior to surgery. Briefly, mice are induced using vaporized isoflurane () at 3% isoflurane/oxygen and flow rate of 1 L/min and maintained at 1.75%. The surgical site is shaved and cleaned with 70% isopropyl alcohol. A single cut is made through the skin and muscle layer dorsally, about 1-2 cm from the spine on either side. A small cut is made in the peritoneal layer and the ovaries are immediately visible. The ovaries are removed and the peritoneal cavity is sealed using a single, simple interrupted suture. A wound clip is used to close the skin. A more detailed protocol is available in the supplementary section.

DOX treatment: DOX (D-4000, LC Laboratories, Woburn, MA) was dissolved in DMSO to make a stock at 100 mg/ml, aliquoted, and kept at -20°C. A thawed aliquot was kept at 4°C and used within 3 days of thawing. On PND23 females were randomly assigned into three groups to receive a single i.p. injection of vehicle control (100 μl of <2% DMSO in sterile 1x PBS, the % of DMSO was the same as that in DOX-treated group), DOX-10 (10 mg/kg, mouse body weight (kg) x 10 mg/kg (final dose) / 100 mg/ml (stock concentration) = ml of stock solution diluted into sterile 1x PBS in 100 ul), or DOX-2 (2 mg/kg/day over 5 days, mouse body weight (kg)). Number of animals in each group and aim can be found in Table 1. PBS and DOX-

10 mice received 100 uL sterile 1x PBS injection from PND24-27 to mimic sustained treatment in DOX-2 group. Although it is unclear about the half-life of DOX in the mouse ovaries via i.p. injection, studies reported a half-life of DOX ranging from 11 hours to 45 hours in different mouse tissues upon a single i.p. injection of 11-12 mg/kg (Siemann and Sutherland, 1979; Johansen, 1981). Our treatment cycle will evaluate the toxicity of DOX on the uterus in response to a bolus dose or multiple lower doses.

Hormonal dose: On PND 56-58, ovariectomized mice in all four groups in both Set A and Set B will undergo hormonal priming (s.c. injection): 100 ng E2 daily on PND56-58; no treatment on PND59-60; 10 ng E2 + 1 mg P4 daily on PND61-63 (Fig. X.1) as previously described (Diao, Xiao, Li, *et al.*, 2013; Andersen *et al.*, 2019).

Artificial decidualization and Aim 1 dissection: On PND63, the hormonally primed mice will undergo oil infusion in the dorsal right side uterine lumen as we described previously (Diao *et al.*, 2010, 2011; Diao, Xiao, Howerth, *et al.*, 2013; Xiao, Li, *et al.*, 2017). On PND64 ~11:00-12:00 h (corresponding to D4.5 in natural pregnancy), the mice will be injected with blue dye to detect early decidualization and uterine images will be taken. Observations on the amount of fat pad are made. Each uterine horn will be cut into segments with blue bands (if there is any) distributed for histology (fixed in 10% formalin) and gene expression (flash-frozen in liquid N_2 and stored at -80^{o}C). The % of mice with clear or faint blue bands, indicating on time or delayed uterine receptivity, respectively, will be recorded (Diao, Xiao, Howerth, *et al.*, 2013; Xiao, Li, *et al.*, 2017). Liver and spleen are flash-frozen in liquid N_2 and stored at -80^{o}C to serve as a control for chemotherapy treatment and determine individual response to chemotherapy treatment (Jadapalli *et al.*, 2018).

Aim 2 dissection: On PND63, 6 hours after hormonal treatment, mice are euthanized. In mice, a surge of estrogen around 11:00 hrs on GD3.5 (GD0.5 is defined as the day a copulatory plug is found), with the window of implantation (WOI) beginning shortly (within 6 hrs) after (Hirota, 2016; Ye, 2020). We have timed our experimental timeline to collect tissue for understanding the mechanisms associated with the WOI and uterine receptivity. The uterine horns are removed, a small section is fixed in 10% formalin for histology and the rest is flash-frozen in liquid N_2 and stored at -80^{o}C for RNAseq.

Serum hormone analysis: Serum was collected from the blood samples after clotting at room temperature for 45 minutes and stored at -80°C. Serum P4 and E2 were measured in the Ligand Assay and Analysis Core of the Center for Research in Reproduction at the University of Virginia (Charlottesville, Virginia).

Histology: Dark blue bands were excised from the oil injected uterine horn for fixation, while the uterine region closest to the oviduct was used for the non-injected uterine horn. Uteri were fixed at 27°C for 24 hrs then placed in 70% ethanol at 4C until dehydration. Uteri were dehydrated and embedded longitudinally. Paraffin sections (6 µm) were cut until the lumen was visible and H&E staining was performed as previously described (Diao *et al.*, 2015).

Alkaline Phosphatase activity assay: Alkaline phosphatase (AP) is exclusively upregulated in the primary and secondary decidual zone of implantation sites and a hallmark of decidualization (Herington *et al.*, 2009; Lei *et al.*, 2013; Fullerton *et al.*, 2017). Frozen uteri sections containing blue-dye were split and sectioned (6 µm). Briefly, frozen sections were fixed in 4% PFA for 15 minutes, then washed in 1X PBS for 2X5 minutes. Slides were then washed in 0.1 M Tris-HCL (pH 9.5) for 2X5 minutes. BCIP/NBT (Sigma Aldrich, 72091) assay working solution was prepared as recommend by manufacturer. Slides were incubated at 55C for 25 min with working

solution and routinely monitored for coloration. Samples from both the oil stimulated and non-stimulated side (negative control) were used for reference. Sections were rinsed in 0.1 M Tris_HCL (pH 9.5) for 2X5 minutes and mounted with glycerol for imaging.

Total RNA isolation for RNAseq and gene expression: Frozen uteri were homogenized in liquid N2 with mortar and pestle, then transferred to TRIzol Reagent (Ambion, 15596-026) and dissolved. Total RNA was extracted using RNA Purification Kit (Invitrogen, 12183555) according to manufacture's protocol.

RNAsequencing: Transcriptomic analysis was performed by the Georgia Genomics and Bioinformatics Core (Athens, GA). RNA integrity was assessed using Agilent Bioanalyzer. 2x150bp paired-end read length is sequenced on NextSeq500 platform.

RNAseq analysis: FASTQ files were downloaded from Illumina's BaseSpace cloud storage service. Currently there are many methods for analyzing RNA-seq data. The pipeline created by Pertea et. al. was selected to analyze the uterine transcriptome. Raw reads first underwent a quality control step to analyze potential biases introduced within the sequencing step or library generation. Reads wear trimmed of the Illumina adapter sequences. HISAT2 was used for alignment to GRCm8 reference genome index. The murine reference assemblies were downloaded from the prebuilt indexes found at the Johns Hopkins University Center for Computational Biology. The indexes and FASTQ files were stored on the University of Georgia's cluster computing network housed at the Georgia Advanced Computing Resource Center. Transcripts were assembled, again using the reference genome, and merged into a single, comprehensive file using StringTie. This merged reference was used to estimate abundances of transcripts on the original assemblies. Lastly, the Ballgown package in R was used to perform differential expression at both the gene and transcript level. The alignment and assembly were run as a single BASH script using the parallel-

processing computer network of the Georgia Advanced Computing Resource Center, methods previously described (Andersen *et al.*, 2019).

Statistical analysis: Data are presented as dots or mean±SD where applicable. A linear mixed model fit by REML using Satterthwaite's method was used to analyze the percent weight change from PND23-64. The percent weight change data were analyzed in R (Version 4.0.2, package lmerTest 3.1-3). Chi-squared test was used to test the correlation between treatment group and blue dye accumulation.

Results

Effects of DOX treatment on body weight

C57Bl6/J mice were all between 9.0-9.4 weeks of age at dissection. Mice were initially weighed at PND23 before ovariectomy, then weighed at PND30, 37, 44, and 64. DOX treatment significantly reduced percent body weight gain 1 week after treatment (week2) (Figure 4.2, A) compared to PBS control. Control mice had an average percent weight gain of 20.1 ± 9.1, while DOX-2 had an average percent weight gain of 9.97 ± 7.6 ($p = .0217$) and DOX-10 had even more reduction with -0.79 ± 12.4 ($p < .0001$). By week 3 and week 6 DOX treated mice had comparable percent weight gain as control. These effects are likely due to the immediate effect to weight loss observed 1-day post-treatment (Andersen, C.L. et al. 2021 submitted BoR). While mice quickly gain weight comparable to control 2 and 3 days after treatment, the effects to the fat pad could persist to keep raw weight significantly below control levels at PND37, 44, and 64 in the DOX-10 group (Figure 4.2, B).

Effects of DOX treatment on blue dye accumulation

During early pregnancy, around the mid-late morning of D3.5, a spike in E2 induces changes to the uterus to initiate the window of implantation (WOI). Fundamental changes include

increasing uterine blood flow and invasion of the arteries in the mesometrial fat pad (Maliqueo, Echiburú and Crisosto, 2016). Once implantation begins further invasion and formation of the early spiral artery occur. This increased vasculature can be observed by using an absorbable blue dye that will preferentially collect at sites of uterine stimulation during the WOI, where significant increased vascular permeability is present (Cha *et al.*, 2018). Upon dissection, uterine images were collected to observe the blue dye reaction. All 8 PBS mice had significant blue dye reaction in the oil stimulated uterus, however, a subset of mice in the treatment groups did not have blue dye accumulation in the oil stimulated uterus (Figure 4.3 A and B). In the DOX-2 group, 56% of mice had blue dye accumulation in the oil stimulated uterus, while in the DOX-10 group had 50% (Figure 4.3 B). A trend towards the DOX-10 group being correlated with the absence of blue dye was found using a Pearson's chi-squared test (p=.06). These observations indicated that DOX can have effect on the uterus to prevent decidualization as a marker for uterine receptivity.

Primary decidual zone histology

After collection of uterine images, dark blue bands were excised from the uterus and fixed for histology. Multiple sections were collected to insure ample coverage of the site of increased vascular permeability signifying the decidual area. Some latitudinal sections were taken to insure ample coverage of uteri without blue dye accumulation (Data not shown). Key events during implantation and decidualization cause structural changes to the site of contact with the blastocyst or oil droplet (reviewed in Chapter 1). Briefly, the LE will dissolve to allow access to the underlying stromal region, the uterine lumine will close, edema will be present in the stromal area, and stromal cells will undergo differentiation to decidual cell, which is characterized by swelling of the cytoplasm. In the PBS group, histology from the oil injected horn shows typical characteristics of an implantation. Edema of the stromal region can be seen (area of white in the

stromal region near myometrium, Figure 4.4 B1 and D1), as well as accumulation of decidual cells near the incased oil droplet (Figure 4.4 B3). Both are absent in the control uterine horn. Similar changes were observed in DOX treated animals, however a subset of animals had uteri similar to metestrus or diestrus (Figure 4.4 F1).

Discussion

Doxorubicin (DOX) is a widely used chemotherapeutic agent. A major side effect of DOX is intestinal mucositis. We observed significant alterations to mouse body weight and percent body weight gain throughout the experimental timeline. Significant reduction in body weight was observed in the DOX-10 group till dissection, indicating that the single dose at PND30 contributed to lasting effects on body weight, but not percent body weight gain. During dissection DOX-10 mice were noted as having a limited uterine fat pad compared to control animals (data not shown). The I.P. injection of DOX at 10 mg/kg could cause adipocyte apoptosis in the fat pad, which can lead to alterations to proper body weight gain (Faust, Johnson and Hirsch, 1976; Batatinha *et al.*, 2014). Of the 3 mice with the most drastic reduction to percent body weight gain and lowest PND64 bodyweight, 2 of them had the most intense blue dye reaction indicating that DOX weight effects did not correlate with uterine defects (data not shown).

Reductions in blue dye accumulation in the oil injected uterine horn of DOX treated mice could be due to disruptions to uterine vasculature that stims from the mesometrial fat pad. As previously stated, reductions in fat pad were observed in DOX treated animals. Fat pad observations were not a goal of the experimental procedure and were only noted after observations seen during dissection. No data exists on how depletions in the uterine fat pad could lead to disruptions to uterine health, but it was observed that the loss of the ovarian fat pad reduced ovarian hormonal steroids in circulation (Wang *et al.*, 2017). Further investigations into loss of

uterine/ovarian fat pads and uterine health are needed. It has been observed that DOX causes disruptions to endothelial cells and microvasculature of other reproductive tissues (Andersen, C.L., et al. 2021 submitted BoR).

Observations of reduced blue dye accumulation in DOX treated uteri after oil stimulation, along with previously published data on the effects to uterine gene expression after DOX treatment, provide evidence that continued investigations of the molecular mechanisms behind DOX targeting of the uterus is needed. During our experiment, uterine tissue from mice treated with hormones similar to the artificial decidualization timeline without the intraluminal uterine oil injection were collected. These tissues will be used for transcriptomic analysis to investigate molecular mechanisms associated with DOX targeting of the uterus. Previous data found that DOX altered the uterine transcriptomic response to E2. However full E2 signaling in the uterus is only partial regulated by ERa, P4 is also necessary for maximal response to E2 (Wetendorf and DeMayo, 2012). Future plans to analyze the transcriptomic data are not within the scope of this dissertation but are needed to answer questions posed above.

Previous analysis of DOX effects on the female reproductive tract found significant alterations to molecular mechanisms associated with uterine health and function, however due to confounding effects of intact ovaries little insight can be gained on direct uterine effects (Nishi *et al.*, 2018; Samare-Najaf, Zal and Safari, 2020). Significant reduction in uterine *Era* gene expression was seen, similar to previous results published by our group (Andersen *et al.*, 2019; Samare-Najaf, Zal and Safari, 2020). However no functional outcomes were tested. We hypothesize that DOX treatment prior to OVX could provide protective effects to the uterus through ovarian steroid hormone actions. To test this aim, we will use the exact same experimental procedure but include a group that is treated with DOX at PND23 and ovariectomized the

following week, then test functional uterine receptivity through artificial decidualization and compare to the initial set of animal presented above.

In summary, we identify the uterus a target for DOX toxic action during the critical time of uterine receptivity. Molecular mechanisms associated with reduced blue dye accumulation in a subset of DOX treated mice are yet to be investigated, but data and tissues collected during this experiment aim to fill those holes. This study fills in the knowledge gap about toxic effects of chemotherapy on the uterus and provides critical information for risk assessment of chemotherapy in female reproduction.

Conflicts of Interest (COI)

The authors declare that there is no applicable COI.

Data Availability Statement

All the data are available upon request.

Acknowledgements

The authors thank the Office of the Vice President for Research, Interdisciplinary Toxicology Program, and Department of Physiology and Pharmacology at the University of Georgia, and the National Institutes of Health (NIH R03HD100652 and R03HD097384 to XY) for financial support. Serum P4 and E2 levels were determined at The University of Virginia Center for Research in Reproduction Ligand Assay and Analysis Core, which is supported by the Eunice Kennedy Shriver NICHD/NIH (NCTRI) Grant P50-HD28934.

Figure Legend

Figure 4.1. Experimental timeline. Descriptions of treatment groups and aims.

Figure 4.2. Weight effects of Doxorubicin treatment. A) Percent weight change (per week) during the experimental protocol. Significant reductions in percent weight gain were observed at

week 2 (1 week post-treatment), however mice quickly recovered to comparable levels. B) Weight of mice during experimental protocol. Significant reductions in body weight were seen at PND37 in both DOX-2x5 and DOX 10x1, while those reductions continued throughout the protocol in DOX 10x1. *p< 0.05; #p<.001.

Figure 4.3. Effect of DOX on blue dye accumulation during artificial decidualization. A) Uterine images taken at dissection. All PBS mice showed blue dye accumulation in the oil injected uterine horn, while a subset of mice in both treatment groups did not show blue dye accumulation. B) Percent blue dye or no blue dye in each treatment group (PBS: 100% blue dye, 0% no blue dye; DOX-2x5: 56% blue dye, 44% no blue dye; DOX-10x1: 50% blue dye, 50% no blue dye). A chi-square test found trending significance in the correlation of treatment group with blue dye accumulation (p=.06)

Figure 4.4. Histological analysis of area of blue dye accumulation. A1, A2, A3: PBS un-injected uterine horn (control). B1, B2, B3: PBS uterine horn that received oil injection. C1, C2, C3: DOX-2x5 un-injected uterine horn (control). D1, D2, D3: DOX-2x5 uterine horn that received oil injection. E1, E2, E3: DOX-10x1 un-injected uterine horn (control). E1, E2, E3: DOX-10x1 uterine horn that received oil injection. Green arrow heads show areas of decidual cells (large, circular), black arrow head show area of LE dissolving.

FIGURES

Figure 4.1

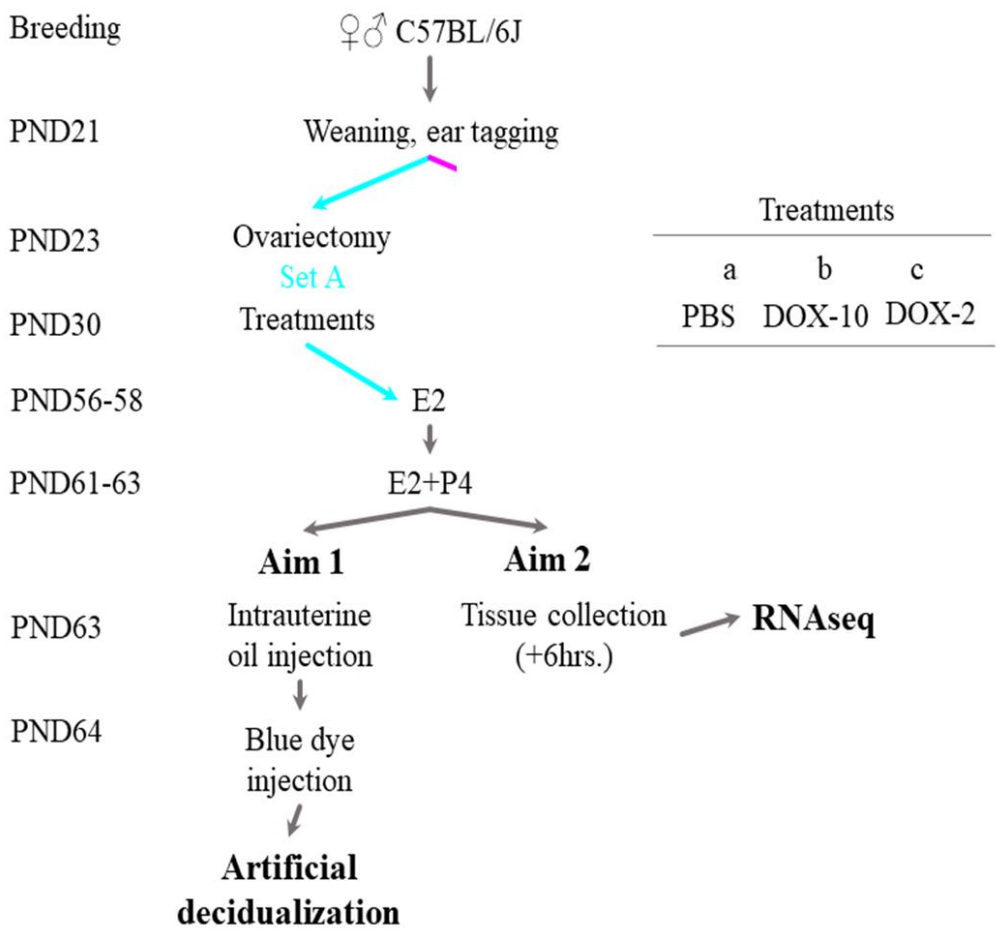

Figure 4.2

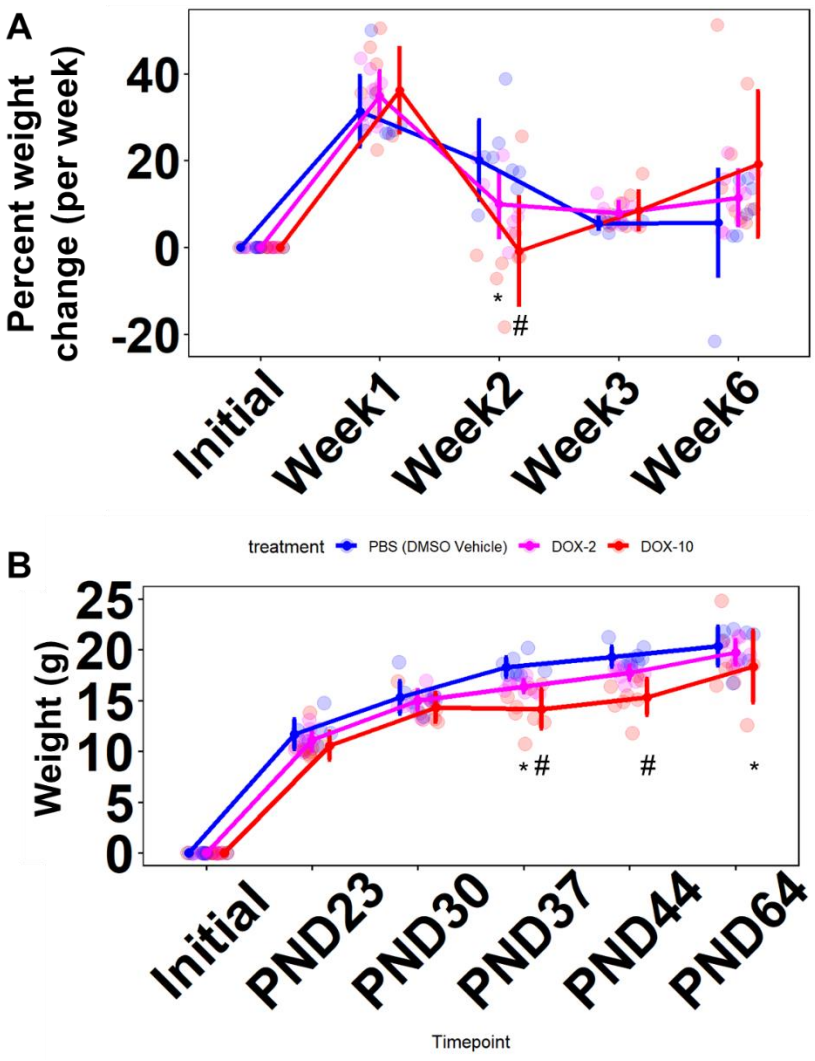
A
Percent weight change (per week)
40
20
0
-20
*
#
Initial
Week1
Week2
Week3
Week6
treatment
PBS (DMSO Vehicle)
DOX-2
DOX-10
B
Weight (g)
25
20
15
10
5
0
* #
#
*
Initial
PND23
PND30
PND37
PND44
PND64
Timepoint

Figure 4.3

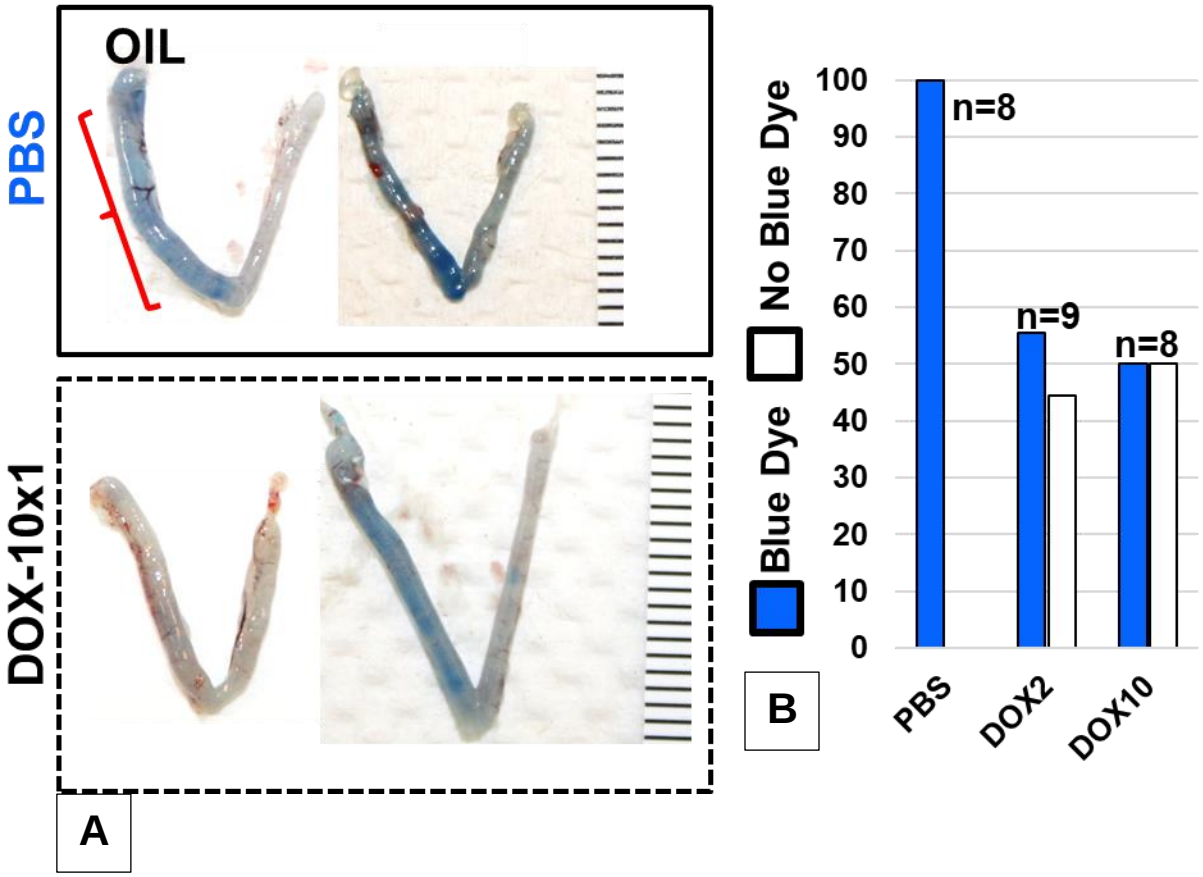
OIL
PBS
DOX-10x1
A
B
No Blue Dye
Blue Dye
100
90
80
70
60
50
40
30
20
10
0
n=8
n=9
n=8
PBS
DOX2
DOX10

Figure 4.4

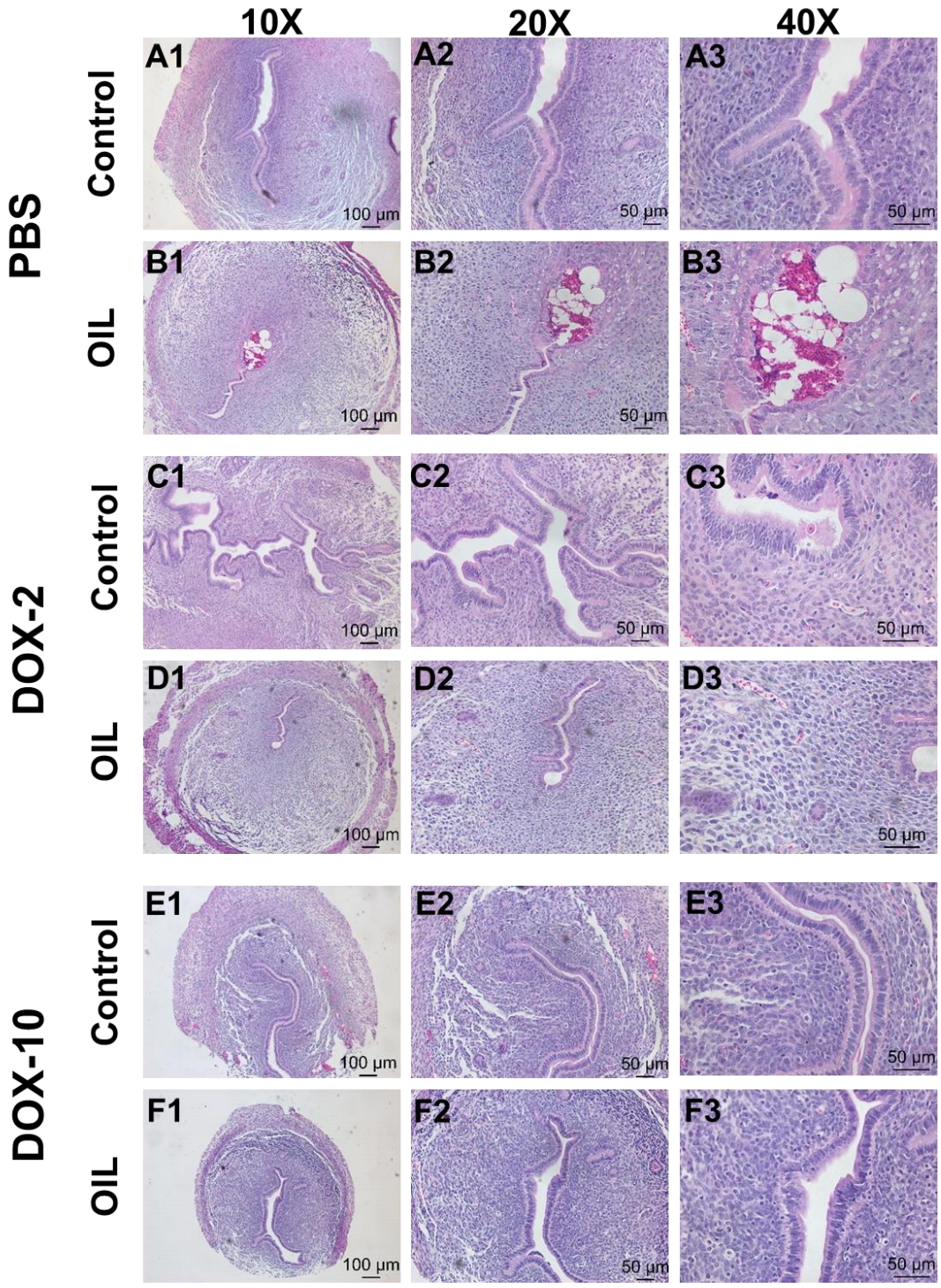
10X
20X
40X
PBS
DOX-2
DOX-10
Control
OIL
A1
A2
A3
B1
B2
B3
C1
C2
C3
D1
D2
D3
E1
E2
E3
F1
F2
F3
100 µm
50 µm

CHAPTER 5

Summary and future directions

The goal of the dissertation research presented was to fill knowledge gaps in our understanding of how chemotherapeutic drugs may target aspects of the female reproductive tract to influence fertility. Millions of prepubescent girls and reproductive aged women suffer from cancers. A unique side effect of concern from anti-cancer treatments, including chemotherapy and radiotherapy, in premenopausal cancer patients is fertility impairment. Oncofertility thus becomes an emerging discipline with the expressed goal to protect the future reproductive health of cancer patients. Prominent gonadotoxicity of chemotherapeutic drugs has focused the oncofertility field on effects in the ovary, primarily on the follicles. The follicle is the functional unit of the ovary and is home to the reserve of oocytes necessary for fertilization, but the ovary is a heterogenous organ. CL development and maintenance is critical for pregnancy establishment hypothesized that DOX affects corpus luteum function, through aberrations of luteal and endothelial cell functions, and effects ovarian hormone signaling in the uterus, disrupting mechanisms needed for uterine receptivity. The published research and draft manuscripts offer compelling evidence that chemotherapy can target both the CL and uterus, information previously unknown to the field of oncofertility.

Chapter 2 focused on the molecular mechanisms in the CL associated with P4 reductions observed during early pregnancy. Using a well-studied model and treatment post-ovulation, we targeted acute effects of DOX on CL development and function. We identify multiple effects of DOX treatment in the preimplantation CLs. Both endothelial cells and luteal cells are targeted.

There are three types of effects from DOX treatment during early pregnancy: 1) effects are present in all DOX-treated CLs but not correlated with the key function of CLs in P4 steroidogenesis, such as lipid droplet accumulation and disrupted cytoskeleton; 2) effects varied greatly and are correlated with P4 levels, such as StAR expression in the luteal cells and impaired morphology of luteal cords, which are surrounded by endothelial cells; and 3) varied effects un-correlated with P4 levels, such as body weight change on D1.5. While an inbred mouse (C57BL6/J) was used for these studies, significant individual variation in the timing of ovulation and thus CL formation could contribute to the varied effects observed. Future work should use a separate model, such as superovulation using immature mice to better sync ovulation timing to ensure effects seen are due to individual variation of DOX sensitivity and not due to differences in ovulation timing. The molecular mechanisms for DOX-induced effects, e.g., reduced StAR expression, in the CL remain to be investigated. While DOX may not directly disrupt mitochondria formation, reductions in the cristae (not observed here) could contribute to reduced StAR expression. Future work should examine aspects of luteal cord formation and regulation of the microvasculature in the CL, such as spatiotemporal expression of pericyte markers and vascular endothelial growth factor (VEGF) that are critical for vasculature establishment. There is extensive published work on DOX induced lipid droplet accumulation in various cell types and tissues, as well as reductions in genes important in lipid droplet metabolism (hormone sensitive lipase, HSL) (Mehdizadeh *et al.*, 2017; Shyu Jr *et al.*, 2018; Mentoor *et al.*, 2020). These mechanisms appear to be cell specific and further investigations into the effects in luteal cells, such as ROS generation, is warranted. Further, DOX has been shown to be toxic to follicles, follicles that do not undergo atresia or apoptosis from DOX treatment will eventually form a corpus luteum. Based on preliminary data presented here, it is important to understand how DOX effects on the follicle could alter CL development, maintenance

and function potentially disrupting cycles even after exposure. This would answer the question, *how well do remaining follicles maintain luteinization competency years after exposure if the follicle is selected for ovulation?* This study fills in the knowledge gap about toxic effects of chemotherapy on the CL and provides critical information for risk assessment of chemotherapy in female reproduction.

Chapters 3 and 4 focused on DOX targeting of important aspects to uterine function and health. Chapter 3 examined the long-term uterine response to ovarian hormones, critical to early pregnancy and fertility, after DOX treatment. The manuscript published from the work in Chapter 3 was highlighted as being the only data available on *in-vivo*, targeted effects DOX can have on the uterus. A stated goal of this dissertation was to fill knowledge gaps in the field of oncofertility, therefore we made the data publicly available from this project in hopes it will be used to provide preliminary data on the potential for DOX to target the uterus. Our main finding was the DOX differential regulated the uterine transcriptomic environment in response to E2. There was significant downregulation of many E2-responsive genes, potentially through ERa actions. Recent research into DOX effects in the uterus found downregulation of *ERa* in response to DOX treatment, however the ovaries were left intact. *ERa* downregulation was observed in our data but not significantly, increased samples could shows significance (Samare-Najaf, Zal and Safari, 2020). Pathway analysis revealed disruptions to gene networks related to secretion of proteins (critical to GE function in the uterus), glycoproteins (critical in uterine preparation for implantation), and the extracellular matrix (major network responsible for many aspects to early pregnancy). Using data on uterine preparation for uterine receptivity, we compared genes involved in DOX alterations to uterine response to E2, finding significant overlap between the genes. Dysregulation of gene networks important to uterine receptivity and early pregnancy, as well as

disruptions to estrogen signaling led us to hypothesize that DOX could disrupt functional uterine receptivity. We addressed this hypothesis in Chapter 4. Utilizing artificial decidualization as a marker for uterine receptivity, we treated mice during adolescence and tested functional responses at maturity. This experimental timeline recapitulated the increasingly common scenario of children and adolescents undergoing cancer therapy to provide more applicable results for risk assessment (Group, 2020). Significant weight effects observed in DOX treated animals suggested that DOX through i.p, causes disruption to long-term weight homeostasis in rodents. Future methods should investigate easier techniques for intra-veinous administration in mice as current methods are time-consuming and require restraint of animals outside of simple scruffing. Due to constraints of the COVID-19 pandemic many of the procedures in this study had to be done by myself without assistance, making I.P. injections a requirement for ease, by offering a single-handed technique. DOX injection in the intraperitoneal cavity could cause apoptosis of adipocytes in the utero fat pad leading to disruptions to weight post-treatment. However, the lower multiple doses of DOX (2 mg/kg/day, across 5 days) did prevent many of the long-term weight effects and suggests multiple lower doses could be less toxic. Regardless of weight effects, the goal should be to mimic the dosing route of exposure in humans, so further confirmatory experiments should strive to include the I.V. dosing route through the tail vein. Our experiment showed that DOX treatment (DOX-2x5 and DOX-10) reduced blue dye accumulation in the uterus during artificial decidualization. This suggests potential disruptions to vascular invasion of the uterus during uterine preparation for uterine receptivity, as well as potential disruptions to events involved in implantation. Histology revealed the absence of decidual zones in a subset of DOX treated animals, further evidence that decidualization never occurred. Clearly individual sensitivity to DOX targeting of the uterus, similar to effects observed in the CL, play a role in mediating uterine preparation for uterine

receptivity. Molecular mechanisms associated with the reduced artificial decidualization are yet to be investigated, however tissues collected in these experiments will aid in understanding DOX disruptions. In conjunction with the artificial decidualization aims of Chapter 4, we also collected tissues to be used for RNAseq. Significant individual variations in the uterine response to estrogen were observed in Chapter 3, since an outbred strain (CD1) was used, we decided to reduce genetic variation in the RNAseq analysis that an inbred strain would be more useful (C57BL6/J). Due to unforeseen circumstances, including the repercussions of the novel coronavirus pandemic, we were unable to submit these tissues in a timely manner. However plans to continue this research have been made and we hope to provide more publicly available data on the targeted effects DOX can have on uterine functions. Furthermore, we plan to include other chemotherapeutic drugs, such as cyclophosphamide and cisplatin, to better understand the effects of chemotherapeutic induced disruptions to uterine function.

In summary, the research submitted in this dissertation fills gaps in our knowledge of the effects of DOX on female fertility. We published novel research on disruptions to P4 synthesis in the CL, showing varying individual sensitivities and disruptions to molecular mechanisms control CL function. We were the first to publish unequivocal evidence of DOX targeting of the uterus in mice, highlighted as a significant contribution to the field of oncofertility. Finally, we continued to investigate disruptions to uterine functions by providing preliminary evidence that DOX disrupts uterine preparation for receptivity using artificial decidualization as a model. We continue to investigate the effects of chemotherapies on female fertility and provide advancements to better aid in risk assessment for premenopausal cancer patients.

REFERENCES

Accialini, P. *et al.* (2017) 'The Rodent Corpus Luteum BT - The Life Cycle of the Corpus Luteum', in Meidan, R. (ed.). Cham: Springer International Publishing, pp. 117–131. doi: 10.1007/978-3-319-43238-0_7.

Allen, C. M. *et al.* (2020) 'Comparative gonadotoxicity of the chemotherapy drugs cisplatin and carboplatin on prepubertal mouse gonads', *Molecular human reproduction*, 26(3), pp. 129–140. doi: 10.1093/molehr/gaaa008.

Almeida, J. Z. *et al.* (2021) '5-Fluorouracil disrupts ovarian preantral follicles in young C57BL6J mice', *Cancer Chemotherapy and Pharmacology*, 87(4), pp. 567–578. doi: 10.1007/s00280-020-04217-7.

Anazodo, A. *et al.* (2018) 'Oncofertility-An emerging discipline rather than a special consideration', *Pediatric Blood & Cancer*, 65(11), p. e27297. doi: 10.1002/pbc.27297.

Andersen, C. L. *et al.* (2019) 'Chemotherapeutic agent doxorubicin alters uterine gene expression in response to estrogen in ovariectomized CD-1 adult mice†', *Biology of reproduction*, 100(4), pp. 869–871. doi: 10.1093/biolre/ioy259.

Anupriwan, A. *et al.* (2008) 'Presence of Arylsulfatase A and Sulfogalactosylglycerolipid in Mouse Ovaries: Localization to the Corpus Luteum', *Endocrinology*, 149(8), pp. 3942–3951. doi: 10.1210/en.2008-0281.

Aplin, J. D. and Singh, H. (2008) 'Bioinformatics and Transcriptomics Studies of Early Implantation', *Annals of the New York Academy of Sciences*, 1127(1), pp. 116–120. doi: https://doi.org/10.1196/annals.1434.005.

Asperen, J. van *et al.* (1998) ‘Increased accumulation of doxorubicin and doxorubicinol in cardiac tissue of mice lacking mdr1a P-glycoprotein’, *British Journal of Cancer*, 79(1), pp. 108–113. doi: 10.1038/sj.bjc.6690019.

Bachelot, A. *et al.* (2009) ‘Prolactin independent rescue of mouse corpus luteum life span: identification of prolactin and luteinizing hormone target genes’, *American journal of physiology. Endocrinology and metabolism*. 2009/06/16, 297(3), pp. E676–E684. doi: 10.1152/ajpendo.91020.2008.

Bachelot, A. and Binart, N. B. T.-C. T. in D. B. (2005) ‘Corpus Luteum Development: Lessons from Genetic Models in Mice’, in. Academic Press, pp. 49–84. doi: https://doi.org/10.1016/S0070-2153(05)68003-9.

Baddela, V. S. *et al.* (2018) ‘Global gene expression analysis indicates that small luteal cells are involved in extracellular matrix modulation and immune cell recruitment in the bovine corpus luteum’, *Molecular and Cellular Endocrinology*, 474, pp. 201–213. doi: https://doi.org/10.1016/j.mce.2018.03.011.

Bahr, J. M. (2018) ‘Ovary, Overview’, in Skinner, M. K. B. T.-E. of R. (Second E. (ed.). Oxford: Academic Press, pp. 3–7. doi: https://doi.org/10.1016/B978-0-12-801238-3.64389-1.

Bar-Joseph, H. *et al.* (2020) ‘Cancer During Pregnancy: The Role of Vascular Toxicity in Chemotherapy-Induced Placental Toxicity’, *Cancers*, 12(5), p. 1277. doi: 10.3390/cancers12051277.

Batatinha, H. *et al.* (2014) ‘Adipose tissue homeostasis is deeply disrupted by doxorubicin treatment’, *Cancer & Metabolism*, 2(Suppl 1), pp. P5–P5. doi: 10.1186/2049-3002-2-S1-P5.

Bazer, F. W. *et al.* (2010) ‘Novel pathways for implantation and establishment and maintenance of pregnancy in mammals’, *Molecular human reproduction*. 2009/10/30, 16(3), pp. 135–152.

doi: 10.1093/molehr/gap095.

Bell, M. R. (2018) ‘Comparing Postnatal Development of Gonadal Hormones and Associated Social Behaviors in Rats, Mice, and Humans’, *Endocrinology*, 159(7), pp. 2596–2613. doi: 10.1210/en.2018-00220.

Ben-Aharon, I. *et al.* (2010) ‘Doxorubicin-induced ovarian toxicity’, *Reproductive biology and endocrinology : RB&E*, 8, p. 20. doi: 10.1186/1477-7827-8-20.

Bertolin, K. and Murphy, B. D. (2014) ‘7 - Reproductive Tract Changes During the Mouse Estrous Cycle’, in Croy, B. A. et al. (eds). Boston: Academic Press, pp. 85–94. doi: https://doi.org/10.1016/B978-0-12-394445-0.00007-2.

Bildik, G. *et al.* (2020) ‘Terminal differentiation of human granulosa cells as luteinization is reversed by activin-A through silencing of Jnk pathway’, *Cell Death Discovery*, 6(1), p. 93. doi: 10.1038/s41420-020-00324-9.

BINGEL, A. S. and SCHWARTZ, N. B. (1969) ‘TIMING OF LH RELEASE AND OVULATION IN THE CYCLIC MOUSE’, *Reproduction*, 19(2), pp. 223–229. doi: 10.1530/jrf.0.0190223.

Bleyer, A. *et al.* (2017) ‘Global assessment of cancer incidence and survival in adolescents and young adults’, *Pediatric Blood & Cancer*, 64(9), p. e26497. doi: https://doi.org/10.1002/pbc.26497.

Carr, J. S., King, S. and Dekaney, C. M. (2017) ‘Depletion of enteric bacteria diminishes leukocyte infiltration following doxorubicin-induced small intestinal damage in mice’, *PLOS ONE*, 12(3), p. e0173429. doi: 10.1371/journal.pone.0173429.

Cha, J. M. *et al.* (2018) ‘Aspects of Rodent Implantation’, in Skinner, M. K. B. T.-E. of R. (Second E. (ed.). Oxford: Academic Press, pp. 291–297. doi: https://doi.org/10.1016/B978-0-12-

801238-3.64402-1.

Chang, C. *et al.* (2014) 'Developmental Toxicity of Doxorubicin Hydrochloride in Embryo-larval Stages of Zebrafish', *Bio-Medical Materials and Engineering*, 24(1), pp. 909–916. doi: 10.3233/bme-130885.

Chang, X.-L. *et al.* (2017) 'The function of high-density lipoprotein and low-density lipoprotein in the maintenance of mouse ovarian steroid balance†', *Biology of Reproduction*, 97(6), pp. 862–872. doi: 10.1093/biolre/iox134.

Chen, J. R. *et al.* (2000) 'Leukemia Inhibitory Factor Can Substitute for Nidatory Estrogen and Is Essential to Inducing a Receptive Uterus for Implantation But Is Not Essential for Subsequent Embryogenesis*', *Endocrinology*, 141(12), pp. 4365–4372. doi: 10.1210/endo.141.12.7855.

Chen, Y. *et al.* (2020) 'The Factors and Pathways Regulating the Activation of Mammalian Primordial Follicles in vivo ', *Frontiers in Cell and Developmental Biology* , p. 1018. Available at: https://www.frontiersin.org/article/10.3389/fcell.2020.575706.

Cheng, M. Y., Hartl, F.-U. and Norwich, A. L. (1990) 'The mitochondrial chaperonin hsp60 is required for its own assembly', *Nature*, 348(6300), pp. 455–458. doi: 10.1038/348455a0.

Chow, E. J. *et al.* (2016) 'Pregnancy after chemotherapy in male and female survivors of childhood cancer treated between 1970 and 1999: a report from the Childhood Cancer Survivor Study cohort', *The Lancet Oncology*, 17(5), pp. 567–576. doi: 10.1016/s1470-2045(16)00086-3.

Christenson, L. K. and Devoto, L. (2003) 'Cholesterol transport and steroidogenesis by the corpus luteum', *Reproductive biology and endocrinology : RB&E*, 1, p. 90. doi: 10.1186/1477-7827-1-90.

Clayton, Z. S. *et al.* (2020) 'Doxorubicin-Induced Oxidative Stress and Endothelial Dysfunction in Conduit Arteries Is Prevented by Mitochondrial-Specific Antioxidant Treatment', *JACC:*

CardioOncology, 2(3), pp. 475–488. doi: 10.1016/j.jaccao.2020.06.010.

Couse, J. F. *et al.* (2005) 'Estrogen Receptor-β Is Critical to Granulosa Cell Differentiation and the Ovulatory Response to Gonadotropins', *Endocrinology*, 146(8), pp. 3247–3262. doi: 10.1210/en.2005-0213.

Das, J. *et al.* (2011) 'Taurine protects rat testes against doxorubicin-induced oxidative stress as well as p53, Fas and caspase 12-mediated apoptosis', *Amino Acids*, 42(5), pp. 1839–1855. doi: 10.1007/s00726-011-0904-4.

Davies, K. J. and Doroshow, J. H. (1986) 'Redox cycling of anthracyclines by cardiac mitochondria. I. Anthracycline radical formation by NADH dehydrogenase.', *Journal of Biological Chemistry*, 261(7), pp. 3060–3067. doi: 10.1016/s0021-9258(17)35746-0.

Davis, J. S., Rueda, B. R. and Spanel-Borowski, K. (2003a) 'Microvascular endothelial cells of the corpus luteum', *Reproductive biology and endocrinology : RB&E*, 1, p. 89. doi: 10.1186/1477-7827-1-89.

Davis, J. S., Rueda, B. R. and Spanel-Borowski, K. (2003b) 'Microvascular endothelial cells of the corpus luteum', *Reproductive biology and endocrinology : RB&E*, 1, p. 89. doi: 10.1186/1477-7827-1-89.

Dekel, N. *et al.* (2014) 'The role of inflammation for a successful implantation', *American journal of reproductive immunology (New York, N.Y. : 1989)*. 2014/05/09, 72(2), pp. 141–147. doi: 10.1111/aji.12266.

Dey, S. K. *et al.* (2004) 'Molecular cues to implantation', *Endocr Rev*, 25(3), pp. 341–373. doi: 10.1210/er.2003-0020.

Dey, S. K. and Lim, H. (2006) 'CHAPTER 4 - Implantation A2 - Neill, Jimmy D', in *Knobil and Neill's Physiology of Reproduction (Third Edition)*. St Louis: Academic Press, pp. 147–188. doi:

https://doi.org/10.1016/B978-012515400-0/50009-9.

Diao, H. *et al.* (2010) 'Uterine luminal epithelium–specific proline-rich acidic protein 1 (PRAP1) as a marker for successful embryo implantation', *Fertility and Sterility*, 94(7), pp. 2808-2811.e1. doi: https://doi.org/10.1016/j.fertnstert.2010.06.034.

Diao, H. *et al.* (2011) 'Temporal expression pattern of progesterone receptor in the uterine luminal epithelium suggests its requirement during early events of implantation', *Fertility and sterility*. 2011/03/03, 95(6), pp. 2087–2093. doi: 10.1016/j.fertnstert.2011.01.160.

Diao, H., Xiao, S., Howerth, E. W., *et al.* (2013) 'Broad Gap Junction Blocker Carbenoxolone Disrupts Uterine Preparation for Embryo Implantation in Mice1', *Biology of Reproduction*, 89(2). doi: 10.1095/biolreprod.113.110106.

Diao, H., Xiao, S., Li, R., *et al.* (2013) 'Distinct spatiotemporal expression of serine proteases Prss23 and Prss35 in periimplantation mouse uterus and dispensable function of Prss35 in fertility', *PloS one*. 2013/02/22, 8(2), pp. e56757–e56757. doi: 10.1371/journal.pone.0056757.

Diao, H. *et al.* (2015) 'Deletion of Lysophosphatidic Acid Receptor 3 (Lpar3) Disrupts Fine Local Balance of Progesterone and Estrogen Signaling in Mouse Uterus During Implantation', *Biology of reproduction*. 2015/10/07, 93(5), p. 123. doi: 10.1095/biolreprod.115.131110.

Duffy, D. M. *et al.* (2018) 'Ovulation: Parallels With Inflammatory Processes', *Endocrine Reviews*, 40(2), pp. 369–416. doi: 10.1210/er.2018-00075.

Eldani, M. *et al.* (2020) 'Continuous treatment with cisplatin induces the oocyte death of primordial follicles without activation', *The FASEB Journal*, 34(10), pp. 13885–13899. doi: 10.1096/fj.202001461rr.

Fan, X. *et al.* (2019) 'Single-cell reconstruction of follicular remodeling in the human adult ovary', *Nature Communications*, 10(1), p. 3164. doi: 10.1038/s41467-019-11036-9.

Faust, I. M., Johnson, P. R. and Hirsch, J. (1976) 'Noncompensation of adipose mass in partially lipectomized mice and rats', *American Journal of Physiology-Legacy Content*, 231(2), pp. 538–544. doi: 10.1152/ajplegacy.1976.231.2.538.

FDA, U. S. F. D. and F. A. (2013) *Doxorubicin Label*, *FDA Label*. Available at: https://www.google.com/url?sa=t&rct=j&q=&esrc=s&source=web&cd=&cad=rja&uact=8&ved=2ahUKEwj4tO2FrfLwAhURH80KHQ7fC3UQFjAAegQIAhAD&url=https%3A%2F%2Fwww.accessdata.fda.gov%2Fdrugsatfda_docs%2Flabel%2F2013%2F050467s073lbl.pdf&usg=AOvVaw1adoMmTuqqfGXk1FJicKkn.

Feng, Y. *et al.* (2017) 'CLARITY reveals dynamics of ovarian follicular architecture and vasculature in three-dimensions', *Scientific reports*, 7, p. 44810. doi: 10.1038/srep44810.

Fortune, J. E. (2018) 'Ovarian Production of Estradiol: The Two-Cell, Two-Gonadotropin Model', in Skinner, M. K. B. T.-E. of R. (Second E. (ed.). Oxford: Academic Press, pp. 165–171. doi: https://doi.org/10.1016/B978-0-12-801238-3.64637-8.

Fullerton, P. T. *et al.* (2017) 'Follistatin is critical for mouse uterine receptivity and decidualization', *Proceedings of the National Academy of Sciences*, 114(24), p. E4772 LP-E4781. doi: 10.1073/pnas.1620903114.

Goad, J. *et al.* (2017) 'Differential Wnt signaling activity limits epithelial gland development to the anti-mesometrial side of the mouse uterus', *Developmental Biology*, 423(2), pp. 138–151. doi: https://doi.org/10.1016/j.ydbio.2017.01.015.

Green, D. M. *et al.* (2009) 'Fertility of Female Survivors of Childhood Cancer: A Report From the Childhood Cancer Survivor Study', *Journal of Clinical Oncology*, 27(16), pp. 2677–2685. doi: 10.1200/jco.2008.20.1541.

Green, D. M., Sklar, C. A. and Boice, J. D. (2009) 'No Title', *J Clin Oncol*, 27(14), p. 2374.

Griffiths, M. J., Winship, A. L. and Hutt, K. J. (2020) 'Do cancer therapies damage the uterus and compromise fertility?', *Human Reproduction Update*, 26(2), pp. 161–173. doi: 10.1093/humupd/dmz041.

Group, U. S. C. S. W. (2020) *United States Cancer Statistics: Data Visualizations, U.S. Cancer Statistics Data Visualizations Tool*. Available at: https://gis.cdc.gov/Cancer/USCS/DataViz.html (Accessed: 5 November 2020).

Gura, M. A. and Freiman, R. N. (2018) 'Primordial Follicle', in Skinner, M. K. B. T.-E. of R. (Second E. (ed.). Oxford: Academic Press, pp. 65–71. doi: https://doi.org/10.1016/B978-0-12-801238-3.64394-5.

Gurney, H. (2002) 'How to calculate the dose of chemotherapy', *British journal of cancer*, 86(8), pp. 1297–1302. doi: 10.1038/sj.bjc.6600139.

Hannon, P. R. and Curry, T. E. (2018) 'Folliculogenesis', in Skinner, M. K. B. T.-E. of R. (Second E. (ed.). Oxford: Academic Press, pp. 72–79. doi: https://doi.org/10.1016/B978-0-12-801238-3.64628-7.

Harada, M. and Osuga, Y. (2018) 'Fertility preservation for female cancer patients', *International Journal of Clinical Oncology*, 24(1), pp. 28–33. doi: 10.1007/s10147-018-1252-0.

Henley, S. J. *et al.* (2020) 'Annual report to the nation on the status of cancer, part I: National cancer statistics', *Cancer*, 126(10), pp. 2225–2249. doi: https://doi.org/10.1002/cncr.32802.

Hennebold, J. D. (2018) 'Corpus Luteum', in Skinner, M. K. B. T.-E. of R. (Second E. (ed.). Oxford: Academic Press, pp. 99–105. doi: https://doi.org/10.1016/B978-0-12-801238-3.64396-9.

Herington, J. L. *et al.* (2009) 'Paracrine Signals from the Mouse Conceptus Are Not Required for the Normal Progression of Decidualization', *Endocrinology*, 150(9), pp. 4404–4413. doi: 10.1210/en.2009-0036.

Herington, J. L. *et al.* (2016) 'Gene profiling the window of implantation: Microarray analyses from human and rodent models', *Journal of reproductive health and medicine*. 2016/12/09, 2(Suppl 2), pp. S19–S25. doi: 10.1016/j.jrhm.2016.11.006.

Hewitt, S. C., Winuthayanon, W. and Korach, K. S. (2016) 'What's new in estrogen receptor action in the female reproductive tract', *Journal of molecular endocrinology*, 56(2), pp. R55–R71. doi: 10.1530/JME-15-0254.

Hirota, Y. (2016) 'Uterine Receptivity in Mouse Embryo Implantation BT - Uterine Endometrial Function', in Kanzaki, H. (ed.). Tokyo: Springer Japan, pp. 11–25. doi: 10.1007/978-4-431-55972-6_2.

Hryciuk, M. M. *et al.* (2019) 'Functional and Morphological Characterization of Small and Large Steroidogenic Luteal Cells From Domestic Cats Before and During Culture ', *Frontiers in Endocrinology* , p. 724. Available at: https://www.frontiersin.org/article/10.3389/fendo.2019.00724.

Iwamoto, T. *et al.* (2020) 'NSAS-BC02 substudy of chemotherapy-induced amenorrhea (CIA) in premenopausal patients who received either taxane alone or doxorubicin(A) cyclophosphamide(C) followed by taxane as postoperative chemotherapy', *Breast Cancer Research and Treatment*, 182(2), pp. 325–332. doi: 10.1007/s10549-020-05692-5.

Jadapalli, J. K. *et al.* (2018) 'Doxorubicin triggers splenic contraction and irreversible dysregulation of COX and LOX that alters the inflammation-resolution program in the myocardium', *American journal of physiology. Heart and circulatory physiology*. 2018/08/03, 315(5), pp. H1091–H1100. doi: 10.1152/ajpheart.00290.2018.

Jiménez, L. M. *et al.* (2010) 'Scavenger receptor-B1 and luteal function in mice', *Journal of lipid research*. 04/19, 51(8), pp. 2362–2371. doi: 10.1194/jlr.M006973.

Johansen, P. B. (1981) ‘Doxorubicin pharmacokinetics after intravenous and intraperitoneal administration in the nude mouse’, *Cancer Chemotherapy and Pharmacology*, 5(4), pp. 267–270. doi: 10.1007/bf00434396.

Johnson-Arbor, K. and Dubey, R. (2020) *Doxorubicin*. StatPearls Publishing. doi: NBK430685.

Kabarowski, J. H. S. (2001) ‘Lysophosphatidylcholine as a Ligand for the Immunoregulatory Receptor G2A’, *Science*, 293(5530), pp. 702–705. doi: 10.1126/science.1061781.

Kelleher, A. M., DeMayo, F. J. and Spencer, T. E. (2019) ‘Uterine Glands: Developmental Biology and Functional Roles in Pregnancy’, *Endocrine Reviews*, 40(5), pp. 1424–1445. doi: 10.1210/er.2018-00281.

Kojima, K. *et al.* (2001) ‘Progesterone inhibits apolipoprotein-mediated cellular lipid release: a putative mechanism for the decrease of high-density lipoprotein’, *Biochimica et Biophysica Acta (BBA) - Molecular and Cell Biology of Lipids*, 1532(3), pp. 173–184. doi: https://doi.org/10.1016/S1388-1981(01)00124-X.

Kojima, Y., Tam, O. H. and Tam, P. P. L. (2014) ‘Timing of developmental events in the early mouse embryo’, *Seminars in Cell & Developmental Biology*, 34, pp. 65–75. doi: 10.1016/j.semcdb.2014.06.010.

Koot, Y. E. M. *et al.* (2016) ‘An endometrial gene expression signature accurately predicts recurrent implantation failure after IVF’, *Scientific Reports*, 6(1), p. 19411. doi: 10.1038/srep19411.

Kotamraju, S. *et al.* (2000a) ‘Doxorubicin-induced Apoptosis in Endothelial Cells and Cardiomyocytes Is Ameliorated by Nitrone Spin Traps and Ebselen: ROLE OF REACTIVE OXYGEN AND NITROGEN SPECIES’, *Journal of Biological Chemistry*, 275(43), pp. 33585–33592. doi: 10.1074/jbc.M003890200.

Kotamraju, S. *et al.* (2000b) 'Doxorubicin-induced Apoptosis in Endothelial Cells and Cardiomyocytes Is Ameliorated by Nitrone Spin Traps and Ebselen', *Journal of Biological Chemistry*, 275(43), pp. 33585–33592. doi: 10.1074/jbc.m003890200.

Krischke, M. *et al.* (2016) 'Pharmacokinetic and pharmacodynamic study of doxorubicin in children with cancer: results of a "European Pediatric Oncology Off-patents Medicines Consortium" trial', *Cancer Chemotherapy and Pharmacology*, 78(6), pp. 1175–1184. doi: 10.1007/s00280-016-3174-8.

Lee-Thacker, S. *et al.* (2018) 'Core Binding Factor β Expression in Ovarian Granulosa Cells Is Essential for Female Fertility', *Endocrinology*, 159(5), pp. 2094–2109. doi: 10.1210/en.2018-00011.

Lee, G. Y., Croop, J. M. and Anderson, E. (1998) 'Multidrug Resistance Gene Expression Correlates with Progesterone Production in Dehydroepiandrosterone-lnduced Polycystic and Equine Chorionic Gonadotropin-Stimulated Ovaries of Prepubertal Rats1', *Biology of Reproduction*, 58(2), pp. 330–337. doi: 10.1095/biolreprod58.2.330.

Lee, K. Y. *et al.* (2007) 'Mouse models of implantation', *Trends in Endocrinology & Metabolism*, 18(6), pp. 234–239. doi: https://doi.org/10.1016/j.tem.2007.06.002.

Lei, L. *et al.* (2020) 'The mouse Balbiani body maintains primordial follicle quiescence via RNA storage', *bioRxiv*, p. 2020.01.17.911040. doi: 10.1101/2020.01.17.911040.

Lei, W. *et al.* (2013) 'Alkaline phosphatases contribute to uterine receptivity, implantation, decidualization, and defense against bacterial endotoxin in hamsters', *Reproduction (Cambridge, England)*, 146(5), pp. 419–432. doi: 10.1530/REP-13-0153.

Levine, J. (2012) 'Gonadotoxicity of Cancer Therapies in Pediatric and Reproductive-Age Females', in Gracia, C. and Woodruff, T. K. (eds) *Oncofertility Medical Practice: Clinical*

Issues and Implementation. New York, NY: Springer New York, pp. 3–14. doi: 10.1007/978-1-4419-9425-7_1.

Lim, H. J. and Wang, H. (2010) 'Uterine disorders and pregnancy complications: insights from mouse models', *The Journal of Clinical Investigation*, 120(4), pp. 1004–1015. doi: 10.1172/JCI41210.

Lu, J., Kong, S. and Wang, H. (2018) 'Uterine Receptivity: The Status of Uterus for Implantation', in Skinner, M. K. B. T.-E. of R. (Second E. (ed.). Oxford: Academic Press, pp. 394–399. doi: https://doi.org/10.1016/B978-0-12-801238-3.64660-3.

Luu, A. Z. *et al.* (2018) 'Role of Endothelium in Doxorubicin-Induced Cardiomyopathy', *JACC: Basic to Translational Science*, 3(6), pp. 861–870. doi: 10.1016/j.jacbts.2018.06.005.

Luu, A. Z. *et al.* (2021) 'Loss of endothelial cell-specific autophagy-related protein 7 exacerbates doxorubicin-induced cardiotoxicity', *Biochemistry and Biophysics Reports*, 25, p. 100926. doi: 10.1016/j.bbrep.2021.100926.

Maliqueo, M., Echiburú, B. and Crisosto, N. (2016) 'Sex Steroids Modulate Uterine-Placental Vasculature: Implications for Obstetrics and Neonatal Outcomes ', *Frontiers in Physiology* , p. 152. Available at: https://www.frontiersin.org/article/10.3389/fphys.2016.00152.

Manna, P. R., Dyson, M. T. and Stocco, D. M. (2009) 'Regulation of the steroidogenic acute regulatory protein gene expression: present and future perspectives', *Molecular Human Reproduction*, 15(6), pp. 321–333. doi: 10.1093/molehr/gap025.

Martin, J. *et al.* (2014) 'The Weaned Pig as a Model for Doxorubicin-Induced Mucositis', *Chemotherapy*, 60(1), pp. 24–36. doi: 10.1159/000365725.

Massarotti, C. *et al.* (2019) 'Beyond fertility preservation: role of the oncofertility unit in the reproductive and gynecological follow-up of young cancer patients', *Human Reproduction*,

34(8), pp. 1462–1469. doi: 10.1093/humrep/dez108.

Matsumoto, H. (2017) ‘Molecular and cellular events during blastocyst implantation in the receptive uterus: clues from mouse models’, *The Journal of reproduction and development*. 2017/06/22, 63(5), pp. 445–454. doi: 10.1262/jrd.2017-047.

McRae, R. S. *et al.* (2005) ‘Changes in Mouse Granulosa Cell Gene Expression during Early Luteinization’, *Endocrinology*, 146(1), pp. 309–317. doi: 10.1210/en.2004-0999.

Mehdizadeh, A. *et al.* (2017) ‘Common chemotherapeutic agents modulate fatty acid distribution in human hepatocellular carcinoma and colorectal cancer cells’, *BioImpacts*, 7(1), pp. 31–39. doi: 10.15171/bi.2017.05.

Meng, L. *et al.* (2018) ‘Preantral follicular atresia occurs mainly through autophagy, while antral follicles degenerate mostly through apoptosis’, *Biology of Reproduction*, 99(4), pp. 853–863. doi: 10.1093/biolre/ioy116.

Mentoor, I. *et al.* (2020) ‘Decreased Efficacy of Doxorubicin Corresponds With Modifications in Lipid Metabolism Markers and Fatty Acid Profiles in Breast Tumors From Obese vs. Lean Mice’, *Frontiers in oncology*, 10, p. 306. doi: 10.3389/fonc.2020.00306.

Miller, K. D. *et al.* (2020) ‘Cancer statistics for adolescents and young adults, 2020’, *CA: A Cancer Journal for Clinicians*, n/a(n/a). doi: https://doi.org/10.3322/caac.21637.

Misset, J. L. *et al.* (1999) ‘Dose-finding study of docetaxel and doxorubicin in first-line treatment of patients with metastatic breast cancer’, *Annals of oncology*, 10(5), pp. 553–560.

Moravek, M. B. *et al.* (2019) ‘Development of a Pediatric Fertility Preservation Program: A Report From the Pediatric Initiative Network of the Oncofertility Consortium’, *Journal of Adolescent Health*, 64(5), pp. 563–573. doi: https://doi.org/10.1016/j.jadohealth.2018.10.297.

Nair, A. B. and Jacob, S. (2016) ‘A simple practice guide for dose conversion between animals

and human', *Journal of basic and clinical pharmacy*, 7(2), pp. 27–31. doi: 10.4103/0976-0105.177703.

Nelson, S. E. *et al.* (1992) 'Isolation, characterization, and culture of cell subpopulations forming the pregnant rat corpus luteum.', *Endocrinology*, 130(2), pp. 954–966. doi: 10.1210/endo.130.2.1733737.

Nishi, K. *et al.* (2018) 'Doxorubicin-induced female reproductive toxicity: an assessment of ovarian follicular apoptosis, cyclicity and reproductive tissue histology in Wistar rats', *Drug and Chemical Toxicology*, 41(1), pp. 72–81. doi: 10.1080/01480545.2017.1307851.

Niswender, G. D. *et al.* (2000) 'Mechanisms Controlling the Function and Life Span of the Corpus Luteum', *Physiological Reviews*, 80(1), pp. 1–29. doi: 10.1152/physrev.2000.80.1.1.

Nowak, R. A. (2018) 'Estrous and Menstrual Cycles', in Skinner, M. K. B. T.-E. of R. (Second E. (ed.). Oxford: Academic Press, pp. 114–120. doi: https://doi.org/10.1016/B978-0-12-801238-3.64631-7.

Ojeda, S. R. and Skinner, M. K. (2006) 'CHAPTER 38 - Puberty in the Rat A2 - Neill, Jimmy D', in *Knobil and Neill's Physiology of Reproduction (Third Edition)*. St Louis: Academic Press, pp. 2061–2126. doi: https://doi.org/10.1016/B978-012515400-0/50043-9.

Okuno, T. *et al.* (2020) 'Zygotic Nuclear F-Actin Safeguards Embryonic Development', *Cell Reports*, 31(13), p. 107824. doi: 10.1016/j.celrep.2020.107824.

Padmanabhan, V., Puttabyatappa, M. and Cardoso, R. C. (2018) 'Hypothalamus–Pituitary–Ovary Axis', in Skinner, M. K. B. T.-E. of R. (Second E. (ed.). Oxford: Academic Press, pp. 121–129. doi: https://doi.org/10.1016/B978-0-12-801238-3.64632-9.

Parr, E. L., Tung, H.-N. and Parr, M. B. (1988) 'Endocytosis in the epithelium of the mouse oviduct', *American Journal of Anatomy*, 181(4), pp. 393–400. doi: 10.1002/aja.1001810407.

Pate, J. L. (2018) ‘Luteolysis’, in Skinner, M. K. B. T.-E. of R. (Second E. (ed.). Oxford: Academic Press, pp. 106–113. doi: https://doi.org/10.1016/B978-0-12-801238-3.64397-0.

Plewes, M. R. *et al.* (2018) ‘Trafficking of Cholesterol from Lipid Droplets to Mitochondria in Bovine Luteal Cells: Acute Control of Progesterone Synthesis<sup>1</sup&gt’, *bioRxiv*, p. 409599. doi: 10.1101/409599.

Ramathal, C. Y. *et al.* (2010) ‘ENDOMETRIAL DECIDUALIZATION: OF MICE AND MEN’, *Seminars in reproductive medicine*, 28(1), pp. 17–26. doi: 10.1055/s-0029-1242989.

Richards, J. S. (2018a) ‘Ovulation’, in Skinner, M. K. B. T.-E. of R. (Second E. (ed.). Oxford: Academic Press, pp. 92–98. doi: https://doi.org/10.1016/B978-0-12-801238-3.64630-5.

Richards, J. S. (2018b) ‘Theca Cells’, in Skinner, M. K. B. T.-E. of R. (Second E. (ed.). Oxford: Academic Press, pp. 14–20. doi: https://doi.org/10.1016/B978-0-12-801238-3.64624-X.

Rodvold, K. A., Rushing, D. A. and Tewksbury, D. A. (1988) ‘Doxorubicin clearance in the obese.’, *Journal of Clinical Oncology*, 6(8), pp. 1321–1327. doi: 10.1200/JCO.1988.6.8.1321.

Romereim, S. M. *et al.* (2017a) ‘Gene expression profiling of bovine ovarian follicular and luteal cells provides insight into cellular identities and functions’, *Molecular and Cellular Endocrinology*, 439, pp. 379–394. doi: https://doi.org/10.1016/j.mce.2016.09.029.

Romereim, S. M. *et al.* (2017b) ‘Transcriptomes of bovine ovarian follicular and luteal cells’, *Data in Brief*, 10, pp. 335–339. doi: https://doi.org/10.1016/j.dib.2016.11.093.

Samare-Najaf, M., Zal, F. and Safari, S. (2020) ‘Primary and Secondary Markers of Doxorubicin-Induced Female Infertility and the Alleviative Properties of Quercetin and Vitamin E in a Rat Model’, *Reproductive Toxicology*, 96, pp. 316–326. doi: https://doi.org/10.1016/j.reprotox.2020.07.015.

Sarvazyan, N. (1996) ‘Visualization of doxorubicin-induced oxidative stress in isolated cardiac

myocytes', *American Journal of Physiology-Heart and Circulatory Physiology*, 271(5), pp. H2079–H2085. doi: 10.1152/ajpheart.1996.271.5.h2079.

Seiler, K. M. *et al.* (2015) 'Tissue underlying the intestinal epithelium elicits proliferation of intestinal stem cells following cytotoxic damage', *Cell and Tissue Research*, 361(2), pp. 427–438. doi: 10.1007/s00441-015-2111-1.

Shrestha, B. *et al.* (2019) 'Engineering Streptomyces peucetius for Doxorubicin and Daunorubicin Biosynthesis BT - Pharmaceuticals from Microbes: The Bioengineering Perspective', in Arora, D. et al. (eds). Cham: Springer International Publishing, pp. 191–209. doi: 10.1007/978-3-030-01881-8_7.

Shyu Jr, P. *et al.* (2018) 'Dropping in on lipid droplets: insights into cellular stress and cancer', *Bioscience Reports*, 38(5). doi: 10.1042/BSR20180764.

Siemann, D. W. and Sutherland, R. M. (1979) 'A comparison of the pharmacokinetics of multiple and single dose administrations of adriamycin', *International Journal of Radiation Oncology*Biology*Physics*, 5(8), pp. 1271–1274. doi: 10.1016/0360-3016(79)90652-7.

Da Silva-Buttkus, P. *et al.* (2008) 'Effect of cell shape and packing density on granulosa cell proliferation and formation of multiple layers during early follicle development in the ovary', *Journal of Cell Science*, 121(23), pp. 3890 LP – 3900. doi: 10.1242/jcs.036400.

Singh, R. and Cuervo, A. M. (2012) 'Lipophagy: Connecting Autophagy and Lipid Metabolism', *International Journal of Cell Biology*, 2012, pp. 1–12. doi: 10.1155/2012/282041.

Smith, C. J. *et al.* (1989) 'The Response of Large and Small Luteal Cells from the Pregnant Rat to Substrates and Secretagogues1', *Biology of Reproduction*, 41(6), pp. 1123–1132. doi: 10.1095/biolreprod41.6.1123.

Soleilhavoup, C. *et al.* (2016) 'Proteomes of the Female Genital Tract During the Oestrous

Cycle', *Molecular & Cellular Proteomics : MCP*, 15(1), pp. 93–108. doi: 10.1074/mcp.M115.052332.

Stocco, C., Djiane, J. and Gibori, G. (2003) 'Prostaglandin F2α (PGF2α) and Prolactin Signaling: PGF2α-Mediated Inhibition of Prolactin Receptor Expression in the Corpus Luteum', *Endocrinology*, 144(8), pp. 3301–3305. doi: 10.1210/en.2003-0420.

Stocco, C., Telleria, C. and Gibori, G. (2007) 'The Molecular Control of Corpus Luteum Formation, Function, and Regression', *Endocrine Reviews*, 28(1), pp. 117–149. doi: 10.1210/er.2006-0022.

Strauss, J. F. *et al.* (1977) 'Lipid metabolism in regressing rat corpora lutea of pregnancy', *Journal of Lipid Research*, 18(2), pp. 246–258. doi: 10.1016/s0022-2275(20)41704-3.

Sun, Y.-C. *et al.* (2017) 'The role of germ cell loss during primordial follicle assembly: a review of current advances', *International journal of biological sciences*, 13(4), pp. 449–457. doi: 10.7150/ijbs.18836.

Szymanska, K. J., Tan, X. and Oktay, K. (2020) 'Unraveling the mechanisms of chemotherapy-induced damage to human primordial follicle reserve: road to developing therapeutics for fertility preservation and reversing ovarian aging', *Molecular human reproduction*. doi: 10.1093/molehr/gaaa043.

Talbott, H. A. *et al.* (2020) 'Formation and characterization of lipid droplets of the bovine corpus luteum', *Scientific Reports*, 10(1), p. 11287. doi: 10.1038/s41598-020-68091-2.

Talbott, H. and Davis, J. S. (2017) 'Lipid Droplets and Metabolic Pathways Regulate Steroidogenesis in the Corpus Luteum', in Meidan, R. (ed.) *The Life Cycle of the Corpus Luteum*. Cham: Springer International Publishing, pp. 57–78. doi: 10.1007/978-3-319-43238-0_4.

Terasawa, E. and Fernandez, D. L. (2001) 'Neurobiological Mechanisms of the Onset of Puberty in Primates*', *Endocrine Reviews*, 22(1), pp. 111–151. doi: 10.1210/edrv.22.1.0418.

Thorn, C. F. *et al.* (2011) 'Doxorubicin pathways', *Pharmacogenetics and Genomics*, 21(7), pp. 440–446. doi: 10.1097/fpc.0b013e32833ffb56.

Tingen, C., Kim, A. and Woodruff, T. K. (2009) 'The primordial pool of follicles and nest breakdown in mammalian ovaries', *Molecular human reproduction*. 2009/08/26, 15(12), pp. 795–803. doi: 10.1093/molehr/gap073.

Tomao, F. *et al.* (2016) 'Special issues in fertility preservation for gynecologic malignancies', *Critical Reviews in Oncology/Hematology*, 97, pp. 206–219. doi: 10.1016/j.critrevonc.2015.08.024.

Ujah, G. A. *et al.* (2021) 'Tert-butylhydroquinone attenuates doxorubicin-induced dysregulation of testicular cytoprotective and steroidogenic genes, and improves spermatogenesis in rats', *Scientific Reports*, 11(1). doi: 10.1038/s41598-021-85026-7.

Völler, S. *et al.* (2017) 'Towards a model-based dose recommendation for doxorubicin in children', *Clinical pharmacokinetics*, 56(3), pp. 215–223.

Vue, Z. *et al.* (2018) 'Fetal and Postnatal Female Tract Development', in Skinner, M. K. B. T.-E. of R. (Second E. (ed.). Oxford: Academic Press, pp. 261–268. doi: https://doi.org/10.1016/B978-0-12-801238-3.64399-4.

Wagner, M. *et al.* (2020) 'Single-cell analysis of human ovarian cortex identifies distinct cell populations but no oogonial stem cells', *Nature Communications*, 11(1), p. 1147. doi: 10.1038/s41467-020-14936-3.

Wang, C.-W. (2016) 'Lipid droplets, lipophagy, and beyond', *Biochimica et Biophysica Acta (BBA) - Molecular and Cell Biology of Lipids*, 1861(8), pp. 793–805. doi:

10.1016/j.bbalip.2015.12.010.

Wang, H.-H. *et al.* (2017) 'Removal of mouse ovary fat pad affects sex hormones, folliculogenesis and fertility', *Journal of Endocrinology*, 232(2), pp. 155–164. doi: 10.1530/JOE-16-0174.

Wang, Haibin and Dey, S. K. (2006) 'Roadmap to embryo implantation: clues from mouse models', *Nature Reviews Genetics*, 7(3), p. 185. doi: 10.1038/nrg1808.

Wang, H and Dey, S. K. (2006) 'Roadmap to embryo implantation: clues from mouse models', *Nat Rev Genet*, 7(3), pp. 185–199. doi: 10.1038/nrg1808.

WANG, Q.-L. *et al.* (2012) 'Doxorubicin Induces Early Embryo Apoptosis by Inhibiting Poly(ADP ribose) Polymerase', *In Vivo*, 26(5), pp. 827 LP – 834. Available at: http://iv.iiarjournals.org/content/26/5/827.abstract.

Wang, W. *et al.* (2019) 'Single cell RNAseq provides a molecular and cellular cartography of changes to the human endometrium through the menstrual cycle', *bioRxiv*, p. 350538. doi: 10.1101/350538.

Wang, Y. *et al.* (2018) 'Multidrug Resistance Protein 1 Deficiency Promotes Doxorubicin-Induced Ovarian Toxicity in Female Mice', *Toxicological Sciences*, 163(1), pp. 279–292. doi: 10.1093/toxsci/kfy038.

Wang, Y. *et al.* (2019) 'Doxorubicin obliterates mouse ovarian reserve through both primordial follicle atresia and overactivation', *Toxicology and Applied Pharmacology*. doi: 10.1016/j.taap.2019.114714.

Wang, Z. *et al.* (2019) 'Association of luteal cell degeneration and progesterone deficiency with lysosomal storage disorder mucolipidosis type IV in Mcoln1−/− mouse model†', *Biology of Reproduction*, 101(4), pp. 782–790. doi: 10.1093/biolre/ioz126.

Weber, D. M. *et al.* (1987) 'Functional Differences between Small and Large Luteal Cells of the Late-Pregnant vs. Nonpregnant Cow1', *Biology of Reproduction*, 37(3), pp. 685–697. doi: 10.1095/biolreprod37.3.685.

Wei, L. *et al.* (2015) 'Dissecting the Mechanisms of Doxorubicin and Oxidative Stress-Induced Cytotoxicity: The Involvement of Actin Cytoskeleton and ROCK1', *PLOS ONE*, 10(7), p. e0131763. doi: 10.1371/journal.pone.0131763.

Wetendorf, M. *et al.* (2017) 'Decreased epithelial progesterone receptor A at the window of receptivity is required for preparation of the endometrium for embryo attachment†', *Biology of Reproduction*, 96(2), pp. 313–326. doi: 10.1095/biolreprod.116.144410.

Wetendorf, M. and DeMayo, F. J. (2012) 'The progesterone receptor regulates implantation, decidualization, and glandular development via a complex paracrine signaling network', *Molecular and cellular endocrinology*. 2011/11/17, 357(1–2), pp. 108–118. doi: 10.1016/j.mce.2011.10.028.

Wiltbank, M. C. *et al.* (2012) 'Comparison of endocrine and cellular mechanisms regulating the corpus luteum of primates and ruminants', *Animal reproduction*, 9(3), pp. 242–259. Available at: https://pubmed.ncbi.nlm.nih.gov/23750179.

Winship, A. L. *et al.* (2019) 'Vincristine Chemotherapy Induces Atresia of Growing Ovarian Follicles in Mice', *Toxicological Sciences*, 169(1), pp. 43–53. doi: 10.1093/toxsci/kfz022.

Xiao, S., Li, R., *et al.* (2017) 'Acidification of uterine epithelium during embryo implantation in mice', *Biology of reproduction*, 96(1), pp. 232–243. doi: 10.1095/biolreprod.116.144451.

Xiao, S., Zhang, J., *et al.* (2017) 'Doxorubicin has dose-dependent toxicity on mouse ovarian follicle development, hormone secretion, and oocyte maturation', *Toxicological Sciences*. doi: 10.1093/toxsci/kfx047.

Yang, F. *et al.* (2014) ‘Doxorubicin, DNA torsion, and chromatin dynamics’, *Biochimica et Biophysica Acta (BBA) - Reviews on Cancer*, 1845(1), pp. 84–89. doi: https://doi.org/10.1016/j.bbcan.2013.12.002.

Ye, X. *et al.* (2005) ‘LPA3-mediated lysophosphatidic acid signalling in embryo implantation and spacing’, *Nature*, 435(7038), p. 104. doi: 10.1038/nature03505.

Ye, X. (2020) ‘Uterine Luminal Epithelium as the Transient Gateway for Embryo Implantation’, *Trends in Endocrinology & Metabolism*, 31(2), pp. 165–180. doi: 10.1016/j.tem.2019.11.008.

Yen, H.-C. *et al.* (1999) ‘Manganese Superoxide Dismutase Protects Mitochondrial Complex I against Adriamycin-Induced Cardiomyopathy in Transgenic Mice’, *Archives of Biochemistry and Biophysics*, 362(1), pp. 59–66. doi: 10.1006/abbi.1998.1011.

Yoshinaga, K. (2013) ‘A sequence of events in the uterus prior to implantation in the mouse’, *Journal of assisted reproduction and genetics*, 30(8), pp. 1017–1022. doi: 10.1007/s10815-013-0093-z.

Young, J. M. and McNeilly, A. S. (2010) ‘Theca: the forgotten cell of the ovarian follicle’, *REPRODUCTION*, 140(4), pp. 489–504. doi: 10.1530/REP-10-0094.

Zhang, C. *et al.* (2013) ‘Liver receptor homolog-1 is essential for pregnancy’, *Nature Medicine*, 19(8), pp. 1061–1066. doi: 10.1038/nm.3192.

Zhang, C. and Murphy, B. D. (2013) ‘Progesterone is critical for the development of mouse embryos’, *Endocrine*, 46(3), pp. 615–623. doi: 10.1007/s12020-013-0140-7.

Zhang, S. *et al.* (2013) ‘Physiological and molecular determinants of embryo implantation’, *Mol Aspects Med*, 34(5), pp. 939–980. doi: 10.1016/j.mam.2012.12.011.

Zhang, W.-Q. *et al.* (2018) ‘Comparative Transcriptomic Analysis of Embryo Implantation in Mice and Rats’, *Cellular Physiology and Biochemistry*, 50(2), pp. 668–678. doi:

10.1159/000494187.

Zhao, F. *et al.* (2013) 'Postweaning Exposure to Dietary Zearalenone, a Mycotoxin, Promotes Premature Onset of Puberty and Disrupts Early Pregnancy Events in Female Mice', *Toxicological Sciences*, 132(2), pp. 431–442. Available at: http://proxy-remote.galib.uga.edu/login?url=http://search.ebscohost.com/login.aspx?direct=true&db=eih&AN=86227247&site=eds-live.

Zhao, F. *et al.* (2014) 'Timing and recovery of postweaning exposure to diethylstilbestrol on early pregnancy in CD-1 mice', *Reproductive Toxicology*, 49, pp. 48–54. doi: 10.1016/j.reprotox.2014.07.072.

Zhao, M., Zhang, W.-Q. and Liu, J.-L. (2017) 'A study on regional differences in decidualization of the mouse uterus', *Reproduction*, 153(5), pp. 645–653. doi: 10.1530/REP-16-0486.

El Zowalaty, A. E., Li, R., Zheng, Y., *et al.* (2017) 'Deletion of RhoA in Progesterone Receptor-Expressing Cells Leads to Luteal Insufficiency and Infertility in Female Mice', *Endocrinology*, 158(7), pp. 2168–2178. doi: 10.1210/en.2016-1796.

El Zowalaty, A. E., Li, R., Chen, W., *et al.* (2017) 'Seipin deficiency leads to increased endoplasmic reticulum stress and apoptosis in mammary gland alveolar epithelial cells during lactation†', *Biology of Reproduction*, 98(4), pp. 570–578. doi: 10.1093/biolre/iox169.

APPENDICE A

SUPPLEMENTARY CHAPTER 6: EFFECTS OF MYCOESTROGENS ON FEMALE REPRODUCTION[1]

[1]Andersen, C.L., F. Zhao, X. Ye. 2018. *Reproductive and Developmental Medicine*. 1:52-58.

Reprinted here with permissions of the publisher

Abstract

Zearalenone (ZEA) is produced by *Fusarium* species and a common contaminant in food. ZEA and its metabolites α- and β-zearalenol, α- and β-zearalanol, and zearalanone are mycoestrogens that can interfere with estrogen signaling. Epidemiological studies correlated mycoestrogens with precocious puberty in girls. Animal studies established causal roles of mycoestrogens in accelerating female pubertal onset. High levels of mycoestrogens reduced female fertility in farm animals and rodents, in which adverse effects of mycoestrogens on major events in female reproduction, including ovarian folliculogenesis, ovulation, ovarian steroidogenesis, fertilization, preimplantation embryo development and transport, embryo implantation, placentation, parturition, and lactation, have been reported in different experimental settings.

(Key words: Zearalenone (ZEA), mycoestrogens, puberty, female reproduction)

Introduction

Mycotoxins are toxic substances produced by fungi and ubiquitously found in the environment. Major mycotoxins include aflatoxins, citrinin, ergot alkaloids, fumonisins, ochratoxin, patulin, trichothecenes, and zearalenone (ZEA), etc. [1] Among them, ZEA and its derivatives are also called mycoestrogens due to their estrogenicity. [2-4] Other mycotoxins may have endocrine disrupting effects, but are not specifically estrogenic. [5, 6]

ZEA is produced by several *Fusarium* species. [7] It is commonly found in livestock feed and human food, such as corn, rice, oats and wheat. One study indicated quantifiable ZEA contamination in 15% of food samples in Europe. [8] ZEA contamination levels in food are usually in the range of ppb and low ppm, with the highest reported reaching 600 ppm. [7-10] Contaminated food is the primary source of mycoestrogen exposure for mammals. ZEA is quickly absorbed and the unconjugated ZEA has an elimination half-life of 16.8 hours after oral administration in male rats. [8] ZEA is mainly metabolized in the liver to α- and β-zearalenol, which can be further metabolized to form α-zearalanol (zeranol), β-zearalanol (teranol), and zearalanone. [7, 11-14] Because of their structural similarity with 17β-estradiol (E2) and their interactions with

estrogen receptors, [2-4] ZEA and its metabolites have estrogenicity with α-zearalenol being the most potent one. [11, 15, 16]

Female reproduction follows pubertal development, which prepares the ovaries, the female reproductive track, and the mammary glands for sexual maturation and reproductive capabilities. [17] Female reproduction involves multiple integral processes, including ovarian folliculogenesis, ovulation, ovarian steroidogenesis, fertilization, preimplantation embryo development and transport, embryo implantation, placentation, parturition, and lactation. Female reproduction is regulated by hormones and estrogen is an essential one. Estrogen mainly acts through estrogen receptors, ERα, ERβ, and potentially G protein coupled ER (GPER/GPR30). [18, 19] Estrogen receptor(s)-modified animal models have revealed the essential *in vivo* roles of estrogen signaling in all the above events except placentation, parturition, and lactation due to defective early pregnancy and defective mammary gland development that prevent the study of these later events in the animal models. [18, 20-23]

Mycoestrogens pose risks on female reproduction because of their ubiquitous presence in the environment and their estrogenicity in interfering with endogenous estrogen signaling. They have been linked to reduced female fertility in farm animals and rodents. [24-30] Here, we review the *in vivo* effects of mycoestrogens on the main events in female reproduction.

Pubertal development

Puberty is a multistage process with dramatic changes in physical appearance and hormonal levels to obtain sexual maturation and reproductive capabilities. Although the precise mechanisms behind pubertal initiation remain largely unknown, the hypothalamic–pituitary–gonadal (HPG)-axis and ERα are essential for pubertal development. [31-34] Pubertal period represents an important stage of development with extreme sensitivity to exogenous estrogens, which can potentially regulate neuronal HPG-axis via positive or negative feedback to influence pubertal development. [31, 32, 35, 36]

Epidemiological studies have correlated mycoestrogens with precocious puberty in girls (onset of secondary sex characteristics by 8 years old). An early epidemiological study suggested a correlation

between α-zearalanol exposure and a rise of precocious puberty in Puerto Rican girls, although the evaluation criteria for precocious puberty were questioned. [37, 38] Elevated urinary and serum ZEA levels were found in Turkish girls and Chinese girls with precocious puberty, respectively. [39, 40] A study in Italy found high levels of ZEA and α-zearalenol in ~20% of girls with precocious puberty. [41]

Animal studies have established a cause-effect relationship between mycoestrogens and pubertal development. In rodents, vaginal opening is an early sign of puberty that can be affected by endocrine disruptors. [26, 27] We found that postweaning exposure to 10 ppm~40 ppm ZEA diet (1.25-5 mg/kg/day) accelerated vaginal opening in mice and multigenerational exposure to 20 ppm ZEA diet did not have an accumulative effect on accelerating vaginal opening. [26, 27] Accelerated vaginal opening by ZEA treatment (10 mg/kg/day, gavage, from postnatal day (PND) 18 for 10 days; or 5 mg/kg/day, gavage, from PND15 for 5 days) was also seen in rats. [42, 43] Although prepubertal (~PND15 in rodents) represent a critical window when the HPG axis begins to function, neonatal exposure to ZEA (2 mg/kg/day, subcutaneous (s.c.) injection, PND1-5) still accelerated vaginal opening in mice. [44] Over-stimulation of the kisspeptin-GPR54-GnRH signaling pathway within the HPG-axis has been implicated in ZEA-induced acceleration of pubertal development in rodents. [42-44]

Results from the animal studies support mycoestrogens, especially ZEA, to be a cause for early puberty onset, which may agree with the correlation of mycoestrogens and precocious puberty in girls from epidemiological studies. However, the levels of mycoestrogens that affect puberty onset in animal models are high and are irrelevant to the exposure levels of general population. On the other hand, humans are exposed to various endocrine disruptors, the precocious puberty in girls could be the net result of genetic factors and exposure to multiple endocrine disruptors.

Ovarian folliculogenesis, ovulation, corpus luteum steroidogenesis

Ovarian functions in folliculogenesis, ovulation, and corpus luteum formation and steroidogenesis not only prepare female germ cells for pregnancy but also produce ovarian hormones to support early embryo development and to prepare the uterus for embryo implantation. ZEA can cause ovarian follicle

atresia in sexually immature gilts. [45] Mice exposed to 40 ppm ZEA during premating (3-8 weeks old) did not affect the number of oocytes and embryos detected in D1.5 oviducts, [27] suggesting that ovarian folliculogenesis and ovulation were not affected under the experimental setting that impaired later events. However, another study showed that prenatal (D15-D19) ZEA treatment (10 mg/kg/day s.c. injection on dams) led to anovulation detected at 4-16 weeks old in mice. [46] The discrepancy in the effects of ZEA on ovulation could be contributed by the differences in animal strains, doses, exposure routes, and exposure windows.

The corpus luteum is a temporary endocrine gland developed in an ovulated follicle. It is the main site for progesterone production to support early pregnancy in all mammalian species. [47] ZEA has been implicated in disrupting corpus luteum formation and/or steroidogenesis. Exposure to ZEA diets (60 ppm, 90 ppm) from postmating D2 to D15 caused fetal loss and progesterone deficiency in gilts detected during 2-6 weeks postmating. [25] ZEA treatment (8 mg/kg/day, s.c.) from D0.5-D4.5 caused significant reduction of plasma progesterone in mice. [28] Reduced number of corpora lutea upon multigenerational treatment with 10 mg/kg/day ZEA diet was demonstrated in F1 and F2 rats, [29] indicating impaired ovarian folliculogenesis, ovulation, and/or corpus luteum formation.

Fertilization

In vivo fertilization occurs in the oviduct where the newly ovulated oocyte meets sperm. Our study in mice revealed reduced fertilization upon premating exposure to 40 ppm ZEA diet. [27] Successful *in vivo* fertilization requires timely presence of functional oocytes and sperm as well as an optimal oviductal environment. *In vitro* studies have showed adverse effects of mycoestrogens on sperm motility and acrosome reaction; [48] and on the response of oviductal epithelial cells to sperm. [49] However, our *in vivo* study showed no adverse effect on male fertility upon 40 ppm ZEA dietary exposure (a dose that severely impaired female fertility) for 3 weeks. [27] Considering the essential role of estrogen signaling for sperm migration in the female reproductive tract, [22] and the impaired embryo transport in the oviduct of mice treated with ZEA, [27] ZEA may disrupt timely migration of sperm to oviduct, without affecting the function

of sperm per se, to impair fertilization. Any adverse effect of ZEA on *in vivo* oocyte quality leading to impaired fertilization cannot be excluded.

Preimplantation embryo development and embryo transport

We demonstrated it in mice that exposure to 40 ppm ZEA diet had adverse effects on preimplantation embryo development. [27] Premating ZEA exposure (3-8 weeks old) reduced fertilization rate. Interestingly, all the embryos from the vehicle control mice were in 2-cell stage, while the majority of embryos recovered from 40 ppm ZEA-treated mice were in 4-8-cell stage on D1.5. This seemingly accelerated early embryo development was most likely caused by the prolonged estrus stage thus earlier mating activity, shortly after setting up for mating between 1100 h and 1700 h in the ZEA-treated mice instead of ~midnight in the control. [27] Postmating exposure (D0.5-D3.5) to 40 ppm ZEA diet did not affect fertilization but delayed embryo development detected on D3.5. [27] Dietary ZEA (1 mg/kg body weight) exposure of sows from D7 to D10 caused blastocyst degeneration. [50] We found that postmating ZEA treatment also delayed embryo transport from oviduct to uterus and the embryos retained in the D3.5 oviduct were more delayed in development than those already transported to the uterus. [27] The effect of ZEA on delaying/blocking embryo transport from oviduct to uterus was also observed in mice treated with ZEA (2-8 mg/kg/day, s.c.) from D0.5-D4.5. [28]

It is unknown whether delayed embryo development caused delayed embryo transport or vice versa, or ZEA affected both events independently. [27] The correlation between delayed embryo development and delayed embryo transport in postmating ZEA exposure may reflect the varied sensitivity of individual mice to ZEA treatment, e.g., both embryo transport and embryo development are more affected in mice that are potentially more sensitive to ZEA exposure. Since estrogen can influence the expression of oviductal glycoprotein(s) that could interact with the gametes and early embryos, [51, 52] it is possible that the estrogenic property of ZEA may affect preimplantation development via altered oviductal environment. Lack of oviductal epithelial ERα leads to elevated protease activity and lysis of early embryos in the oviduct. [22] It remains to be investigated if enhanced estrogen signaling by estrogenic chemicals like

ZEA would disrupt protease balance in the oviduct to affect early embryo development. ZEA can impair corpus luteum thus reduce progesterone production. [28, 29] Progesterone deficiency not only could delay preimplantation embryo development [53] but also could further tilt the unbalanced ratio of estrogen / progesterone signaling towards even stronger estrogen signaling, resulting in defective embryo transport from oviduct to uterus in mice. Although progesterone levels were not measured in our study, the assumed reduced progesterone levels and known enhanced estrogen signaling upon ZEA treatment could explain the correlation between delayed embryo development and retention of embryos in the oviduct. [27] ZEA increased cell proliferation in the oviduct of immature gilts. [45] The molecular mechanism of mycoestrogens on oviductal transport is largely unknown.

Embryo implantation

Embryo implantation is the critical initial step for establishing physical fetal-maternal interactions. It requires synchronized readiness of a competent embryo and a receptive uterus, as well as their mutual signal communications. Any disruption in the preimplantation events (e.g., fertilization, embryo development and transport) will result in impaired embryo implantation. Uterine receptivity is controlled by ovarian hormones estrogen and progesterone. Imbalanced estrogen and progesterone signaling can lead to delayed establishment of uterine receptivity [54, 55] or a non-receptive uterus [56] to impair embryo implantation.

ZEA at high doses (e.g., 20-40 ppm in diet, 8 mg/kg/day s.c. injection) can disrupt embryo implantation in mice. [26-28] Postweaning mice fed with 40 ppm ZEA diet had disrupted embryo implantation and a distended uterus with disrupted expression of the progesterone receptor, [27] representing enhanced estrogen signaling that could also be aggravated by the potential progesterone deficiency. [28] Multigenerational exposure to 20 ppm ZEA diet did not affect embryo implantation in F0 females but reduced implantation rates and delayed embryo implantation in those F1 and F2 females with implantation sites, [26] indicating an accumulative effect upon ZEA exposure. In both studies, no obvious adverse effect on embryo implantation was observed in mice treated with ≤4 ppm ZEA diets, [26, 27] indicating a threshold

exposure level for ZEA to affect embryo implantation; and we noticed that cessation of exposure to 20 ppm or 40 ppm ZEA diets could lead to restoration of embryo implantation in most cases. [26, 27]

Decidualization occurs in the stromal cells at the implantation site a few hours after embryo attachment [57] to prepare the uterus for embryo invasion into the endometrium. Decidualization detected on D7.5 was impaired in mice treated with ZEA (8 mg/kg/day ZEA, s.c., D0.5~D4.5), which could be due to the reduced progesterone level. [28] Distended uterus on D4.5 [27] and impaired decidualization on D7.5 [28] demonstrate that ZEA at high doses has direct effects on the uterus to disrupt embryo implantation, most likely due to enhanced estrogen signaling resulted from the estrogenicity of ZEA and reduced progesterone signaling. Enhanced estrogen signaling is also supported by the observation that ZEA increased cell proliferation in the uterus of immature gilts. [45]

Placental development and function

The placenta is a transient organ serving as the sole bridge between the mother and the fetus in eutherians, thus a functional placenta is essential for fetal development and maternal health. A placenta has three major layers: the outer maternal layer that includes decidual cells and maternal vasculature; the middle "junctional" zone that attaches the fetal placenta to the uterus and contains trophoblast cells invading the uterine wall and maternal vessels; and the inner labyrinth layer with highly branched villi for efficient nutrient exchange and fetal waste disposal. [58] The placenta is an important organ for toxicological evaluations but is seriously understudied. To address this issue, the National Institute of Environmental Health Sciences in USA recently put out a Funding Opportunity, 'Environmental influences on Placental Origins of Development (ePOD)'.

Several studies have alluded to the placenta as a target of mycoestrogens. Bioactivation of ZEA in placental cells [59] could make the placenta more sensitive to mycoestrogen insult. Upon exposure to 2.76 ppm ZEA diet from D35 to D70 of pregnancy, ZEA level in the D70 placenta of sow was 130 fold and 20 fold higher than that in the D70 plasma and fetal liver, respectively, suggesting accumulation of ZEA in the placenta. This study also found reduced placenta weights at D70 and farrowing as well as reduced live fetus

weight at D70 and live piglet weight at birth, [60] implying impaired placental function that was not furthered investigated. Multigenerational studies indicated increased post-implantational death in F1 and F2 mice [26] and rats, [29] which could be contributed by delayed embryo implantation, [55, 61] compromised placental functions, and/or direct adverse effect on the fetus as mycoestrogens can pass through placenta to fetus. [62, 63] Rats exposed to ZEA diet (20 ppm, D0.5 to D20.5) had viable newborns with reduced birth weight and placentas with reduced *Esr1* (ERα) mRNA levels. [64] Mice treated with zeranol (10 and 100 mg/kg/day, gavage, D13.5~D16.5) had D17.5 placentas with dysregulation of genes involved in cell cycle and apoptosis, but any related cellular effects were not reported. [65] Overall, well-designed experiments to address the effects and mechanisms of mycoestrogens on placental development and function are still lacking.

Parturition

Parturition is the last step of pregnancy in which the uterus transits from quiescence to contraction to propel the fetus. The timing of parturition is critical for the health of the mother and newborn. Research from past decades has provided critical insights into parturition, but the molecular mechanisms involved in the initiation of parturition remain largely unknown. [66, 67] Limited studies have referred to potential effects of mycoestrogens on parturition. We noticed delayed parturition in the F1 and F2 mice treated with 20 ppm ZEA diet in the multigenerational setting, which was most likely caused by delayed embryo implantation thus prolonged gestation period. [26] Pregnant gilts (89 +/- 2 days gestation) fed an experimental diet with 5.08 ppm deoxynivalenol, 0.09 ppm ZEA and 21.6 ppm fusaric acid had a prolonged parturition process. [68] Because of the low concentration of ZEA compared to the other chemicals in the diet, the contribution of ZEA on the parturition is questionable. When pregnant ICR mice were given zeranol (100 mg/kg/day, gavage, D13.5-D16.5), there was an increased percentage of mice with preterm birth, which was not observed in mice treated with 1 or 10 mg/kg/day. [65] Our studies [26, 27] suggested that a dose of 100 mg/kg/day zeranol in mice would be equivalent to ~800 ppm zeranol in the diet, which would exceed the

reported highest concentration of its parent compound ZEA in a contaminated diet (600 ppm). [7] Therefore, effects of mycoestrogens at environmental relevant exposure levels on parturition remain to be investigated.

Mammary gland development and lactation

Mammary gland development is characterized by branching morphogenesis to form a ductal tree filling the fat pad. [69-71] During pregnancy, the mammary gland undergoes tremendous side-branching and alveologenesis to prepare for lactation. [69] These processes are regulated by estrogen signaling [71-74] and can be targeted by mycoestrogens. Limited studies have shown effects of mycoestrogens on mammary gland development and lactation. Prenatal (D15-D19) ZEA treatment (10 mg/kg/day, s.c.) led to anovulation and growth retardation of mammary glands in most mice but those ZEA-treated mice with corpora lutea showed increased alveolar differentiation at 4 weeks old. [46] Prenatal (D9-delivery) and neonatal (PND1-5) ZEA exposure (20 ug/kg/day~5 mg/kg/day, s.c.) of rats led to increased mean terminal end buds at PND30 and increased mammary gland epithelial cell proliferation at PND180.[75] Sows exposed to 2.76 ppm ZEA diet from D35 to D70 had decreased levels of total solids, protein, fat, and lactose in the colostrum and milk. [60] The cellular, molecular, and functional effects of mycoestrogens on the mammary gland remain to be investigated.

Endometrial and breast cancer

Because of their estrogenicity, mycoestrogens potentially have tumor-promoting activity in estrogen-dependent tissues, such as endometrium and mammary gland. Although a cause-effect relationship has not been established *in vivo*, ZEA and α-zearalenol were frequently detected in human endometrial cancer tissues but undetectable in normal human endometrial tissues, [76, 77] and there was a correlation between increased urine α-zearalenol level and increased risk of breast cancer. [78]

Conclusion and future directions

Mycoestrogens at levels found in highly contaminated food have been demonstrated to affect mammalian female pubertal development and reproduction. Future directions shall fill in knowledge gaps, such as systematic time-course and dose-response *in vivo* effects of mycoestrogens on main reproduction events (e.g., placental development); effects of real life exposure to mixtures of mycoestrogens with other mycotoxins on mammalian reproduction; as well as endocrine, cellular and molecular mechanisms involved.

References

1. Bennett JW, Klich M. Mycotoxins. Clinical Microbiology Reviews 2003; 16:497-516. doi:10.1128/CMR.16.3.497-516.2003
2. Gromadzka K, Waskiewicz A, Golinski P, Swietlik J. Occurrence of estrogenic mycotoxin - Zearalenone in aqueous environmental samples with various NOM content. Water Res 2009; 43:1051-1059. doi:10.1016/j.watres.2008.11.042
3. Li Y, Burns KA, Arao Y, Luh CJ, Korach KS. Differential estrogenic actions of endocrine-disrupting chemicals bisphenol A, bisphenol AF, and zearalenone through estrogen receptor alpha and beta in vitro. Environ Health Perspect 2012; 120:1029-1035. doi:10.1289/ehp.1104689
4. He J, Wei C, Li Y, Liu Y, Wang Y, Pan J, Liu J, Wu Y, Cui S. Zearalenone and alpha-zearalenol inhibit the synthesis and secretion of pig follicle stimulating hormone via the non-classical estrogen membrane receptor GPR30. Mol Cell Endocrinol 2018; 461:43-54. doi:10.1016/j.mce.2017.08.010
5. Streit E, Schatzmayr G, Tassis P, Tzika E, Marin D, Taranu I, Tabuc C, Nicolau A, Aprodu I, Puel O, Oswald IP. Current Situation of Mycotoxin Contamination and Co-occurrence in Animal Feed—Focus on Europe. Toxins 2012; 4:788-809. doi:10.3390/toxins4100788
6. Demaegdt H, Daminet B, Evrard A, Scippo M-L, Muller M, Pussemier L, Callebaut A, Vandermeiren K. Endocrine activity of mycotoxins and mycotoxin mixtures. Food and Chemical Toxicology 2016; 96:107-116. doi:https://doi.org/10.1016/j.fct.2016.07.033

7. Zinedine A, Soriano JM, Molto JC, Manes J. Review on the toxicity, occurrence, metabolism, detoxification, regulations and intake of zearalenone: an oestrogenic mycotoxin. Food Chem Toxicol 2007; 45:1-18. doi:S0278-6915(06)00243-2 [pii]10.1016/j.fct.2006.07.030

8. EFSA. Scientific Opinion on the risks for public health related to the presence of zearalenone in food. EFSA Journal 2011; 9:2197. doi:10.2903

9. Sangare-Tigori B, Moukha S, Kouadio HJ, Betbeder AM, Dano DS, Creppy EE. Co-occurrence of aflatoxin B1, fumonisin B1, ochratoxin A and zearalenone in cereals and peanuts from Cote d'Ivoire. Food Addit Contam 2006; 23:1000-1007. doi:10.1080/02652030500415686

10. Price WD, Lovell RA, McChesney DG. Naturally occurring toxins in feedstuffs: Center for Veterinary Medicine Perspective. J Anim Sci 1993; 71:2556-2562

11. Kuiper-Goodman T, Scott PM, Watanabe H. Risk assessment of the mycotoxin zearalenone. Regul Toxicol Pharmacol 1987; 7:253-306

12. Mirocha CJ, Pathre SV, Robison TS. Comparative metabolism of zearalenone and transmission into bovine milk. Food Cosmet Toxicol 1981; 19:25-30

13. Bravin F, Duca RC, Balaguer P, Delaforge M. In vitro cytochrome p450 formation of a mono-hydroxylated metabolite of zearalenone exhibiting estrogenic activities: possible occurrence of this metabolite in vivo. Int J Mol Sci 2009; 10:1824-1837. doi:10.3390/ijms10041824

14. Belhassen H, Jimenez-Diaz I, Ghali R, Ghorbel H, Molina-Molina JM, Olea N, Hedili A. Validation of a UHPLC-MS/MS method for quantification of zearalenone, alpha-zearalenol, beta-zearalenol, alpha-zearalanol, beta-zearalanol and zearalanone in human urine. J Chromatogr B Analyt Technol Biomed Life Sci 2014; 962:68-74. doi:10.1016/j.jchromb.2014.05.019

15. Frizzell C, Ndossi D, Verhaegen S, Dahl E, Eriksen G, Sorlie M, Ropstad E, Muller M, Elliott CT, Connolly L. Endocrine disrupting effects of zearalenone, alpha- and beta-zearalenol at the level of nuclear receptor binding and steroidogenesis. Toxicol Lett 2011; 206:210-217. doi:10.1016/j.toxlet.2011.07.015

16. Ueno Y, Tashiro F. alpha-Zearalenol, a major hepatic metabolite in rats of zearalenone, an estrogenic mycotoxin of Fusarium species. J Biochem 1981; 89:563-571

17. Blaustein JD, Ismail N, Holder MK. Review: Puberty as a time of remodeling the adult response to ovarian hormones. The Journal of steroid biochemistry and molecular biology 2016; 160:2-8. doi:10.1016/j.jsbmb.2015.05.007

18. Hewitt SC, Winuthayanon W, Korach KS. What's new in estrogen receptor action in the female reproductive tract. J Mol Endocrinol 2016; 56:R55-71. doi:10.1530/JME-15-0254

19. Stefkovich ML, Arao Y, Hamilton KJ, Korach KS. Experimental models for evaluating non-genomic estrogen signaling. Steroids 2017. doi:10.1016/j.steroids.2017.11.001

20. Hamilton KJ, Arao Y, Korach KS. Estrogen hormone physiology: reproductive findings from estrogen receptor mutant mice. Reprod Biol 2014; 14:3-8. doi:10.1016/j.repbio.2013.12.002

21. Pawar S, Laws MJ, Bagchi IC, Bagchi MK. Uterine Epithelial Estrogen Receptor-alpha Controls Decidualization via a Paracrine Mechanism. Mol Endocrinol 2015; 29:1362-1374. doi:10.1210/me.2015-1142

22. Winuthayanon W, Bernhardt ML, Padilla-Banks E, Myers PH, Edin ML, Hewitt SC, Korach KS, Williams CJ. Oviductal estrogen receptor alpha signaling prevents protease-mediated embryo death. Elife 2015; 4:e10453. doi:10.7554/eLife.10453

23. Feng Y, Manka D, Wagner KU, Khan SA. Estrogen receptor-alpha expression in the mammary epithelium is required for ductal and alveolar morphogenesis in mice. Proc Natl Acad Sci U S A 2007; 104:14718-14723. doi:10.1073/pnas.0706933104

24. Chang K, Kurtz HJ, Mirocha CJ. Effects of the mycotoxin zearalenone on swine reproduction. Am J Vet Res 1979; 40:1260-1267

25. Long GG, Diekman MA. Effect of purified zearalenone on early gestation in gilts. J Anim Sci 1984; 59:1662-1670

26. Zhao F, Li R, Xiao S, Diao H, El Zowalaty AE, Ye X. Multigenerational exposure to dietary zearalenone (ZEA), an estrogenic mycotoxin, affects puberty and reproduction in female mice. Reprod Toxicol 2014; 47C:81-88. doi:10.1016/j.reprotox.2014.06.005

27. Zhao F, Li R, Xiao S, Diao H, Viveiros MM, Song X, Ye X. Postweaning exposure to dietary zearalenone, a mycotoxin, promotes premature onset of puberty and disrupts early pregnancy events in female mice. Toxicol Sci 2013; 132:431-442. doi:10.1093/toxsci/kfs343

28. Kunishige K, Kawate N, Inaba T, Tamada H. Exposure to Zearalenone During Early Pregnancy Causes Estrogenic Multitoxic Effects in Mice. Reprod Sci 2017; 24:421-427. doi:10.1177/1933719116657194

29. Becci PJ, Johnson WD, Hess FG, Gallo MA, Parent RA, Taylor JM. Combined two-generation reproduction-teratogenesis study of zearalenone in the rat. J Appl Toxicol 1982; 2:201-206

30. Zhang Y, Jia Z, Yin S, Shan A, Gao R, Qu Z, Liu M, Nie S. Toxic effects of maternal zearalenone exposure on uterine capacity and fetal development in gestation rats. Reprod Sci 2014; 21:743-753. doi:10.1177/1933719113512533

31. Clarke IJ. Control of GnRH secretion: one step back. Front Neuroendocrinol 2011; 32:367-375. doi:10.1016/j.yfrne.2011.01.001

32. d'Anglemont de Tassigny X, Fagg LA, Carlton MB, Colledge WH. Kisspeptin can stimulate gonadotropin-releasing hormone (GnRH) release by a direct action at GnRH nerve terminals. Endocrinology 2008; 149:3926-3932. doi:10.1210/en.2007-1487

33. Quaynor SD, Stradtman EW, Jr., Kim HG, Shen Y, Chorich LP, Schreihofer DA, Layman LC. Delayed puberty and estrogen resistance in a woman with estrogen receptor alpha variant. N Engl J Med 2013; 369:164-171. doi:10.1056/NEJMoa1303611

34. Luo Y, Liu Q, Lei X, Wen Y, Yang YL, Zhang R, Hu MY. Association of estrogen receptor gene polymorphisms with human precocious puberty: a systematic review and meta-analysis. Gynecol Endocrinol 2015; 31:516-521. doi:10.3109/09513590.2015.1031102

35. Braun JM. Early Life Exposure to Endocrine Disrupting Chemicals and Childhood Obesity and Neurodevelopment. Nature reviews. Endocrinology 2017; 13:161-173. doi:10.1038/nrendo.2016.186

36. RAMIREZ VD, SAWYER CH. Advancement of puberty in the female rat by estrogen. Endocrinology 1965; 76:1158-1168

37. Environmental Hormone Contamination in Puerto Rico. New England Journal of Medicine 1984; 310:1741-1742. doi:10.1056/nejm198406283102612

38. Ingle M, Martin B. Precocious puberty in puerto rico. The Journal of pediatrics 1986; 109:390

39. Asci A, Durmaz E, Erkekoglu P, Pasli D, Bircan I, Kocer-Gumusel B. Urinary zearalenone levels in girls with premature thelarche and idiopathic central precocious puberty. Minerva Pediatr 2014; 66:571-578

40. Deng F, Tao FB, Liu DY, Xu YY, Hao JH, Sun Y, Su PY. Effects of growth environments and two environmental endocrine disruptors on children with idiopathic precocious puberty. Eur J Endocrinol 2012; 166:803-809. doi:10.1530/EJE-11-0876

41. Massart F, Meucci V, Saggese G, Soldani G. High Growth Rate of Girls with Precocious Puberty Exposed to Estrogenic Mycotoxins. The Journal of Pediatrics 2008; 152:690-695.e691. doi:https://doi.org/10.1016/j.jpeds.2007.10.020

42. Kriszt R, Winkler Z, Polyak A, Kuti D, Molnar C, Hrabovszky E, Kallo I, Szoke Z, Ferenczi S, Kovacs KJ. Xenoestrogens Ethinyl Estradiol and Zearalenone Cause Precocious Puberty in Female Rats via Central Kisspeptin Signaling. Endocrinology 2015; 156:3996-4007. doi:10.1210/en.2015-1330

43. Yang R, Wang YM, Zhang L, Zhao ZM, Zhao J, Peng SQ. Prepubertal exposure to an oestrogenic mycotoxin zearalenone induces central precocious puberty in immature female rats through the mechanism of premature activation of hypothalamic kisspeptin-GPR54 signaling. Mol Cell Endocrinol 2016; 437:62-74. doi:10.1016/j.mce.2016.08.012

44. Parandin R, Behnam-Rassouli M, Mahdavi-Shahri N. Effects of Neonatal Exposure to Zearalenone on Puberty Timing, Hypothalamic Nuclei of AVPV and ARC, and Reproductive Functions in Female Mice. Reprod Sci 2017; 24:1293-1303. doi:10.1177/1933719116683808

45. Obremski K, Gajecki M, Zwierzchowski W, Zielonka L, Otrocka-Domagala I, Rotkiewicz T, Mikolajczyk A, Gajecka M, Polak M. Influence of zearalenone on reproductive system cell proliferation in gilts. Pol J Vet Sci 2003; 6:239-245

46. Nikaido Y, Yoshizawa K, Danbara N, Tsujita-Kyutoku M, Yuri T, Uehara N, Tsubura A. Effects of maternal xenoestrogen exposure on development of the reproductive tract and mammary gland in female CD-1 mouse offspring. Reprod Toxicol 2004; 18:803-811. doi:10.1016/j.reprotox.2004.05.002 S0890623804000899 [pii]

47. Bazer FW, Wu G, Spencer TE, Johnson GA, Burghardt RC, Bayless K. Novel pathways for implantation and establishment and maintenance of pregnancy in mammals. Mol Hum Reprod 2010; 16:135-152. doi:gap095 [pii]10.1093/molehr/gap095

48. Filannino A, Stout TA, Gadella BM, Sostaric E, Pizzi F, Colenbrander B, Dell'Aquila ME, Minervini F. Dose-response effects of estrogenic mycotoxins (zearalenone, alpha- and beta-zearalenol) on motility, hyperactivation and the acrosome reaction of stallion sperm. Reprod Biol Endocrinol 2011; 9:134. doi:10.1186/1477-7827-9-134

49. Yousef MS, Takagi M, Talukder AK, Marey MA, Kowsar R, Abdel-Razek AK, Shimizu T, Fink-Gremmels J, Miyamoto A. Zearalenone (ZEN) disrupts the anti-inflammatory response of bovine oviductal epithelial cells to sperm in vitro. Reprod Toxicol 2017; 74:158-163. doi:10.1016/j.reprotox.2017.09.012

50. Long GG, Turek J, Diekman MA, Scheidt AB. Effect of zearalenone on days 7 to 10 post-mating on blastocyst development and endometrial morphology in sows. Vet Pathol 1992; 29:60-67. doi:10.1177/030098589202900108

51. Bhatt P, Kadam K, Saxena A, Natraj U. Fertilization, embryonic development and oviductal environment: role of estrogen induced oviductal glycoprotein. Indian J Exp Biol 2004; 42:1043-1055

52. Niu BY, Xiong YZ, Li FE, Jiang SW, Deng CY, Ding SH, Guo WH, Lei MG, Zheng R, Zuo B, Xu DQ, Li JL. Oviduct-specific glycoprotein 1 locus is associated with litter size and weight of ovaries in pigs. Asian-Australasian Journal of Animal Sciences 2006; 19:632-637

53. Zhang C, Murphy BD. Progesterone is critical for the development of mouse embryos. Endocrine 2014; 46:615-623. doi:10.1007/s12020-013-0140-7

54. Diao H, Li R, El Zowalaty AE, Xiao S, Zhao F, Dudley EA, Ye X. Deletion of Lysophosphatidic Acid Receptor 3 (Lpar3) Disrupts Fine Local Balance of Progesterone and Estrogen Signaling in Mouse Uterus During Implantation. Biol Reprod 2015; 93:123. doi:10.1095/biolreprod.115.131110

55. Ye X, Hama K, Contos JJ, Anliker B, Inoue A, Skinner MK, Suzuki H, Amano T, Kennedy G, Arai H, Aoki J, Chun J. LPA3-mediated lysophosphatidic acid signalling in embryo implantation and spacing. Nature 2005; 435:104-108

56. El Zowalaty AE, Li R, Zheng Y, Lydon JP, DeMayo FJ, Ye X. Deletion of RhoA in Progesterone Receptor-Expressing Cells Leads to Luteal Insufficiency and Infertility in Female Mice. Endocrinology 2017; 158:2168-2178. doi:10.1210/en.2016-1796

57. Diao H, Paria BC, Xiao S, Ye X. Temporal expression pattern of progesterone receptor in the uterine luminal epithelium suggests its requirement during early events of implantation. Fertil Steril 2011; 95:2087-2093. doi:S0015-0282(11)00239-1 [pii]10.1016/j.fertnstert.2011.01.160

58. Watson ED, Cross JC. Development of structures and transport functions in the mouse placenta. Physiology (Bethesda) 2005; 20:180-193. doi:10.1152/physiol.00001.2005

59. Huuskonen P, Auriola S, Pasanen M. Zearalenone metabolism in human placental subcellular organelles, JEG-3 cells, and recombinant CYP19A1. Placenta 2015; 36:1052-1055. doi:10.1016/j.placenta.2015.06.014

60. Zhang Y, Gao R, Liu M, Shi B, Shan A, Cheng B. Use of modified halloysite nanotubes in the feed reduces the toxic effects of zearalenone on sow reproduction and piglet development. Theriogenology 2015; 83:932-941. doi:10.1016/j.theriogenology.2014.11.027

61. Ye X, Diao H, Chun J. 11-deoxy prostaglandin F(2alpha), a thromboxane A2 receptor agonist, partially alleviates embryo crowding in Lpar3((-/-)) females. Fertil Steril 2012; 97:757-763. doi:10.1016/j.fertnstert.2011.12.004

62. Bernhoft A, Behrens GH, Ingebrigtsen K, Langseth W, Berndt S, Haugen TB, Grotmol T. Placental transfer of the estrogenic mycotoxin zearalenone in rats. Reprod Toxicol 2001; 15:545-550

63. Lange IG, Daxenberger A, Meyer HH, Rajpert-De Meyts E, Skakkebaek NE, Veeramachaneni DN. Quantitative assessment of foetal exposure to trenbolone acetate, zeranol and melengestrol acetate, following maternal dosing in rabbits. Xenobiotica 2002; 32:641-651. doi:10.1080/00498250210143010

64. Gao X, Sun L, Zhang N, Li C, Zhang J, Xiao Z, Qi D. Gestational Zearalenone Exposure Causes Reproductive and Developmental Toxicity in Pregnant Rats and Female Offspring. Toxins (Basel) 2017; 9. doi:10.3390/toxins9010021

65. Wang Y, Li L, Wang CC, Leung LK. Effect of zeranol on expression of apoptotic and cell cycle proteins in murine placentae. Toxicology 2013; 314:148-154. doi:10.1016/j.tox.2013.09.011

66. Norwitz ER, Bonney EA, Snegovskikh VV, Williams MA, Phillippe M, Park JS, Abrahams VM. Molecular Regulation of Parturition: The Role of the Decidual Clock. Cold Spring Harb Perspect Med 2015; 5. doi:10.1101/cshperspect.a023143

67. Renthal NE, Williams KC, Montalbano AP, Chen CC, Gao L, Mendelson CR. Molecular Regulation of Parturition: A Myometrial Perspective. Cold Spring Harb Perspect Med 2015; 5. doi:10.1101/cshperspect.a023069

68. Jakovac-Strajn B, Vengust A, Pestevsek U. Effects of a deoxynivalenol-contaminated diet on the reproductive performance and immunoglobulin concentrations in pigs. Vet Rec 2009; 165:713-718

69. Macias H, Hinck L. Mammary gland development. Wiley Interdiscip Rev Dev Biol 2012; 1:533-557. doi:10.1002/wdev.35

70. Sinkevicius KW, Burdette JE, Woloszyn K, Hewitt SC, Hamilton K, Sugg SL, Temple KA, Wondisford FE, Korach KS, Woodruff TK, Greene GL. An estrogen receptor-alpha knock-in mutation provides evidence of ligand-independent signaling and allows modulation of ligand-induced pathways in vivo. Endocrinology 2008; 149:2970-2979. doi:10.1210/en.2007-1526

71. Korach KS, Couse JF, Curtis SW, Washburn TF, Lindzey J, Kimbro KS, Eddy EM, Migliaccio S, Snedeker SM, Lubahn DB, Schomberg DW, Smith EP. Estrogen receptor gene disruption: molecular characterization and experimental and clinical phenotypes. Recent Prog Horm Res 1996; 51:159-186; discussion 186-158

72. Palmieri C, Cheng GJ, Saji S, Zelada-Hedman M, Warri A, Weihua Z, Van Noorden S, Wahlstrom T, Coombes RC, Warner M, Gustafsson JA. Estrogen receptor beta in breast cancer. Endocr Relat Cancer 2002; 9:1-13

73. Krege JH, Hodgin JB, Couse JF, Enmark E, Warner M, Mahler JF, Sar M, Korach KS, Gustafsson JA, Smithies O. Generation and reproductive phenotypes of mice lacking estrogen receptor beta. Proc Natl Acad Sci U S A 1998; 95:15677-15682

74. Forster C, Makela S, Warri A, Kietz S, Becker D, Hultenby K, Warner M, Gustafsson JA. Involvement of estrogen receptor beta in terminal differentiation of mammary gland epithelium. Proc Natl Acad Sci U S A 2002; 99:15578-15583. doi:10.1073/pnas.192561299

75. Belli P, Bellaton C, Durand J, Balleydier S, Milhau N, Mure M, Mornex J-F, Benahmed M, Le Jan C. Fetal and neonatal exposure to the mycotoxin zearalenone induces phenotypic alterations in adult rat mammary gland. Food and Chemical Toxicology 2010; 48:2818-2826. doi:https://doi.org/10.1016/j.fct.2010.07.012

76. Pajewska M, Lojko M, Cendrowski K, Sawicki W, Kowalkowski T, Buszewski B, Gadzala-Kopciuch R. The determination of zearalenone and its major metabolites in endometrial cancer tissues. Anal Bioanal Chem 2018; 410:1571-1582. doi:10.1007/s00216-017-0807-7

77. Tomaszewski J, Mitурski R, Semczuk A, Kotarski J, Jakowicki J. [Tissue zearalenone concentration in normal, hyperplastic and neoplastic human endometrium]. Ginekol Pol 1998; 69:363-366

78. Belhassen H, Jimenez-Diaz I, Arrebola JP, Ghali R, Ghorbel H, Olea N, Hedili A. Zearalenone and its metabolites in urine and breast cancer risk: a case-control study in Tunisia. Chemosphere 2015; 128:1-6. doi:10.1016/j.chemosphere.2014.12.055

APPENDICE B

SUPPLEMENTARY CHAPTER 7: DIETARY EXPOSURE TO MYCOTOXIN ZEARALENONE (ZEA) DURING POST-IMPLANTATION ADVERSELY AFFECTS PLACENTAL DEVELOPMENT IN MICE[1]

[1]Li, R., C.L. Andersen, L. Hu, Z. Wang, Y. Li, T. Nagy, X. Ye. 2019. *Reproductive Toxicology*. 85:42-50. Reprinted here with permissions of the publisher

Abstract

Zearalenone (ZEA) is a common food contaminant (ppb~ppm) derived from *Fusarium* fungi. With its estrogenicity and potential chronic exposure, ZEA poses a risk to pregnancy. Our previous studies implied post-implantational lethality by ZEA. Since a functional placenta is essential for fetal development and survival, it was hypothesized that ZEA may have adverse effects on placental development leading to post-implantational lethality. Exposure of young mice to 0, 0.8, 4, 10, and 40 ppm ZEA diets from gestation day 5.5 (D5.5) to D13.5 led to increased resorption of implantation sites, increased placental hemorrhage, decreased placental and fetal weights, proportionally reduced placental layers, and disorganized placental labyrinth vascular spaces in the 40 ppm ZEA group, as well as lipid accumulation in the labyrinth layer of all four ZEA treatment groups examined on D13.5. These data demonstrate adverse effects of ZEA on placental development.

Introduction

Zearalenone (ZEA) is a major mycotoxin derived from *Fusarium* fungi and a common food contaminant in the levels of parts per billion (ppb) ~ parts per million (ppm), with 600 ppm being the highest reported in contaminated food [1-4]. Contaminated food is the primary source of ZEA exposure for mammals. ZEA is quickly absorbed and mainly metabolized in the liver to form α- and β-zearalenol, from which α-zearalanol (zeranol), β-zearalanol (teranol), and zearalanone can be derived [1, 5-8]. Unconjugated ZEA has an elimination half-life of 16.8 hours after oral administration in male rats [4]. Because of their structural similarity with 17β-estradiol (E2) and their interactions with estrogen receptors (ERα, ERβ) [9-11], ZEA and its metabolites are also called mycoestrogens, and among them, α-zearalenol is the most potent [5, 12, 13]. Estrogen receptor(s)-modified animal models have revealed the essential *in vivo* roles of estrogen signaling

in pregnancy [14-18]. The estrogenicity of ZEA gives it the potential to interfere with mammalian pregnancy. Indeed, studies have shown that ZEA and its metabolites can disrupt pregnancy in different species (e.g., pig and mouse) by affecting different pregnancy events, such as preimplantation embryo development and transport, embryo implantation, and potentially placental development (reviewed in [19]).

The placenta is a transient organ bridging the mother and fetus during eutherian pregnancy. It is an important organ for toxicological evaluations but is seriously understudied. This situation is also implicated in studying the effect of ZEA on placental development. Several studies have alluded to the placenta as a target of ZEA: for example, ZEA can be bioactivated in placental cells [20]; ZEA and its metabolites can pass through placentas [21, 22]; ZEA (2.76 ppm diet from D35 to D70 of pregnancy) can be accumulated in pig placentas and reduce placental and fetal weights [23], which may indicate impaired placental function that was not further investigated in the study; ZEA (20 ppm diet, from D0.5 to D20.5 of pregnancy) causes reduced birth weight of rats and reduced *Esr1* (ERα) mRNA levels in the placentas but its effects on placental weight and placental morphology were not reported in the study [24]; rats exposed to 8 mg/kg body weight ZEA via gavage on D6–D19 had increased resorption of implantation sites and decreased fetal viability examined on D20, but the placentas were not examined in the study [25]. Since the placenta is the sole source of nutrients for supporting fetal development, the fetal toxicity from ZEA treatment could be a secondary effect of placental toxicity.

To determine the effect of ZEA on placental development, we use mouse as a model that shares the same hemochorial structure as humans. Mice have a definitive chorioallantoic placenta that develops from the extraembryonic lineages originated from the trophoblasts in gestation day 3.5 (D3.5) blastocysts. Embryo implantation in mice initiates ~D4.0 and trophoblasts penetrate

through uterine luminal epithelium into the uterine stromal layer by D5.0 for the subsequent establishment of a placenta [26]. The mural trophectoderm cells (not in contact with the inner cell mass) become trophoblast giant cells. The polar trophectoderm cells (adjacent to the inner cell mass) form the extraembryonic ectoderm and ectoplacental cone that will give rise to the spongiotrophoblast layer and labyrinth layer of the placenta. Structurally, a mouse placenta has three major layers: the outer maternal layer that includes decidual cells and maternal vasculature; the middle "junctional" zone that includes spongiotrophoblast layer and parietal trophoblast giant cell layer; and the inner labyrinth layer [27]. The labyrinth is the closest to the fetus for nutrient and gas exchanges between maternal and fetal blood as well as for disposal of waste from the fetus [28]. The mouse labyrinth consists of two separate, highly branched, and tortuously intertwined vascular networks, the maternal blood spaces and the fetal capillaries. They are separated by an interhemal membrane that consists of three layers of trophoblasts, which includes a layer of mononuclear sinusoidal trophoblast giant cells lining the maternal blood spaces and two layers of multiple nuclear syncytiotrophoblasts, as well as a layer of fetal blood vessel endothelial cells lining the fetal capillaries [28]. The flexuous network of maternal and fetal vessels in the labyrinth starts to develop following chorioallantoic attachment that occurs ~D8.5 [29], is established ~D10.5, and subsequently undergoes extensive modifications to accommodate fetal growth. The three major layers in the mouse placenta can be clearly defined by D12.5 [30].

Our previous study demonstrated that ZEA diet at 40 ppm blocked embryo implantation in mice [31]. To avoid the adverse effect of ZEA on embryo implantation [31] and to cover the main placental development period [27], in this study, we treated the mice during post-implantation period from D5.5 to D13.5 to determine the effect of ZEA on placental development. Indeed, ZEA at environmental relevant levels can adversely affect placental development.

Materials and methods

2.1. Animals

Wild type mice with C57BL/6 and129 mixed background, which were derived from *Atp6v0d2*$^{+/-}$ mice in C57BL/6 and129 mixed background [32, 33], were used in this study. Prior to treatment, all the mice were fed with regular chow 5053 (Labdiet, St. Louis, MO, USA) and housed in polypropylene cages with free access to food and water from water sip tubes in a reverse osmosis system. The Coverdell animal facility at the University of Georgia is on a 12-hour light/dark cycle (6:00 AM to 6:00 PM) at 23±1°C with 30-50% relative humidity. All methods used in this study were approved by the University of Georgia IACUC Committee (Institutional Animal Care and Use Committee) and conform to National Institutes of Health guidelines and public law.

2.2. Dose selection, treatment, and tissue collection

ZEA doses of 0 ppm (control), 0.8 ppm, 4 ppm, 10 ppm, and 40 ppm in the diets were used in our previous postweaning, premating, postmating, and/or multigenerational studies in mice [31, 34]. These ZEA levels have been reported in the contaminated food [1-4], which must also have contamination of other mycotoxins, including other mycoestrogens. The homemade ZEA diets were prepared by mixing ZEA (Cayman chemical, Ann Arbor, Michigan, USA) in casein-based phytoestrogen-free AIN-93G diet (Bio-Serv, Frenchtown, NJ) as we previously described [31, 34]. Our previous studies established 0.8 ppm, 4 ppm, 10 ppm, and 40 ppm ZEA diets to corresponding ZEA doses of about 0.1, 0.5, 1.25, and 5 mg/kg body weight per day, respectively, in mice [31, 34].

Female mice at 2-3 months old were mated with stud males (3-4 females with one male in a cage) and checked for a vaginal plug the next morning. The day of vaginal plug presence was designated

as gestation day 0.5 (D0.5). The plugged mice were randomly assigned into 5 groups (N=6-9 pregnant mice/group, no littermates in the same treatment group). The weights of the females in different groups were comparable at the beginning of treatment on D5.5. The treatments started on D5.5 and ended on D13.5 when the mice were dissected. Food and water consumptions in each cage were monitored. Since the mice were plugged on different days and treated with different ZEA diets, to reduce the housing cost, up to 5 mice on different gestation days in the same treatment group could be housed in the same cage during treatment. Therefore, food and water consumptions were rough estimations without considering gestation days. Body weights were recorded to determine pregnancy status as we reported previously [35].

On D13.5, the pregnant females were sacrificed by cervical dislocation. The numbers of total implantation sites, absorbed implantation site(s), placentas with live fetus, and weights of placentas and fetuses were recorded. One representative placenta from each mouse was fixed in Bouin's solution and the rest of the placentas were snapped frozen in liquid N_2 and kept at -80^{o}C. The average weight of placentas with a live fetus from each dam was counted as one data point, so as the average weight of all live fetuses from each dam. The body weight gain per implantation site for each dam was calculated as the weight difference between D13.5 and D5.5 divided by the total number of implantation sites in each dam on D13.5. The implantation site resorption rate was counted as the percentage of resorbed implantation sites, which were smaller, could be darker, and without a live fetus compared to the unabsorbed ones, in each pregnant D13.5 mouse. The resorbed implantation sites were classified into two groups in the 40 ppm ZEA group: type I resorption with the implantation site completely dark; and type II resorption with a small and partially pinkish implantation site.

2.3. Histology and quantification of placental layers

After fixation in Bouin's solution for 48 hrs, the placentas were dehydrated in 50%, 70%, 80%, 90% 100% (twice) alcohol for 1 hr each, and subsequently, cleared in xylene for 5-10 min until the tissue becomes transparent, and incubated in paraffin overnight before embedding. The processed placentas were then embedded in the orientation for cross sections. Every 10^{th} cross placental sections in the largest middle part were collected. Haemotoxylin and Eosin staining (H&E) staining was done as previously described [35, 36]. The middle three sections with the largest areas were selected for area quantification. The total area of each placental section and the areas of labyrinth layer, junctional zone, and decidua, which were outlined manually and quantified using Image J (National Institutes of Health, Bethesda, MD, USA) [35-38]. The average of each area from three sections in the same placenta was counted as one data point for statistical analysis. A total of 5-6 placentas from different mice in each group were processed for layer quantification.

2.4. Proliferating cell nuclear antigen (PCNA) immunofluorescence and quantification of PCNA positive cells in the labyrinth layer

Cross sections (10 μm) of the middle part of frozen placentas from 0 ppm and 40 ppm ZEA-treated groups were collected on the same slides for immunofluorescence. The sections were fixed in 4% paraformaldehyde for 15 min, and blocked with 3% hydrogen peroxide in methanol for 10 min at 25°C, and 10% goat serum in 1x phosphate buffered saline (PBS) for 1 hour at 25°C, incubated with rabbit anti-proliferating cell nuclear antigen (PCNA (D3H8P)1:250, 13110XP, Cell Signaling Technology, Danvers, MA, USA) overnight [35, 38, 39]. On the second day, the slides were incubated with goat anti-rabbit secondary antibody (Alexa Fluor 288, 1:200, A-11034, ThermoFisher, Rockford, IL, USA). The sections were counterstained with DAPI. Quantification of PCNA positive cells was done as following: At least 4 representative images at 40x in the

labyrinth layer of each placental section were taken for PCNA staining (green) and DAPI (blue). They were adjusted to the same exposure level on the background. The number of nuclei for each image was counted by ImageJ. The number of PCNA-positive cells in each image was counted manually by three people (two of them were blind to the identity of each image) or by ImageJ with the same criteria for all the images. The ratio of PCNA-positive cells in each image = the average counts of PCNA-positive cells (manually or ImageJ) / the number of nuclei (by DAPI staining). The average ratio of all images for the same section represented one mouse (N=6 mice/group).

2.5. Cytokeratin 19 immunohistochemistry & laminin immunofluorescence

Placental sections were prepared and processed as described in 2.4. For Cytokeratin 19 immunohistochemistry, the slides were incubated with rat anti-Cytokeratin 19 (CK19, 1:200, TROM-III, DSHB, Iowa city, Iowa, USA) at 4°C overnight. On the second day, the slides were incubated with biotinylated goat anti-rat IgG Antibody (1:200, BA-9400, Vector laboratories, Burlingame, CA, USA) for 1 hour at RT, and the signals were developed by DAB substrate kit (SK-4100, Vector lab, Burlingame, CA, USA). The nuclear were counter stained by Hematoxylin Solution, Harris Modified (HHS32-1L, Sigma-Aldrich, St. Louis, MO, USA). For laminin immunofluorescence, the slides were incubated with rat anti-Laminin (1:200, Lam-B, DSHB, Iowa city, Iowa, USA) at 4°C overnight. On the second day, the slides were incubated with goat anti-rat Alexa Fluor 594 (1:200, A11007, Fisher Scientific, Pittsburgh, PA, USA) at RT for 1 hour and mounted with VECTASHIELD Antifade Mounting Medium with DAPI (H-1200, Vector laboratories, Burlingame, CA, USA).

2.6. Oil red O staining and quantification

Oil Red O (O0625, Sigma-Aldrich) is a lysochrome diazo dye that stains neutral lipids including triglycerides on frozen sections. Cross sections (10 μm) of the middle part of frozen placentas from

different treatment groups were placed on the same slides, air dry for 10 min. The slides were fixed in 4% PFA for 15 min, washed in 1xPBS for 10 min, and stained with Oil red O working solution, which was freshly prepared as described [40], for 10 min. The slides were then rinsed in ddH_2O (30 s), 60% isopropyl (30 s), and ddH_2O (30s). One set of slides with all sections was counterstained with Hematoxylin (HHS16-550ML, Sigma Aldrich, St. Louis, MO, USA), washed in tap water for 10 min, and mounted with glycerol (BP229-1, Fisher Scientific, Pittsburgh, PA, USA). Another set of slides with serial sections were mounted with glycerol without further counterstaining for quantification of Oil red O staining using Image J [35-38]. Briefly, three 0.0359 mm^2 representative areas in the labyrinth layer of each section were selected. After converting the pictures into 8 bit images, a threshold of 0-174, 55-255, 45-255 was cut off to calculate the density of staining which is the percentage of positively labeled area in the whole pictures. The average of the density of three areas in one section was used to represent one sample. N=4 mice/group.

2.7. Statistical analyses

Two-tailed Fisher's exact test was used for comparing "% mice w/ placental hemorrhage". Two-tailed unequal variance student's t-test was used to compare other variables between two groups. The significance level was set at $P<0.05$.

Results

3.1. Implantation site on D13.5

Exposure to 0.8 ppm to 40 ppm ZEA diets from D5.5 to D13.5 did not have an obvious effect on food consumption and water consumption of mice (data not shown) as we previously reported [31, 34]. All the mice appeared healthy, indicating no general toxicity caused by the treatment regimens. Since exposure to ZEA diets started on D5.5 after embryo implantation initiation (~D4.0

in mice [26]), ZEA treatments were not expected to affect embryo implantation. Exposure to 40 ppm ZEA diet from D5.5 affected several post-implantation parameters detected on D13.5. *Body weight gain*: The absolute body weight gain (data not shown) or the body weight gain per implantation site during the treatment were comparable among 0 ppm, 0.8 ppm, 4 ppm, and 10 ppm ZEA groups, but were significantly reduced in the 40 ppm ZEA group compared to the other four groups (Fig. B1A, B1C). *Resorption of embryo implantation site*: Although there were mice with resorbed implantation sites in each group and the individual resorption rate, which was the percentage of resorbed implantation sites in each mouse, varied among individual mice, all 9 mice in the 40 ppm ZEA group had resorbed implantation sites and one of them had all implantation sites reabsorbed. The average resorption rate in the 40 ppm ZEA group (54%) was significantly higher than those in the rest of the four groups (<15%), which did not have significant difference among them (Fig. B1B, B1C). The resorbed implantation sites had different appearances in the 40 ppm ZEA group compared to control and other ZEA-treated groups. All the resorbed implantation sites in the control and the majority of those in the 0.8 ppm, 4 ppm, and 10 ppm ZEA groups were small and with part of the implantation site dark and the other part still pinkish (Fig. B1D upper middle panel), and without detectable fetal tissue (data not shown). While in the 40 ppm ZEA group, all 9 mice had resorbed implantation site(s) that was (were) small and completely dark (type I), and without any recognizable structure; and 3 of them also had resorbed implantation site(s) that was (were) small but still partially pinkish (type II) (Table B1 and Fig. B1D lower middle panel), and the degenerating placental and fetal tissues could still be identifiable (data not shown). Type II resorption most likely occurred later than type I resorption. The decreased weight gain in the 40 ppm ZEA group (Fig. B1A) most likely reflected the increased resorption of implantation

sites (Fig. B1B, B1C). These data demonstrate the toxicity of 40 ppm ZEA diet on the post-implantation pregnancy in mice.

3.2. Placental weight and fetus weight on D13.5

Accompanying with the increased resorption of implantation sites (Fig. B1B, B1C), ZEA also affected the placenta. *Placental hemorrhage*: All the 8 mice with unabsorbed implantation site(s) in the 40 ppm ZEA group had placental hemorrhage (100%), which appeared as a dark patch(s), most located within the rim of the placental disk (Fig. B1D), while only one in six mice (16.7%) had obvious placental hemorrhage in the 10 ppm ZEA group and none was observed in the other three groups (Fig. B1C). *Placental weight and fetus weight*: Significantly reduced weights of placentas and fetuses were observed in the 40 ppm ZEA group compared to the rest 4 groups, which were comparable among them (Fig. B1E, B1F). These data demonstrate the toxicity of 40 ppm ZEA diet on placental development in mice.

3.3. Histology of placenta

Quantification of three placental layers, labyrinth, junctional zone, and decidua (Fig. B2A), indicated comparable areas for all these three parameters in the 0 ppm, 0.8 ppm, 4 ppm, and 10 ppm ZEA groups, while those three areas were significant reduced in the 40 ppm group compared to all the other four groups (Fig. B2B). Correspondingly, the same pattern was seen in the total placental area (Fig. B2C). These data were consistent with the reduced placental weight only seen in the 40 ppm ZEA group (Fig. B1E). They also indicated that all placental layers were proportionally reduced in the 40 ppm ZEA group, suggesting overall suppressed placental development in this group.

Histology revealed morphological changes in the ZEA-treated placentas. In the decidual layer, focal necrosis in the superficial decidual cells was observed in multiple placentas of each ZEA-

treated group without an obvious dose-response relationship, while none was observed in the five control placentas (data not shown). The junctional zone did not show obvious structural abnormalities in the ZEA-treated groups. The labyrinth layer had the most abnormalities among the three main placental layers upon ZEA treatment. *Focal necrosis* in the labyrinth layer was observed in 1/5 placenta of 4 ppm ZEA group (data not shown) and 3/7 placentas of the 40 ppm ZEA group (Fig. B3B-B3B2), but none in the control (Fig. B3A-B3A2), 0.8 ppm and 10 ppm ZEA groups that were examined (data not shown). The following abnormalities of vascular spaces were observed in the 40 ppm ZEA-treated group. *Dilated lacunae with accumulation of red blood cells*: Although normally there were nucleated fetal blood cells in the fetal capillaries and enucleated maternal blood cells in the maternal blood spaces of the labyrinth layer, dilated lacunae with abnormal accumulation of red blood cells were observed in the labyrinth layer of 100% of the placentas in the 40 ppm ZEA group (Fig. B3C-B3C2 and data not shown). These observations were consistent with the placental hemorrhage (Fig. B1C, B1D). Such abnormal accumulation of blood cells in the labyrinth layer was also occasionally observed in the 0.8 ppm, 4 ppm, and 10 ppm ZEA groups (data not shown). *Reduced vascular spaces*: Accompanying with the dilated blood spaces, there were areas in the labyrinth layer of 40 ppm ZEA group with reduced blood spaces (Fig. B3C1, B3C2). The histology data revealed disrupted vascular spaces in the labyrinth layer of placentas in the 40 ppm ZEA group (Fig. B3B-B3C2).

3.4. Immunostaining of cytokeratin 19 (CK19) and laminin in placental labyrinth layer

CK19 labels the sinusoidal trophoblast giant cells that line the maternal blood space in the labyrinth [28]. Immunohistochemistry of CK19 showed relatively uniform distribution of maternal blood spaces in the control labyrinth (Fig. 4A), but enlarged or unexpanded maternal blood sinusoids in the 40 ppm ZEA-treated labyrinth associated with thickened intrahemal membrane

(Fig. B4B, B4C). Laminin is a marker of basal laminin surrounding the fetal capillary in the labyrinth [41]. Immunofluorescence revealed laminin staining as stretches of lines, which are supposed to be lining the fetal capillaries, in the control labyrinth (Fig. B4D). In the 40 ppm ZEA group, there were enlarged areas outlined by discontinuous laminin staining (Fig. B4E), most likely indicative of the dilated areas in the labyrinth layer; there were small patches of laminin staining (Fig. B4F), which did not appear to have adjacent lines of laminin staining to form fetal blood space and might be areas with unexpanded fetal capillaries; there were also lines with laminin staining that appeared to be fragmented in the labyrinth layer of 40 ppm ZEA-treated placenta (Fig. B3E). Fig. 3 and Fig. 4 consistently demonstrated disrupted labyrinth structure in the 40 ppm ZEA group.

3.5. PCNA staining of D13.5 placentas

PCNA is involved in DNA synthesis. Many trophoblast cells undergo endoreplication without going through mitosis, resulting in large nuclei. In our study, we found PCNA that was highly expressed in many cells in the placenta. PCNA staining was mainly detected in the labyrinth layer and appeared less in the junctional zone (data not shown). Although disrupted labyrinth structure was found in the 40 ppm ZEA group (Figs. B3, B4), the percentage of PCNA positive cells in the 40 ppm ZEA-treated labyrinth was not significantly different from that of the control, both by manual counting and by ImageJ automatic counting (data not shown). These data indicate that DNA replication in the labyrinth layer was not affected by 40 ppm ZEA treatment.

3.6. Oil red O staining of D13.5 placentas

Fetal growth depends on the supply of nutrients from the placenta. One important class of nutrients is lipid. To obtain a general picture of lipid supply in the placenta, we used a widely used method, Oil red O staining, which reveals neutral lipid droplets in the cell. In the D13.5 placentas, the Oil

red O staining was mainly detected in the labyrinth layer, detectable in trophoblast giant cells and spongiotrophoblast cells in the junctional zones, and to a lesser extent, in some stromal cells in the decidual layer (Fig. B5A, B5B). Since nutrient transfer to the fetus occurs in the labyrinth layer, we quantified Oil red O staining areas in the labyrinth layer using ImageJ. All four ZEA-treated groups had increased Oil red O staining compared to the vehicle control 0 ppm ZEA group (Fig. B5). These data indicate that there was no lack of lipid in the labyrinth layer to support the fetus in the ZEA-treated groups.

Discussion

The dose-response relationship between ZEA diets and placental weight is not linear (Fig. B1). It seems that there is a dose threshold between 10 ppm and 40 ppm ZEA to affect placental weight. Such threshold may reflect placental adaptation. Our previous multigenerational study showed that exposure to 20 ppm ZEA diet in F0 females from weaning to the end of pregnancy did not adversely affect their pregnancy rate, litter size, or offspring body weight measured at one week old [34], suggesting that 20 ppm ZEA diet did not compromise placental function in supporting fetal development and survival in the F0 females. There could be potential cellular and molecular changes in the 20 ppm ZEA-treated placentas of F0 females that were not investigated in the study. However, life time exposure to 20 ppm ZEA diet in F1 and F2 females impaired early pregnancy event(s) leading to reduced pregnancy rates [34]. Interestingly, the fertile F1 and F2 females treated with 20 ppm ZEA diet had comparable numbers of implantation sites to controls on D4.5 but significantly reduced litter sizes at birth, indicating increased post-implantational lethality [34], which could result from defective placentas and/or fetuses that were not further examined. These observations imply that the placenta has certain capacity to handle up to 20 ppm ZEA diet in the

F0 mice. However, 40 ppm ZEA diet impairs multiple pregnancy events in F0 mice, such as fertilization, embryo transport and preimplantation embryo development, and embryo implantation [31], as well as placental development and fetal development demonstrated in this study. These adverse effects of 40 ppm ZEA diet prevent further study on F1 and F2 females.

There are three potential possibilities for the reduced weight of both the placentas and the fetuses in the 40 ppm ZEA group. 1. Since ZEA and its metabolites can pass through the placenta to reach the fetus [21, 22], ZEA may have a direct adverse effect on the fetus to reduce fetal development and the reduced placental weight is an indirect effect to adapt to the slow fetal development; 2) Since ZEA can be bioactivated in placental cells [20] and accumulated in placentas [23], the placenta can be a direct target of ZEA and the reduced fetal weight is the consequence of comprised placental function in transferring adequate nutrients for fetal growth; and 3) ZEA directly targets both the placenta and the fetus to cause their reduced weights. Although the available information cannot exclude any of these three possibilities, our data support that the placenta is a direct target for ZEA. In the event of fetal death, the placenta continues to function for days in rodents [42, 43] or weeks in primates [44, 45]. For example, fetectomy on D13.5 in mice does not affect placental weight, placental area, or labyrinth volume, but significantly decreases the volume of fetoplacental capillaries on D17.5 [42]. ZEA treatment started on D5.5 in our study that covered the entire period of placental formation, from the initial choriovitelline pattern to the subsequent chorioallantoic pattern [30]. In mice, chorioallantoic attachment occurs ~D8.5 [27] that marks the initiation of transition to chorioallantoic placentation. Most of the absorbed implantation sites in the 40 ppm ZEA group were small and completely dark, which were most likely indicative of early resorption. Since ZEA treatment started on D5.5, the increased presence of such small and dark resorbed implantation sites in the 40 ppm ZEA group could be a result from disrupted decidualization,

and/or early nutritional disruption of the visceral yolk sac and its interaction with the antimesometrium during implantation chamber remodeling, or possibly from ZEA toxicity on the embryo. Because the treatment started on D5.5 and decidualization starts by D4.5 in mice [26], it is expected that the embryos were alive beyond D5.5 when ZEA treatment started. If ZEA only targeted the embryo/fetus, the placenta is expected to continue developing for certain period of time. And for the fetuses that were alive on D13.5, it is expected that the associated placentas would be normal if the fetus is the only target. However, we observed placentas with disrupted labyrinth layer, especially in the 40 ppm ZEA group. These observations support the placenta being a target of ZEA.

A recent study highlights the association of placentation defects with embryonic lethality in 103 mutant mouse models [46]. It finds that almost every line that died before embryonic/gestation day 14.5 (E14.5/D14.5) exhibited placental abnormalities, while only 35% of lines that were viable beyond E14.5/D14.5 had placental abnormalities and these lines were associated with a younger developmental stage (delayed fetal development). Although placental defects and embryonic lethality are linked [46], they can be differentiated [47].

Since ZEA treatment (especially at 40 ppm) disrupted the structure of labyrinth layer, it is expected that the maternal-fetal material exchange is impaired. Consequently, it will affect fetal survival and growth. Indeed, the fetuses in the 40 ppm ZEA group had significantly reduced weight. ZEA treatment increases oil red staining in the labyrinth layer of all the ZEA treatment groups from 0.8 ppm to 40 ppm ZEA (Fig. B5), indicating that ZEA has an effect in the placenta at levels as low as 0.8 ppm. The effect of ZEA on fetal survival and growth was only manifested in the 40 ppm ZEA group would suggest that the placenta has certain capacity to accommodate the insult from ZEA in order to protect the developing fetus.

The accumulation of lipid in the ZEA-treated labyrinth layer indicates that there is no lack of lipid in the labyrinth layer. It is possible that the disrupted labyrinth structure in 40 ppm ZEA group would impede the transfer of lipid to fetus leading to lipid accumulation and compromised fetal growth. However, in the lower doses, the morphological changes in the labyrinth layer were not severe or not obvious (e.g., 0.8 ppm ZEA group) and the fetal survival and growth were not affected, yet lipid accumulation still occurred, suggesting that ZEA may affect molecular changes without obvious effects on the cellular level to disrupt lipid homeostasis.

Estrogen has been generally associated with reduction of lipid, while loss of estrogen or estrogen receptor is associated with adiposity and hepatic lipogenesis [48]. Estrogen can reduce lipid accumulation in the liver through ERα-mediated pathways [49]. It may be responsible for the decreased saturate fat acid content in the female brain compared to male brain [50]. Its levels are oppositely related to mouse uterine lipid contents during estrous cycle, with minimum at estrus stage and maximum at diestrus stage [51]. Therefore, it is unlikely that ZEA-induced lipid accumulation observed in our study is directly caused by the estrogenicity of ZEA.

Increased neutral lipid accumulation in placenta has also been observed in women with preeclampsia, gestational diabetes, and fetal growth restriction [52, 53]. One potential cause that has been proposed is the hypoxia in the placenta which can be induced by defects in vasculature development [54]. Unexpanded or dilated blood spaces in the labyrinth layer of the placentas in the 40 ppm ZEA group indicated defective vasculature development, which could contribute to the increased lipid accumulation. The molecular mechanisms of ZEA in affecting the placenta (e.g., lipid homeostasis) and the time course of ZEA in affecting placental development remain to be investigated.

Acknowledgements

The authors thank the Office of the Vice President for Research, Interdisciplinary Toxicology Program, and Department of Physiology and Pharmacology at the University of Georgia, and the National Institutes of Health (NIH R01HD065939 (co-funded by ORWH and NICHD) to XY) for financial support.

Competing interests

The authors declare no conflict of interest.

References

[1] Zinedine A, Soriano JM, Molto JC, Manes J. Review on the toxicity, occurrence, metabolism, detoxification, regulations and intake of zearalenone: an oestrogenic mycotoxin. Food Chem Toxicol. 2007;45:1-18.

[2] Sangare-Tigori B, Moukha S, Kouadio HJ, Betbeder AM, Dano DS, Creppy EE. Co-occurrence of aflatoxin B1, fumonisin B1, ochratoxin A and zearalenone in cereals and peanuts from Cote d'Ivoire. Food Addit Contam. 2006;23:1000-7.

[3] Price WD, Lovell RA, McChesney DG. Naturally occurring toxins in feedstuffs: Center for Veterinary Medicine Perspective. J Anim Sci. 1993;71:2556-62.

[4] EFSA. Scientific Opinion on the risks for public health related to the presence of zearalenone in food. EFSA Journal. 2011;9:2197.

[5] Kuiper-Goodman T, Scott PM, Watanabe H. Risk assessment of the mycotoxin zearalenone. Regul Toxicol Pharmacol. 1987;7:253-306.

[6] Mirocha CJ, Pathre SV, Robison TS. Comparative metabolism of zearalenone and transmission into bovine milk. Food Cosmet Toxicol. 1981;19:25-30.

[7] Bravin F, Duca RC, Balaguer P, Delaforge M. In vitro cytochrome p450 formation of a mono-hydroxylated metabolite of zearalenone exhibiting estrogenic activities: possible occurrence of this metabolite in vivo. Int J Mol Sci. 2009;10:1824-37.

[8] Belhassen H, Jimenez-Diaz I, Ghali R, Ghorbel H, Molina-Molina JM, Olea N, et al. Validation of a UHPLC-MS/MS method for quantification of zearalenone, alpha-zearalenol, beta-zearalenol, alpha-zearalanol, beta-zearalanol and zearalanone in human urine. J Chromatogr B Analyt Technol Biomed Life Sci. 2014;962:68-74.

[9] Gromadzka K, Waskiewicz A, Golinski P, Swietlik J. Occurrence of estrogenic mycotoxin - Zearalenone in aqueous environmental samples with various NOM content. Water Res. 2009;43:1051-9.

[10] Li Y, Burns KA, Arao Y, Luh CJ, Korach KS. Differential estrogenic actions of endocrine-disrupting chemicals bisphenol A, bisphenol AF, and zearalenone through estrogen receptor alpha and beta in vitro. Environ Health Perspect. 2012;120:1029-35.

[11] He J, Wei C, Li Y, Liu Y, Wang Y, Pan J, et al. Zearalenone and alpha-zearalenol inhibit the synthesis and secretion of pig follicle stimulating hormone via the non-classical estrogen membrane receptor GPR30. Mol Cell Endocrinol. 2018;461:43-54.

[12] Frizzell C, Ndossi D, Verhaegen S, Dahl E, Eriksen G, Sorlie M, et al. Endocrine disrupting effects of zearalenone, alpha- and beta-zearalenol at the level of nuclear receptor binding and steroidogenesis. Toxicol Lett. 2011;206:210-7.

[13] Ueno Y, Tashiro F. alpha-Zearalenol, a major hepatic metabolite in rats of zearalenone, an estrogenic mycotoxin of Fusarium species. J Biochem. 1981;89:563-71.

[14] Hewitt SC, Winuthayanon W, Korach KS. What's new in estrogen receptor action in the female reproductive tract. J Mol Endocrinol. 2016;56:R55-71.

[15] Hamilton KJ, Arao Y, Korach KS. Estrogen hormone physiology: reproductive findings from estrogen receptor mutant mice. Reprod Biol. 2014;14:3-8.

[16] Pawar S, Laws MJ, Bagchi IC, Bagchi MK. Uterine Epithelial Estrogen Receptor-alpha Controls Decidualization via a Paracrine Mechanism. Mol Endocrinol. 2015;29:1362-74.

[17] Winuthayanon W, Bernhardt ML, Padilla-Banks E, Myers PH, Edin ML, Hewitt SC, et al. Oviductal estrogen receptor alpha signaling prevents protease-mediated embryo death. Elife. 2015;4:e10453.

[18] Feng Y, Manka D, Wagner KU, Khan SA. Estrogen receptor-alpha expression in the mammary epithelium is required for ductal and alveolar morphogenesis in mice. Proc Natl Acad Sci U S A. 2007;104:14718-23.

[19] Andersen CL, Zhao F, Ye X. Effects of mycoestrogens on female reproduction. Reprod Dev Med. 2018;2:52-8.

[20] Huuskonen P, Auriola S, Pasanen M. Zearalenone metabolism in human placental subcellular organelles, JEG-3 cells, and recombinant CYP19A1. Placenta. 2015;36:1052-5.

[21] Bernhoft A, Behrens GH, Ingebrigtsen K, Langseth W, Berndt S, Haugen TB, et al. Placental transfer of the estrogenic mycotoxin zearalenone in rats. Reprod Toxicol. 2001;15:545-50.

[22] Danicke S, Brussow KP, Goyarts T, Valenta H, Ueberschar KH, Tiemann U. On the transfer of the Fusarium toxins deoxynivalenol (DON) and zearalenone (ZON) from the sow to the full-term piglet during the last third of gestation. Food Chem Toxicol. 2007;45:1565-74.

[23] Zhang Y, Gao R, Liu M, Shi B, Shan A, Cheng B. Use of modified halloysite nanotubes in the feed reduces the toxic effects of zearalenone on sow reproduction and piglet development. Theriogenology. 2015;83:932-41.

[24] Gao X, Sun L, Zhang N, Li C, Zhang J, Xiao Z, et al. Gestational Zearalenone Exposure Causes Reproductive and Developmental Toxicity in Pregnant Rats and Female Offspring. Toxins (Basel). 2017;9.

[25] Collins TF, Sprando RL, Black TN, Olejnik N, Eppley RM, Alam HZ, et al. Effects of zearalenone on in utero development in rats. Food Chem Toxicol. 2006;44:1455-65.

[26] Diao H, Paria BC, Xiao S, Ye X. Temporal expression pattern of progesterone receptor in the uterine luminal epithelium suggests its requirement during early events of implantation. Fertil Steril. 2011;95:2087-93.

[27] Watson ED, Cross JC. Development of structures and transport functions in the mouse placenta. Physiology (Bethesda). 2005;20:180-93.

[28] Simmons DG. Postimplantation Development of the Chorioallantoic Placenta. In: Croy B, Yamada A, DeMayo F, Adamson S, editors. The Guide to the Investigation of Mouse Pregnancy: Elsevier; 2014. p. 143-62.

[29] Rai A, Cross JC. Development of the hemochorial maternal vascular spaces in the placenta through endothelial and vasculogenic mimicry. Dev Biol. 2014;387:131-41.

[30] Malassine A, Frendo JL, Evain-Brion D. A comparison of placental development and endocrine functions between the human and mouse model. Hum Reprod Update. 2003;9:531-9.

[31] Zhao F, Li R, Xiao S, Diao H, Viveiros MM, Song X, et al. Postweaning exposure to dietary zearalenone, a mycotoxin, promotes premature onset of puberty and disrupts early pregnancy events in female mice. Toxicol Sci. 2013;132:431-42.

[32] Lee SH, Rho J, Jeong D, Sul JY, Kim T, Kim N, et al. v-ATPase V0 subunit d2-deficient mice exhibit impaired osteoclast fusion and increased bone formation. Nat Med. 2006;12:1403-9.

[33] Xiao S, Li R, El Zowalaty AE, Diao H, Zhao F, Choi Y, et al. Acidification of uterine epithelium during embryo implantation in mice. Biol Reprod. 2017;96:232-43.

[34] Zhao F, Li R, Xiao S, Diao H, El Zowalaty AE, Ye X. Multigenerational exposure to dietary zearalenone (ZEA), an estrogenic mycotoxin, affects puberty and reproduction in female mice. Reprod Toxicol. 2014;47C:81-8.

[35] El Zowalaty AE, Li R, Zheng Y, Lydon JP, DeMayo FJ, Ye X. Deletion of RhoA in Progesterone Receptor-Expressing Cells Leads to Luteal Insufficiency and Infertility in Female Mice. Endocrinology. 2017;158:2168-78.

[36] Li R, Zhao F, Diao HL, Xiao S, Ye XQ. Postweaning dietary genistein exposure advances puberty without significantly affecting early pregnancy in C57BL/6J female mice. Reproductive Toxicology. 2014;44:85-92.

[37] El Zowalaty AE, Li R, Chen W, Ye X. Seipin deficiency leads to increased ER stress and apoptosis in mammary gland alveolar epithelial cells during lactation. Biol Reprod. 2017.

[38] El Zowalaty AE, Ye X. Seipin deficiency leads to defective parturition in mice. Biol Reprod. 2017;97:378-86.

[39] El Zowalaty AE, Li R, Chen W, Ye X. Seipin deficiency leads to increased endoplasmic reticulum stress and apoptosis in mammary gland alveolar epithelial cells during lactation. Biol Reprod. 2018;98:570-8.

[40] Mehlem A, Hagberg CE, Muhl L, Eriksson U, Falkevall A. Imaging of neutral lipids by oil red O for analyzing the metabolic status in health and disease. Nature Protocols. 2013;8:1149-54.

[41] Senior PV, Critchley DR, Beck F, Walker RA, Varley JM. The localization of laminin mRNA and protein in the postimplantation embryo and placenta of the mouse: an in situ hybridization and immunocytochemical study. Development. 1988;104:431-46.

[42] Isaac SM, Qu D, Adamson SL. Effect of selective fetectomy on morphology of the mouse placenta. Placenta. 2016;46:11-7.

[43] Roby KF, Soares MJ. Trophoblast cell differentiation and organization: role of fetal and ovarian signals. Placenta. 1993;14:529-45.

[44] Albrecht ED, Pepe GJ. The placenta remains functional following fetectomy in baboons. Endocrinology. 1985;116:843-5.

[45] Nathanielsz PW, Figueroa JP, Honnebier MB. In the rhesus monkey placental retention after fetectomy at 121 to 130 days' gestation outlasts the normal duration of pregnancy. Am J Obstet Gynecol. 1992;166:1529-35.

[46] Perez-Garcia V, Fineberg E, Wilson R, Murray A, Mazzeo CI, Tudor C, et al. Placentation defects are highly prevalent in embryonic lethal mouse mutants. Nature. 2018;555:463-8.

[47] Schreiber M, Wang ZQ, Jochum W, Fetka I, Elliott C, Wagner EF. Placental vascularisation requires the AP-1 component fra1. Development. 2000;127:4937-48.

[48] Napso T, Yong HEJ, Lopez-Tello J, Sferruzzi-Perri AN. The Role of Placental Hormones in Mediating Maternal Adaptations to Support Pregnancy and Lactation. Front Physiol. 2018;9:1091.

[49] Palmisano BT, Zhu L, Stafford JM. Role of Estrogens in the Regulation of Liver Lipid Metabolism. Adv Exp Med Biol. 2017;1043:227-56.

[50] Morselli E, Santos RS, Gao S, Avalos Y, Criollo A, Palmer BF, et al. Impact of estrogens and estrogen receptor-alpha in brain lipid metabolism. Am J Physiol Endocrinol Metab. 2018;315:E7-E14.

[51] Beall JR. Uterine lipid metabolism--a review of the literature. Comp Biochem Physiol B. 1972;42:175-95.

[52] Brown SH, Eather SR, Freeman DJ, Meyer BJ, Mitchell TW. A Lipidomic Analysis of Placenta in Preeclampsia: Evidence for Lipid Storage. PLoS One. 2016;11:e0163972.

[53] Stirm L, Kovarova M, Perschbacher S, Michlmaier R, Fritsche L, Siegel-Axel D, et al. BMI-Independent Effects of Gestational Diabetes on Human Placenta. Journal of Clinical Endocrinology & Metabolism. 2018;103:3299-309.

[54] Sadovsky IBWTSBCMMS-YOMOBCS-HTCYBDMNY. PLIN2 is essential for trophoblastic lipid droplet accumulation and cell survival during hypoxia. Endocrinology. 2018:Epub ahead of print.

Table

Table B1. Implantation site resorption rate on D13.5.

ZEA treatment group	Mouse No.	No. of total implantation sites	Unabsorbed (%)	Resorption (%)	
0 ppm	0-1	5	80	20	
	0-2 *	8	87.5	12.5	
	0-3	9	100	0	
	0-4	8	100	0	
	0-5	6	83.3	16.7	
	0-6	4	75	25	
				Type I resorption (%)	Type II resorption (%)
40 ppm	40-1	9	55.6	33.3	11.1
	40-2	11	72.8	27.2	0
	40-3	6	50	50	0
	40-4	6	83.3	16.7	0
	40-5	6	50	16.7	33.3
	40-6 *	7	28.57	42.86	28.57
	40-7	10	20	80	0
	40-8	9	0	100	0
	40-9	7	57.1	42.9	0

* Uterine images of 0-2 and 40-6 were shown in Fig. B1D. Type I resorption: The implantation site was completely dark and without identifiable structure. Type II resorption: The implantation site was partially pinkish and the degenerating placental and fetal tissues could still be identifiable.

Figure legend

Figure B1. Effects of ZEA diets on fetal and placental growth detected on D13.5. A. Body weight gain from gestation day 5.5 (D5.5) to D13.5. B. Resorption rate of implantation site in individual mouse. Each diamond represents one mouse. Red line indicates average. C. Percentage of mice with placental hemorrhage. D. From left to right: images of one D13.5 uterus with implantation sites each from 0 ppm (upper panel) and 40 ppm (lower panel) ZEA groups (see Table 1), enlarged view of resorbed implantation sites, and a fetus with its placenta from an unabsorbed implantation site on the left. . Black arrow, unabsorbed implantation site; blue arrow, a small implantation site being absorbed with part dark tissue on the left side and part pinkish tissue on the right side in 0 ppm ZEA group; blue dotted arrow, an implantation site with complete dark tissue (type I) in 40 ppm ZEA group; red dotted arrow, a small implantation site being absorbed (type II) in 40 ppm ZEA group; red arrow, placental hemorrhage in 40 ppm ZEA group. E. Placental weight. F. Fetal weight. A, E, and F: Error bar, standard deviation; N=6-9 (A) and 6-8 (C, E, F); * $P<0.05$, compared to the rest four groups.

Figure B2. Quantification of D13.5 placental layers. A. Outlines of three layers in a placenta in 0 ppm ZEA group and two placentas in 40 ppm ZEA group. Yellow lined area, labyrinth; blue lined area, junctional zone; green lined area, decidua; black line, width of a 5x image. B. Areas of placental layers. C. Total area of the placentas. B & C: Error bar, standard deviation; N=5-6; * $P<0.05$, compared to the rest four groups.

Figure B3. Histology of D13.5 placentas. A-A2. A representative labyrinth layer in 0 ppm ZEA group. B-B2. Focal necrosis in the labyrinth layer of a placenta in 40 ppm ZEA group. C-C2. Dilation of blood space in the labyrinth layer of a placenta in 40 ppm ZEA group. A1-C1, enlarged from the boxed area in A-C, respectively; A2-C2, enlarged from the boxed area in A1-C1, respectively; laby, labyrinth layer; yellow star in B2, focal necrosis; blue arrow in C2, dilated maternal blood space filled with enucleated red blood cells; black arrow in C2, nucleated fetal blood cells in fetal capillary; scale bar, 400 μm (A-C), 100 μm (A1-C1), or 25 μm (A2-C2).

Figure B4. Immunostaining of cytokeratin 19 (CK19) and laminin in labyrinth layer. A-C. Immunohistochemistry of CK19 in control (A) and 40 ppm ZEA (B, C) labyrinths. CK19 (brown staining) labels sinusoidal trophoblast giant cells that line the maternal blood space in the labyrinth. Blue arrow, expanded maternal blood space; black dotted arrow, unexpanded maternal blood space; scale bar, 50 μm. D-F. Immunofluorescence of laminin in control (D) and 40 ppm ZEA (E, F) labyrinths. Laminin (red staining) is a marker of basal laminin surrounding the fetal capillary in the labyrinth. White arrow in D, fetal capillary lined up by laminin staining; yellow arrow in E, dilated fetal capillary; yellow dotted arrow in E, discontinuous laminin staining; white dotted arrow in F, focal cluster of laminin staining; scale bar, 25 μm.

Figure B5. ZEA diets increase oil red staining in labyrinth layer (Laby) of D13.5 placentas. A-D. Oil red staining counter-stained with Hematoxylin. C & D: Enlarged from A & B, respectively. E-F. Oil red staining only for quantification using ImageJ. A-F: scale bar, 400 μm (A,B) and 25 μm (C-F). G. Oil red staining as % of area. N=4; error bar, standard deviation; * $P<0.05$, compared to 0 ppm group.

Figure B1

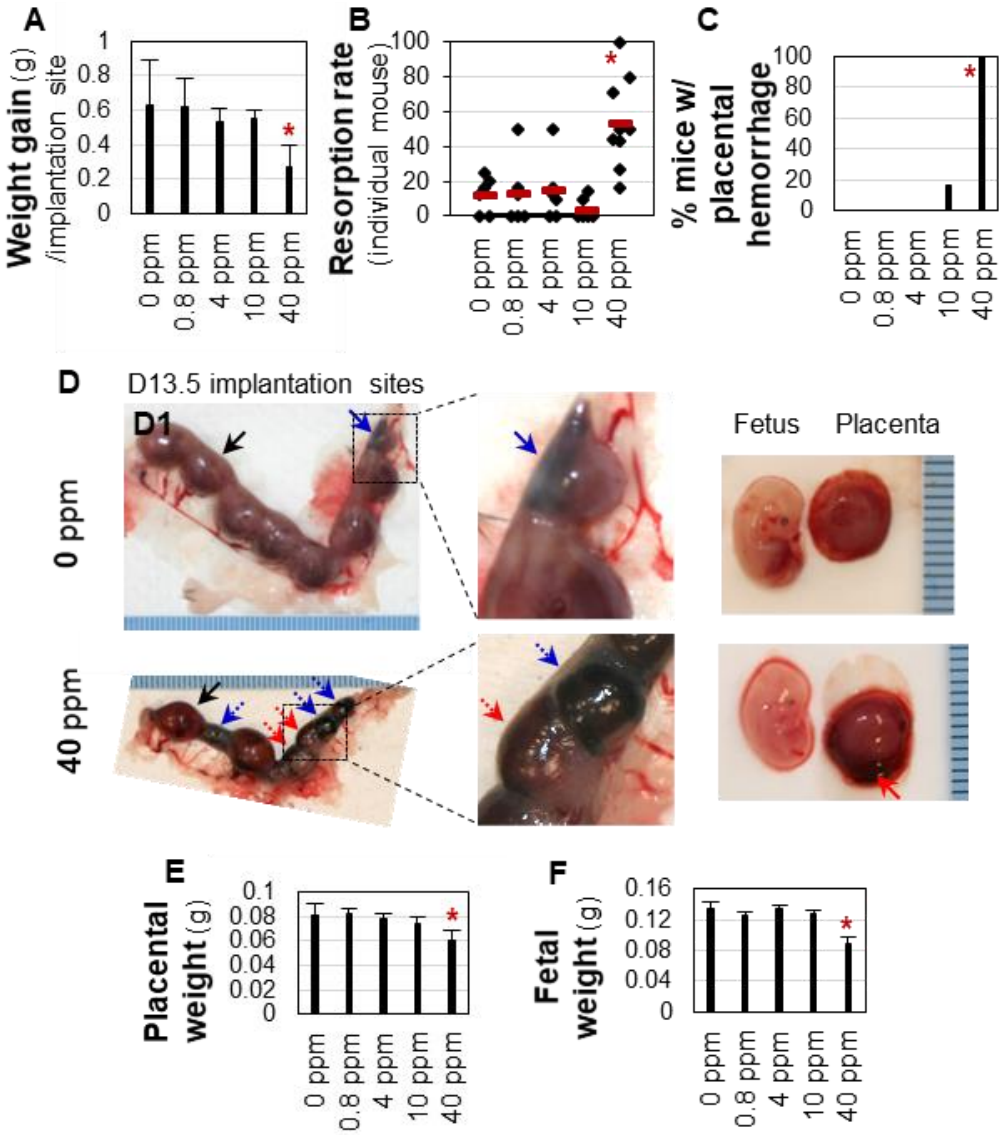
A
Weight gain (g) /implantation site
1
0.8
0.6
0.4
0.2
0
0 ppm
0.8 ppm
4 ppm
10 ppm
40 ppm
B
Resorption rate (individual mouse)
100
80
60
40
20
0
C
% mice w/ placental hemorrhage
D
D13.5 implantation sites
D1
0 ppm
40 ppm
Fetus
Placenta
E
Placental weight (g)
0.1
0.08
0.06
0.04
0.02
0
F
Fetal weight (g)
0.16
0.12
0.08
0.04
0

Figure B2

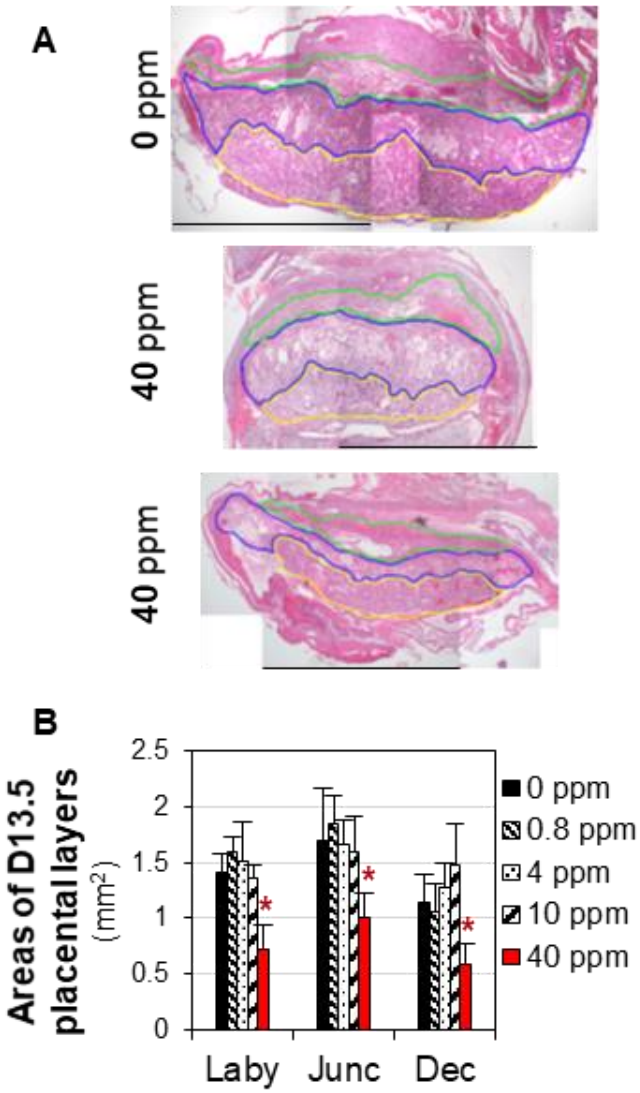
A
0 ppm
40 ppm
40 ppm
B
Areas of D13.5 placental layers (mm²)
2.5
2
1.5
1
0.5
0
Laby
Junc
Dec
0 ppm
0.8 ppm
4 ppm
10 ppm
40 ppm
C
Total area of D13.5 placentas (mm²)
5
4
3
2
1
0
0 ppm
0.8 ppm
4 ppm
10 ppm
40 ppm

Figure B3

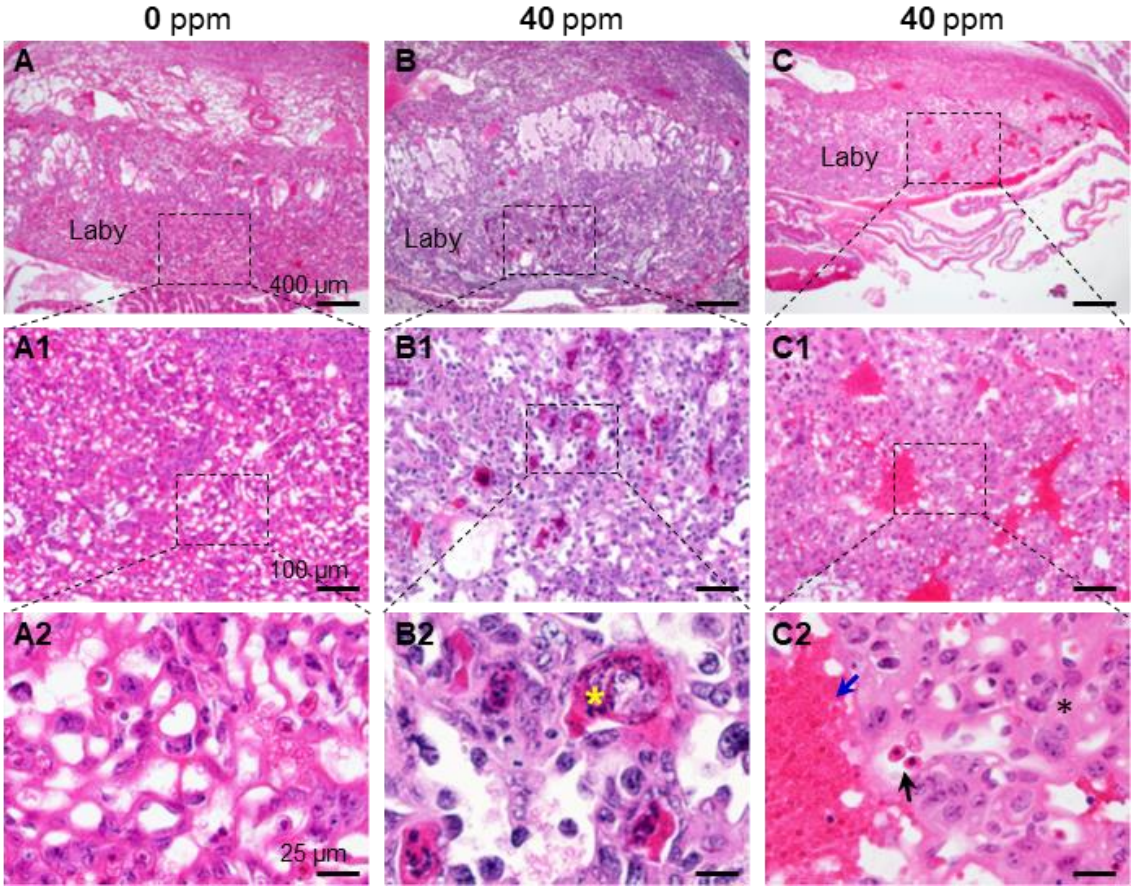
0 ppm
40 ppm
40 ppm
A
B
C
Laby
Laby
Laby
400 µm
A1
B1
C1
100 µm
A2
B2
C2
25 µm

Figure B4

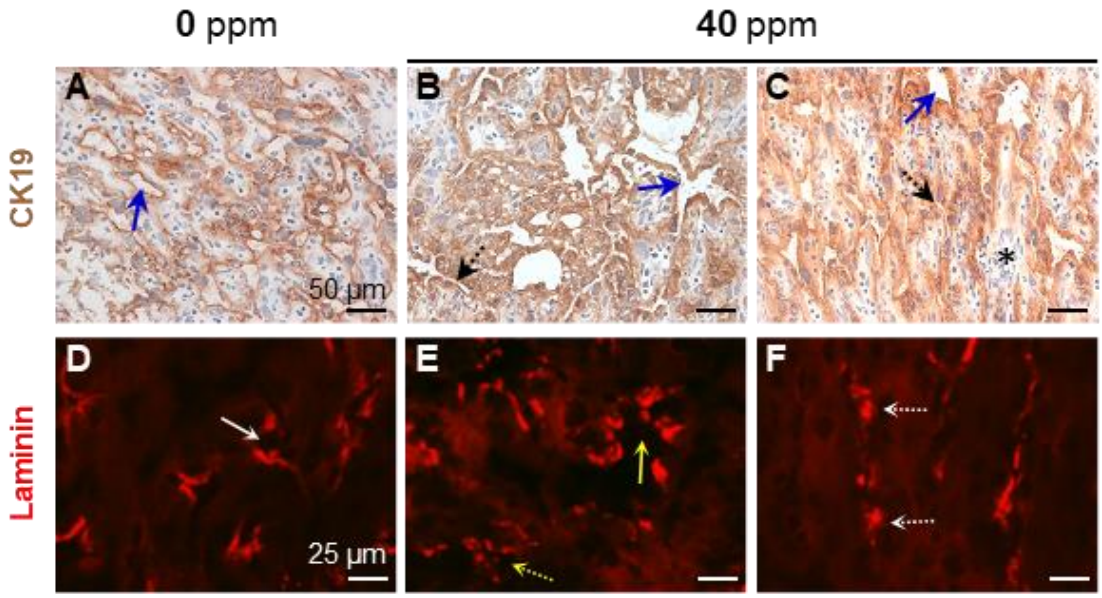

Figure B5

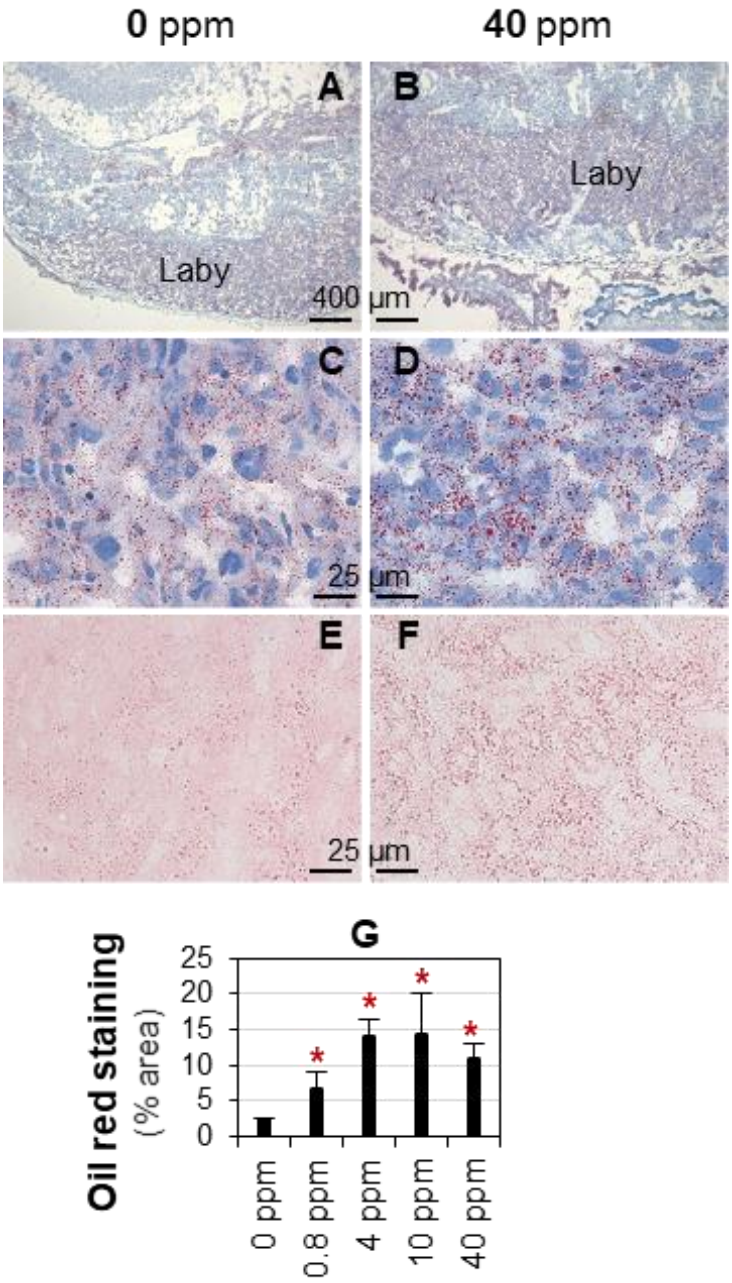
0 ppm
40 ppm
A
B
Laby
Laby
400 µm
C
D
25 µm
E
F
25 µm
G
Oil red staining
(% area)
25
20
15
10
5
0
*
*
*
*
0 ppm
0.8 ppm
4 ppm
10 ppm
40 ppm

APPENDICE C

SUPPLEMENTARY CHAPTER 8: MOUSE PLACENTAL MICRORNA PROFILING UPON ZEARALENONE EXPOSURE[1]

[1]Andersen, C.L., R. Li, X. Ye. 2020. *Biology of Reproduction*. 102:5-7. Reprinted here with permissions of the publisher

Abstract

Mycoestrogen zearalenone (ZEA) is a common food contaminant (ppb ~ low ppm levels) that can interfere with female reproduction. Previously we demonstrated disrupted mouse placental development by 40 ppm ZEA diet. MicroRNAs are sensitive to xenobiotics and have been implicated in placental physiology and pathology. We hypothesized that ZEA could dysregulate microRNA expression in the mouse placenta. Young mice were fed with 0 ppm (control), 4 ppm, and 40 ppm ZEA diets from 5.5 days post-coitum (D5.5). On D13.5, placentas were isolated for microRNA array analysis. In the D13.5 control placentas, ~80% of microRNAs had an average signal intensity <100; the top 20 most abundant microRNAs were predicated to target genes involved in metabolism, vesicle trafficking, and immune function, etc., that are critical for maternal-fetal communications. Using criteria of $Log_2FC \geq 1$ and $Log_2FC \leq -1$ (linear 2 fold change (FC)), a false discovery rate adjusted p-value ≤ 0.05, and an average signal intensity in all three groups >100, R package *limma* identified 8 differentially expressed miRNAs (mmu-miR-133b-5p, mmu-miR-7028-5p, mmu-miR-294-3p, mmu-miR-3970, mmu-miR-20b-5p, mmu-miR-7683-3p, mmu-miR-335-5p, mmu-miR-450b-5p) in the 40 ppm ZEA group that included all 5 differentially expressed miRNAs in the 4 ppm ZEA group. The predicted targets of the 5 differentially expressed microRNAs in both ZEA-treated groups were related to immune function, protein metabolism and post-translational modifications, extracellular matrix organization, and membrane trafficking, etc. These data imply roles of placental microRNAs in regulating expression of genes critical for placental function *in vivo* and in sensing environmental contaminants.

Introduction

Mold contamination is ubiquitous in the environment. Zearalenone (ZEA), a mycotoxin from a common type of mold named *Fusarium*, is a regular food contaminant at levels of ppb ~ low ppm . ZEA and its metabolites can interact with estrogen receptors and are classified as mycoestrogens. Because of the essential roles of estrogen in female reproduction, some mycoestrogens have been shown to interfere with female reproduction [1]. The placenta is indispensable for female reproduction in eutherians, providing nourishment and waste removal for the developing fetus [3]. Because of ethical issues and shared similarities at the molecular level between hemochorial human and mouse placentas, mouse models have often been used to provide important insights into the molecular basis of human placenta.

When young female mice were fed with ZEA diets (0.8, 4, 10, and 40 ppm) from 5.5 days post-coitum (D5.5) to D13.5, their placentas showed various adverse effects, including increased resorption of placentas, placental hemorrhage, decreased placental weight, and disrupted placental labyrinth vascular spaces in the 40 ppm ZEA group, as well as lipid accumulation in the placental labyrinth layer in all ZEA-treated groups. Meanwhile, there were increased fetal resorption and decreased fetal weight in the 40 ppm ZEA group, which were most likely caused by ZEA-induced placental toxicity [2].

Placental development is associated with dynamic gene expression, which can be regulated by epigenetic mechanisms, such as microRNAs (miRNAs). MiRNAs bind to the 3'-untranslated region of target mRNAs to silence target gene expression via mRNA degradation and/or translational suppression. Emerging information has indicated roles for miRNAs in placental development and pregnancy complications [4]. Placental miRNAs are sensitive to xenobiotics, including environmental pollutants [5]. It was hypothesized that ZEA could dysregulate miRNA

expression in the mouse placenta. This hypothesis was tested using miRNA array in D13.5 placentas from control (0 ppm), 4 ppm, and 40 ppm ZEA groups (N=4) [2].

Materials and methods

C57BL/6 female mice (2-3 months old) were fed with ZEA diets: 0 ppm (control), 4 ppm, or 40 ppm zearalenone (ZEA) from gestation day 5.5 (D5.5) to D13.5 as previously described (Li and Andersen *et al*., 2019). On D13.5, pregnant dams were euthanized and placentas were flash frozen in liquid nitrogen and kept in -80^{o}C.

One representative D13.5 whole placenta from each mouse was homogenized in liquid nitrogen for total RNA isolation using Trizol reagent (Invitrogen, ThermoFisher Scientific, #15596018). Four samples from four individual mice in each group that passed QC test were processed for microRNA array at LC Sciences, Houston, TX. Chip images were digitized and microRNA intensity values were generated. Background was subtracted from signal means and then normalized using a LOWESS filter (LC Sciences).

ANOVA (p-value ≤ 0.05) was used to select differentially expressed miRNAs for heatmap plots (supplementary Fig. S2). The R package *limma* was employed for identifying differentially expressed microRNAs (Ritchie *et al.*, 2015). MiRNAs with an average signal intensity <1 were excluded from analysis. Criteria for differential expression include: 1) $Log_2FC \geq 1$ or $Log_2FC \leq -1$ (linear 2 fold change (FC)); 2) an adjusted p-value ≤ 0.05 (Benjamini-Hochber FDR), which would filter out the majority of the differentially expressed miRNAs selected using ANOVA (p-value ≤ 0.05); and 3) an average signal intensity (reading from microRNA array) of all three groups >100 (McCarthy and Smyth, 2009; Xiao *et al.*, 2014). A 3D plot of the first 3 principle components was created to visualize the variation of miRNA expression among three treatment groups and four individual samples in each group (PC1=16.94%, PC2=13.09%, PC3=10.84% of total variation

explained, Figure C1). Five miRNAs (mmu-miR-20b-5p, mmu-miR-294-3p, and mmu-miR-3970, mmu-miR-7683-3p, mmu-miR-450b-5p) were downregulated in both 4 ppm and 40 ppm ZEA groups (Supplementary Table CS1) and were used in downstream analyses.

D13.5 murine placenta transcriptome from publicly available data set GSE119710 was analyzed to determine placenta specific transcripts (McNairn *et al.*, 2019). Raw fastq files were downloaded from GEO and analyzed as previously described (Andersen *et al.*, 2018). 79091/142332 (55.57%) refseq_mrna IDs with at least 1 read count across all samples were used for analysis. Read counts were log transformed and mean expression, standard deviation, and a coefficient of variation (COV ≤ 30%) were generated for each transcript (Sticht *et al.*, 2018). 16551 (11.63%) had an average read count greater than 100 and were considered to be expressed above a basal level. Predicted targets were determined using miRwalk using default settings (Sticht *et al.*, 2018). There were 3672 (2.58%) unique refseq_mrna IDs shared between the differentially expressed miRNA predicted targets and the placenta transcriptome dataset. All transcripts that were both predicted targets and found in the placenta transciptome dataset were used for Reactome pathway enrichment analysis (Fabregat *et al.*, 2017). MiRNA abundance in D13.5 placenta: To analyze pathways involved in the highest expressed miRNAs, miRNAs were determined to be highly expressed if the average signal intensity value was above 1000. A COV less than 30% was used to increase confidence in the expressions of miRNAs. The top 20 miRNA (average signal intensity value > 6000) that matched these criteria were used in the analysis. All predicted targets (44496 refseq_mrna) were compared to placental transcriptome. 5112 unique refseq_mrna IDs were shared between the miRNA predicted targets and the placenta transcriptome. All transcripts were used for Reactome pathway enrichment analysis.

Results

Among the 1,900 miRNA probes in the D13.5 control placentas, 13 (0.68%) had signal intensity over 10,000; 119 (6.26%) between 1,000 and 10,000; 263 (13.84%) between 100 and 1,000; and the remaining 1,505 (79.21%) <100 (Fig. C1A). The top 20 most abundant miRNAs with an average signal intensity >6,000 and a coefficient of variation <30% were selected for target mining. Predicted mRNA targets, including abundantly expressed *Tpbpa* & *Tpbpb* (trophoblast specific proteins alpha and beta) in the D13.5 mouse placenta, were determined using miRwalk with default settings and enriched with D13.5 murine placenta transcriptome GSE119710 (McNairn *et al.*, 2019). Pathway analysis of the enriched placental target genes of the top 20 highest expressed miRNAs revealed the following top pathways: metabolism of proteins, post-translational protein modification, metabolism, membrane trafficking, and vesicle-mediated transport, and many other important signaling pathways (Fig. CS1) that are critical for maternal-fetal communications. These data imply important roles of miRNAs in regulating expression of genes critical for placenta development and function under physiological conditions.

MiRNA profiles were analyzed for differentially expressed miRNAs by ZEA exposure. Visualization of the first three principle components indicated low variability in 0 ppm ZEA group that overlapped with 4 ppm ZEA group, and a well separated 40 ppm ZEA group with large intra-variability. This overall picture indicated a dose-response effect and various individual sensitivity to ZEA exposure (Fig. C1B). The majority of the differentially expressed miRNAs indicated by ANOVA analysis (heatmaps in Fig. CS2) were filtered out when R package *limma* was employed to identify differentially expressed miRNAs, with criteria of $Log_2FC \geq 1$ or $Log_2FC \leq -1$ (linear 2 fold change (FC)), a false discovery rate adjusted p-value ≤ 0.05, and an average signal intensity in all three groups >100 (Ritchie *et al.*, 2015). Under these criteria, 8 differentially expressed

miRNAs were identified in the 40 ppm ZEA group (mmu-miR-133b-5p, mmu-miR-7028-5p, mmu-miR-294-3p, mmu-miR-3970, mmu-miR-20b-5p, mmu-miR-7683-3p, mmu-miR-335-5p, mmu-miR-450b-5p), which included all 5 differentially expressed miRNAs in the 4 ppm ZEA group (Table CS1), shown as the largest red dots in the volcano plots (Fig. C1C, C1D). Two of the 20 most abundantly expressed miRNAs in the D13.5 placentas, mmu-miR-133b-5p and mmu-miR-7028-5p, were downregulated only in the 40 ppm ZEA group (Table CS1). Their predicted target genes were enriched in 'endocytosis' and 'mTOR signaling' pathways (data not shown).

Since the placentas from 40 ppm ZEA group had disrupted structure and function that were not obvious in the placentas from 4 ppm ZEA group, it is possible that differential expression of some miRNAs in the 40 ppm ZEA group could be a consequence of disrupted placental structure and function, whereas those in the 4 ppm ZEA group would more likely be targeted by ZEA and act as sensors of ZEA exposure (Li and Andersen *et al.*, 2019). We focused our analysis on the five microRNAs, mmu-miR-20b-5p, mmu-miR-294-3p, and mmu-miR-3970, mmu-miR-7683-3p, and mmu-miR-450b-5p, which were downregulated in both 4 ppm and 40 ppm ZEA groups (Table CS1). Mmu-miR-294-3p is a member of the miR-290-295 cluster, equivalent to human homologs miR-371-373, which are important for placental growth and maternal-fetal transport (Paikari *et al.*, 2017). Reactome pathway analysis revealed multiple enriched pathways from the predicted targets of these five miRNAs. Three of the top 5 pathways were related to immune function, which is critical for regulating maternal-fetal interface (Ander, Diamond and Coyne, 2019). Protein metabolism and post-translational modifications, extracellular matrix organization, and membrane trafficking are among top predicated pathways (Fig. C1E). These data demonstrate that ZEA has dose-dependent effects on expression of some placental miRNAs that are predicted to target critical genes in placental development and function.

Several miRNAs that are differentially expressed in the placentas from preeclampsia patients, such as miR-20b, have significant expression levels in the control D13.5 placentas and were shown to be dysregulated by ZEA treatment (Wang *et al.*, 2012). MiR-20b is a known angiogenesis-associated miRNA detected in the syncytium and some of the villous mesoblasts of term human placenta. Since the most severe adverse effects induced by ZEA exposure were observed in the labyrinth layer, and several placental miRNAs sensitive to ZEA treatment are associated with functions of cells in the labyrinth layer, this study provides preliminary evidence that miRNAs may mediate ZEA-induced placental toxicity.

Conflict of interest statement

The authors declare that there are no conflicts of interest.

Acknowledgments

We thank the financial support from Interdisciplinary Toxicology Program, Department of Physiology and Pharmacology, College of Veterinary Medicine, and Office of the Vice President for Research at University of Georgia, as well as the National Institutes of Health (R01HD065939 (co-funded by ORWH & NICHD), & R03HD097384).

References

Ander, S. E., Diamond, M. S. and Coyne, C. B. (2019) 'Immune responses at the maternal-fetal interface', *Science immunology*, 4(31), p. eaat6114. doi: 10.1126/sciimmunol.aat6114.

Andersen, C. L. *et al.* (2018) 'Chemotherapeutic agent doxorubicin alters uterine gene expression in response to estrogen in ovariectomized CD-1 adult mice', *Biology of Reproduction*, pp. ioy259–ioy259. doi: 10.1093/biolre/ioy259.

Christian Andersen Xiaoqin Ye, F. Z. *et al.* (2018) 'Effects of Mycoestrogens on Female Reproduction', *Reproductive and Developmental Medicine*, 2(1), pp. 52–58. doi: 10.4103/2096-2924.232875.

Evain-Brion, D. and Malassine, A. (2003) 'Human placenta as an endocrine organ', *Growth Hormone & IGF Research*, 13(Supplement), pp. S34–S37. doi: https://doi.org/10.1016/S1096-6374(03)00053-4.

Fabregat, A. *et al.* (2017) 'Reactome pathway analysis: a high-performance in-memory approach', *BMC bioinformatics*, 18(1), p. 142. doi: 10.1186/s12859-017-1559-2.

Li, Q. *et al.* (2015) 'Exploring the associations between microRNA expression profiles and environmental pollutants in human placenta from the National Children's Study (NCS)', *Epigenetics*. 2015/08/07, 10(9), pp. 793–802. doi: 10.1080/15592294.2015.1066960.

Li, R. *et al.* (2019) 'Dietary exposure to mycotoxin zearalenone (ZEA) during post-implantation adversely affects placental development in mice', *Reproductive Toxicology*, 85, pp. 42–50. doi: 10.1016/j.reprotox.2019.01.010.

Malnou, E. C. *et al.* (2019) 'Imprinted MicroRNA Gene Clusters in the Evolution, Development, and Functions of Mammalian Placenta', *Frontiers in genetics*, 9, p. 706. doi: 10.3389/fgene.2018.00706.

McCarthy, D. J. and Smyth, G. K. (2009) 'Testing significance relative to a fold-change threshold is a TREAT', *Bioinformatics (Oxford, England)*. 01/28, 25(6), pp. 765–771. doi: 10.1093/bioinformatics/btp053.

McNairn, A. J. *et al.* (2019) 'Female-biased embryonic death from inflammation induced by genomic instability', *Nature*. 2019/02/20, 567(7746), pp. 105–108. doi: 10.1038/s41586-019-0936-6.

Paikari, A. *et al.* (2017) 'The eutheria-specific miR-290 cluster modulates placental growth and maternal-

fetal transport', *Development (Cambridge, England)*. 2017/09/21, 144(20), pp. 3731–3743. doi: 10.1242/dev.151654.

Ritchie, M. E. *et al.* (2015) 'limma powers differential expression analyses for RNA-sequencing and microarray studies', *Nucleic acids research*. 2015/01/20, 43(7), pp. e47–e47. doi: 10.1093/nar/gkv007.

Sticht, C. *et al.* (2018) 'miRWalk: An online resource for prediction of microRNA binding sites', *PloS one*, 13(10), pp. e0206239–e0206239. doi: 10.1371/journal.pone.0206239.

Wang, W. *et al.* (2012) 'Preeclampsia Up-Regulates Angiogenesis-Associated MicroRNA (i.e., miR-17, -20a, and -20b) That Target Ephrin-B2 and EPHB4 in Human Placenta', *The Journal of Clinical Endocrinology & Metabolism*, 97(6), pp. E1051–E1059. doi: 10.1210/jc.2011-3131.

Xiao, S. *et al.* (2014) 'Differential gene expression profiling of mouse uterine luminal epithelium during periimplantation', *Reproductive sciences (Thousand Oaks, Calif.)*. 07/24, 21(3), pp. 351–362. doi: 10.1177/1933719113497287.

Figure Legend

Figure C1. Analysis of microRNAs in D13.5 mouse placentas upon ZEA treatment. A. Distribution of microRNAs based on their abundance/reading in the D13.5 control placentas. B. A 3D plot of the first three principle components (PC1=16.94%, PC2=13.09%, PC3=10.84% of total variation explained) to visualize the variations of microRNA expression profiles among the treatment groups and individual samples. C-D. Volcano plots of D13.5 placental microRNAs between 0 ppm and 4 ppm ZEA groups (C) and between 0 ppm and 40 ppm ZEA groups (D). Red dots: significantly differentially expressed miRNAs, $Log_2FC \geq 1$ or $Log_2FC \leq -1$ (linear 2 fold change (FC)), adjusted p-value ≤ 0.05; dot size: Log_2(average signal intensity of all three groups). The 5 miRNAs in C represented by the 5 biggest red dots had average signal intensity >100 (Table S1) and were used for further analysis in E. E. Reactome pathway analysis of predicted targets of 5 significantly differentially expressed microRNAs in both 4 ppm and 40 ppm ZEA groups that fit the criteria of $Log_2FC \geq 1$ or $Log_2FC \leq -1$, adjusted p-value ≤ 0.05, and average signal intensity >100 (Table S1). Reactome pathway adjusted p-value ≤ 0.05, sorted by p-value.

Figure CS1. Reactome pathways (adj. $P \leq .05$) enriched with predicted placenta-specific target genes of the 20 most abundant microRNAs in D13.5 mouse placentas of control group.

Figure CS2. Heat maps of differentially expressed miRNAs (A. $P<0.05$; B. $P<0.01$) in D13.5 mouse placentas upon 0 ppm, 4 ppm, and 40 ppm dietary ZEA treatment from D5.5 to D13.5. N=4; ANOVA analysis.

Table CS1. Differentially expressed microRNAs in D13.5 mouse placentas upon 4 ppm and 40 ppm dietary ZEA treatment from D5.5 to D13.5.

Figure

Figure C1

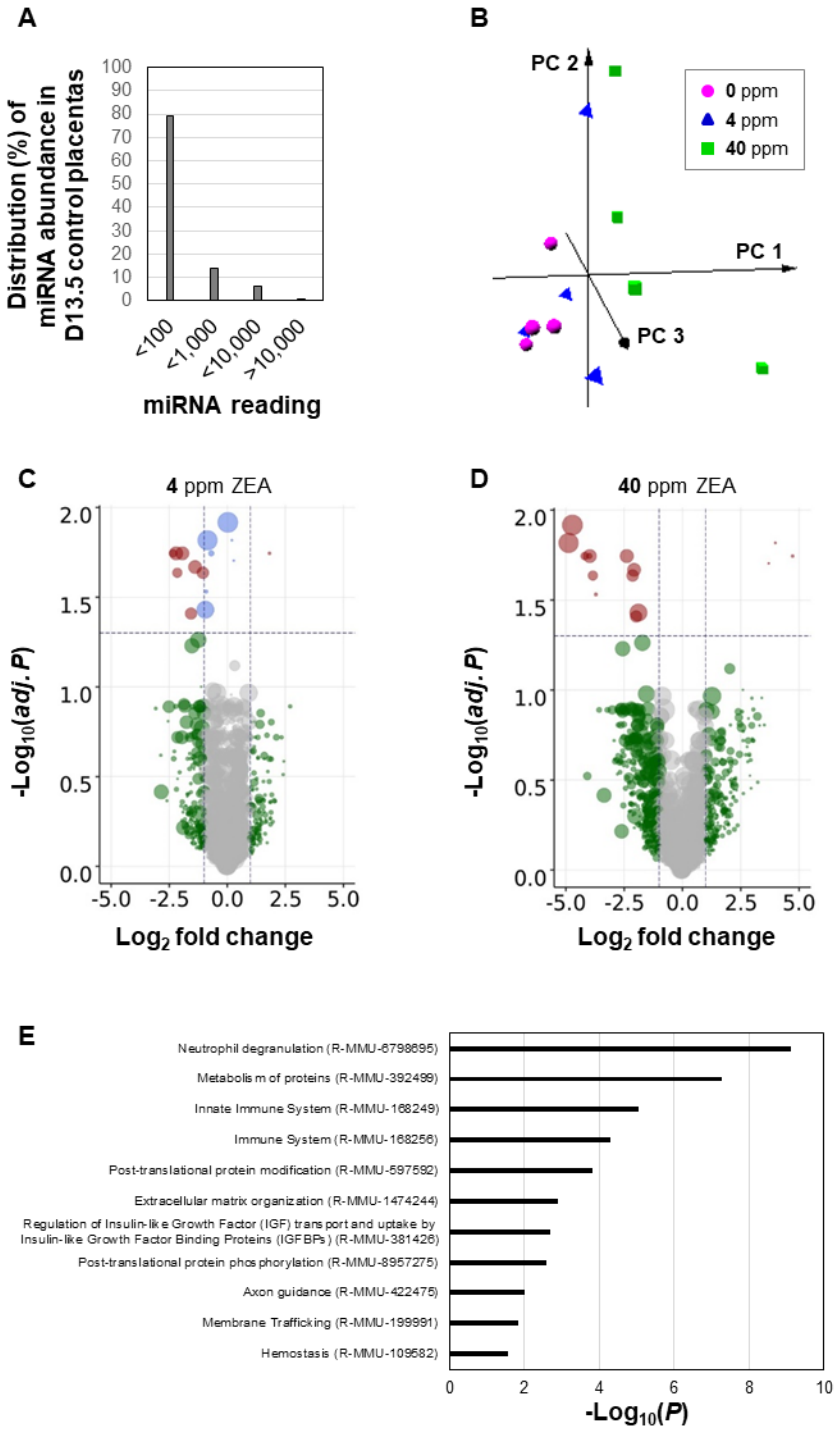

Supplementary

Figure CS1

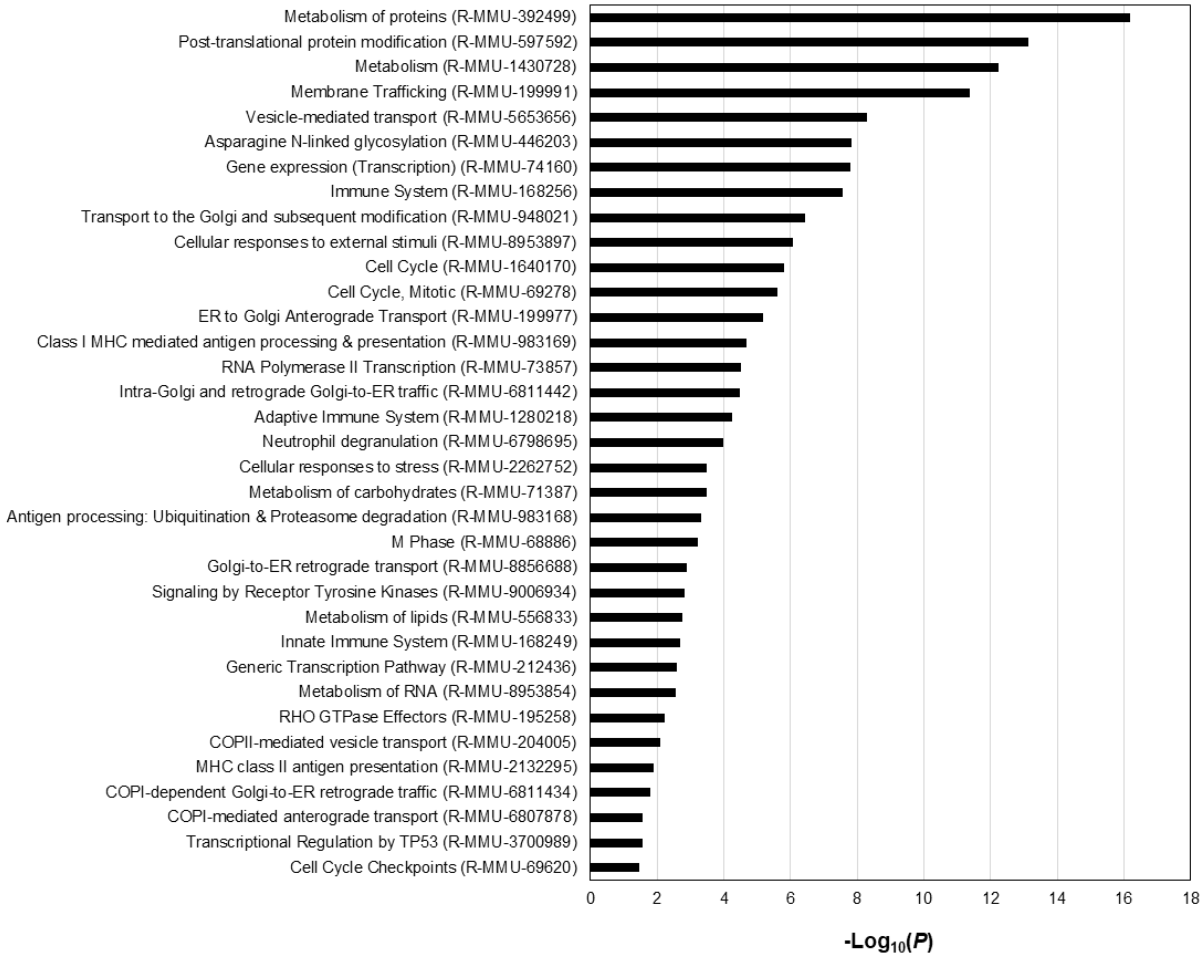

Figure CS2

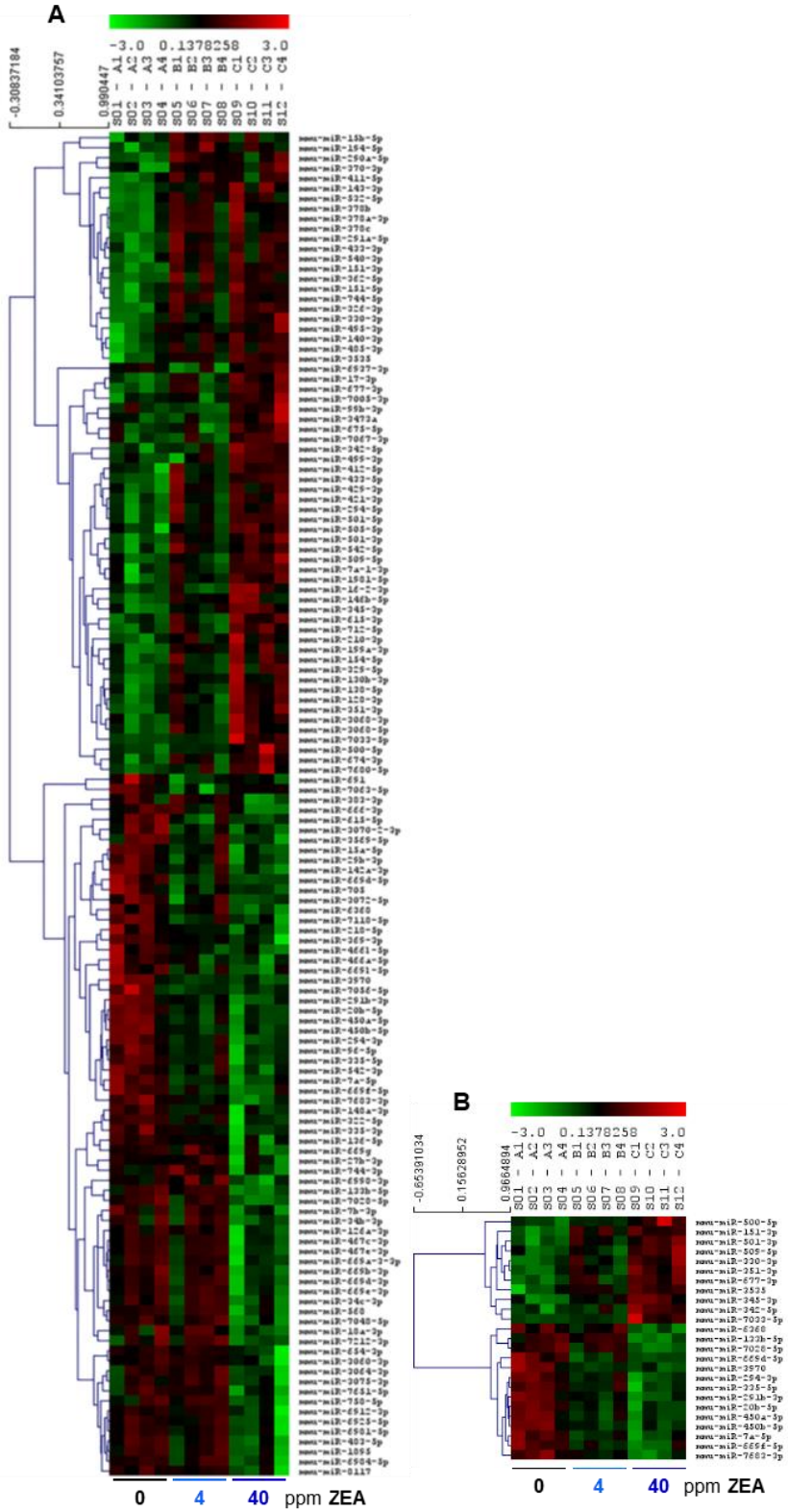

Table CS1

MicroRNA	Log_2(Average signal intensity)	Log_2(FC) 4 ppm vs. 0 ppm ZEA	Log_2(FC) 40 ppm vs. 0 ppm ZEA	p-value (ANOVA)	Adjusted p-value (Benjamini-Hochber FDR)
mmu-miR-133b-5p	13.2564524	0.023427502	-4.719539364	6.85E-06	0.012099
mmu-miR-7028-5p	12.8374876	-0.851913611	-4.883563271	2.49E-05	0.015222
mmu-miR-294-3p	8.65325973	-1.932268423	-3.973355725	6.96E-05	0.017999
mmu-miR-3970	8.74906396	-2.203043077	-2.387934485	5.07E-05	0.017999
mmu-miR-20b-5p	8.59042637	-1.387480707	-2.074759008	0.000122	0.021461
mmu-miR-7683-3p	7.65562713	-1.05264071	-2.137587803	0.000157	0.023099
mmu-miR-335-5p	11.2992763	-0.945557609	-1.888618939	0.000299	0.037122
mmu-miR-450b-5p	7.53545064	-1.562233712	-1.986270139	0.000354	0.039018